UNIVERSITY OF OKLAHOMA

GRADAUTE COLLEGE

SHAPE DESIGN OPTIMIZATION OF PARAMETRIC FLUME SECTIONS

A DISSERTATION

SUBMITTED TO THE GRADUATE FACULTY

In partial fulfillment of the requirement for the

degree of

Doctor of Philosophy

BY

SUNG-HWAN JOO
Norman, Oklahoma
2006

Downloaded from SHAREOK. Persistent Handle URL: https://hdl.handle.net/11244/1057

UMI Number: 3218985



UMI Microform 3218985

Copyright 2006 by ProQuest Information and Learning Company.
All rights reserved. This microform edition is protected against
unauthorized copying under Title 17, United States Code.

ProQuest Information and Learning Company
300 North Zeeb Road
P.O. Box 1346
Ann Arbor, MI 48106-1346

SHAPE DESIGN OPTIMIZATION OF PARAMETRIC FLUME SECTIONS

A DISSERTATION APPROVED FOR THE
SCHOOL OF AEROSPACE AND MECHANICAL ENGINEERING

BY

_____

ALFRED G. STRIZ, CHAIR

_____

KURT GRAMOLL

_____

J. DAVID BALDWIN

_____

ZAHED SIDDIQUE

_____

SHIVAKUMAR RAMAN

© Copyright by SUNG-HWAN JOO 2006

All Rights Reserved.

ACKNOWLEDGMENTS

I would like to express my very sincere appreciation to Dr. Alfred G. Striz for his guidance and support through this work, and for serving as the chair of my advisory committee.

I also wish to express my gratitude to Dr. Kurt Gramoll, Professor of the School of Aerospace and Mechanical Engineering, Dr. J. David Baldwin, Associate Professor of the School of Aerospace and Mechanical Engineering, Dr. Zahed Siddique, Associate Professor of the School of Aerospace and Mechanical Engineering, and Dr. Shivakumar Raman, Professor of the School of Industrial Engineering, for serving as committee members and for their sincere evaluations of this dissertation. Also, I would like to thank Dr. Kuang-Hua Chang, Professor of the School of Aerospace and Mechanical Engineering, for his guidance and support.

I would like to thank my colleagues at the University of Oklahoma, especially Jang-Ho Yoon, Hyun-Wook Gwak, Trey Wheeler, and Mangesh S. Edke. I would like to thank the members of the Norman Korean Baptist Church, especially Pastor Youn Seung Yang and Pastor Jong-Ki Kim for their encouragement and prayers.

There is no word to express my appreciation to my parents, parents-in-law, sisters, sister-in-law, and brothers-in-law for their understanding and support, from the bottom of my heart.

Finally, I thank my wife, Heeyeoun, my son, Hong-Jae, my daughter, Hye-Jun, for their love and support. I could not have succeeded without them.

And, thank God for everything he gave me.

TABLE OF CONTENTS

Acknowledgments iv

Table of Contents v

List of Figures viii

List of Tables xii

Abstract xiii

1. Introduction 1

    1.1 Motivation and Literature Review 4

    1.2 Objective and Scope 7

    1.3 Approach 8

        1.3.1 Design Optimization of B-Spline-Based Flume Sections 8
        1.3.2 Design Optimization of CAD-Based Flume Sections 9

    1.4 Outline 10

2. Construction of B-Spline-Based Flume Section Geometry 12

    2.1. Introduction 12

    2.2 Flume Sections 13

    2.3 General Procedure for Constructing Flume Section Geometry 23

    2.4 Parametric B-Spline Representation 26

        2.4.1 B-Spline Curve 28
        2.4.2 B-Spline Surface 31

    2.5 Curve Fitting and Surface Skinning 32

        2.5.1 Least Squares Fitting Using B-Spline Curves 32
        2.5.2 Surface Skinning 35

    2.6 Flume Section Configuration Examples 38

3. Construction of CAD-Based Flume Section Geometry 41

3.1. Introduction 41

3.2. Mathematic Representation of Basic Flume Sections 41

3.2.1 Equations of Straight Flume Section 42
3.2.2 Equations of Arced Flume Section 43
3.2.3 Equations of Cubic-Curve Flume Section 45

3.3 Continuity Requirements and Design Parameterization 47

4. Motion Analysis Along Flume Sections 53

4.1. Introduction 53

4.2. Lagrange's Equations of Motion 53

4.3. Generalized Equations of Motion 55

4.4. Numerical Calculations 60

4.5. Numerical Examples 63

4.5.1 Numerical Example of B-Spline-Based Flume Sections 63
4.5.2 Numerical Examples of CAD-Based Flume Sections 67

5. Shape Design Analysis and Optimization of Flume Sections 71

5.1. Introduction 71

5.2. Overall Finite Difference Method 72

5.3. Numerical Calculations 80

5.4. Design Sensitivity Verification 81

5.5. Shape Design Optimization of B-Spline-Based Flume Sections 91

5.5.1 Flume Configuration for Optimization 91
5.5.2 Design Optimization Problem 94
5.5.3 Design Optimization Results 95
5.5.4 Off-Design Results 99

5.6. Shape Design Optimization of CAD-Based Flume Sections 102

5.6.1 Flume Configuration for Optimization 102
5.6.2 Design Optimization Problem 105
5.6.3 Design Optimization Results 107
5.6.4 Off-Design Results 111

6. Discussion and Future Work 113

References 116

Appendices 120

Appendix A: Three – Dimensional Transformation 120

Appendix B: Continuity Requirements for CAD-Based Flume Sections 123

Appendix C: Frictional Forces 149

Appendix D: Derivation of Sensitivity Equations 157

LIST OF FIGURES

Figure Pages

1.1 Roman Water Channel 1

1.2 Water Sluice in Middle East Asia 2

1.3 Water Slide 2

1.4 Bobsled Track 3

2.1 Flow Channel Composed of Five Flume Sections 22

2.2 Flume Sections before Transformation 22

2.3 Transformed Flume Sections 23

2.4 General Procedure for Constructing Flow Channel Geometries 24

2.5 Geometric Points of *CTL* and *S68* Flume Sections 24

2.6 Completed Connection of *CTL* and *S68* Flume Sections 25

2.7 B-Spline Surface and Control/Geometric Points of Connected Flume Sections 26

2.8 Parametric Curve in Space 27

2.9 Parametric Surface in Space 28

2.10 Parametric B-Spline Curve with Control Points and Control Polygon 29

2.11 B-Spline Curve Fitting 33, 34

2.12 Computational Algorithm for Curve Fitting 35

2.13 Spline Surface Skinning 36

2.14 Geometric Points of Parker Water Slide after Three-Dimensional Transformation 38

2.15 B-Spline Surface of Parker Water Slide 39

2.16 Control Points and Control Polygon of Parker Water Slide 40

3.1 Straight Flume Section 43

3.2 Arced Flume Section 44

3.3 Spatial Cubic Curve 45

3.4 Cubic-Curve Flume Section 46

3.5 Configuration of Two Straight Flume Sections 50

3.6 Configuration of Straight-Cubic-Straight Flume Configuration 51,52

4.1 Geometric Shape of Parker Configuration 64

4.2 Top View of Particle Trace of Non-Friction Case (Parker) 65

4.3 Isometric View of Particle Trace of Non-Friction Case (Parker) 65

4.4 Top View of Particle Trace of Friction Case (Parker) 66

4.5 Isometric View of Particle Trace of Friction Case (Parker) 66

4.6 Particle Trace of Arced Flume Configuration 68

4.7 Particle Traces of Straight-Cubic-Straight Flume Configuration 70

5.1 Dependence of Object Path on Design Changes 75

5.2 Illustration of DSA Predictions for Variables at Same Time Step 79

5.3 Procedure for Numerical Calculations 81

5.4 Parker Configuration with Particle Trace 82

5.5 Location of Object $u(t)$ in Time Domain 83

5.6a Sensitivity Verification for $w(t)$ due to Change of $B^z_{20,6}$ 85

5.6b Sensitivity Verification for $u(t)$ due to Change of $B^z_{20,6}$ 86

5.6c Sensitivity Verification for $w(t)$ due to Change of $B^y_{5,7}$ 87

5.6d Sensitivity Verification for $u(t)$ due to Change of $B^y_{5,7}$ 88

5.6e Sensitivity Verification for $w(t)$ due to Change of $B_{8,8}^{x}$ 89

5.6f Sensitivity Verification for u(t) due to Change of $B_{8,8}^{x}$ 90

5.7a Isometric View of William Configuration 92

5.7b Front View of William Configuration 92

5.7c Top View of William Configuration 93

5.8a Isometric View of William Configuration with Particle Trace
before Optimization 96

5.8b Top View of William Configuration with Particle Trace
before Optimization 97

5.9 Comparisons of Particle Traces in William Configuration
before and after Optimization 98

5.10 Paths of Friction Cases in B-Spline-Based Optimized Slide 100

5.11 Combined Paths of Friction Cases in B-Spline-Based Optimized Slide 101

5.12 Top View of Center Points of Cubic-Curve Sections 102

5.13a Isometric View of David Configuration 103

5.13b Top View of David Configuration.....104

5.14a Isometric View of David Configuration with Particle Trace
before Optimization 107

5.14b Top View of David Configuration with Particle Trace
before Optimization 108

5.15 Comparisons of Center Points before and after Optimization 109

5.16a Top View of David Configuration with Particle Trace after Optimization 109

5.16b Isometric View of David Configuration with Particle Trace after Optimization 110

5.17 Combined Paths of Friction Cases on CAD-Based Optimized Slide 111

5.18 Combined Paths of Friction Cases on CAD-Based Optimized Slide 112

A.1 Homogeneous Coordinate System in Two Dimensions 120

B.1 Straight Flume Section 124

B.2 90º Arced Flume Section 128

C.1 Vectors of Particle on Surface 150

C.2 Normal Reaction Force and Unit Normal Vector 154

LIST OF TABLES

Table		Pages
2.1a	Straight Flume Sections	14,15,16
2.1b	Connection Flume Sections	17,18
2.1c	Curved Flume Sections	19,20
4.1	Coefficients of Adams-Bashforth Methods	62
4.2	Coefficients of Adams-Moulton Methods	62
4.3	Coefficients of Gear Methods	63
4.4	Physical Sizes of Parker Configuration	67
4.5	Physical Sizes of Arced Flume Configuration	69
4.6	Physical Sizes of Straight and Cubic Mixed Flume Configuration	69
5.1	Physical Sizes of William Configuration	91
5.2	Physical Parameters for Off-Design Friction/Weight Cases	99

ABSTRACT

This research presents a shape design analysis and optimization methodology for parametric surface flume sections. Flume sections or flow channels have been used widely in many areas such as water chutes in civil and agricultural engineering and water slides and bob sled tracks in the recreational and sports fields. Designing such a flow channel in a CAD environment can provide many advantages such as time and resource savings to the designer. In addition, optimizing such flow channels in a virtual environment is especially efficient.

In this research, geometric modeling was addressed first. Two types of parametric surface flume section models were created: B-Spline-based flume sections and parametric CAD-based flume sections as used in water chutes or water slides. The B-Spline-based flume sections were based on the dimensions of fifteen flume sections, provided by a commercial water slide firm. These flume sections presented the basis for building up realistic flume section configurations. In addition, three different kinds of CAD-based flume sections were developed by the author. Sets of differential equations based on Lagrange's equations of motion were derived that describe the motion of an object traveling in the flow channel. These ordinary differential equations were solved using *Mathematica*®. Continuity requirements were derived from the equations of motion. An analytical shape design sensitivity analysis (DSA) methodology was developed and employed to support the optimization of the B-Spline-based and the CAD-based flume section models.

Optimization of parametric surfaces is a reasonably new area. Although research has been done in this area, most of it has been focused on developing better parametric surfaces, i.e., surface fitting schemes. Here, the B-Spline-based models, based on bi-cubic B-Spline surfaces, were optimized first. The control point positions were used as design variables in the optimization. Using the B-Spline control points as design variables provides more flexibility and allows for local design changes. However, the fact that no CAD software provides the control points as design parameters significantly limits their usefulness in a real design environment. The CAD-based flume section models consisted of sets of key dimensions, which were again defined as design variables for optimization. Using dimensions as design variables provided an easy and realistic avenue for design changes. However, the limited number of dimensions also limits the flexibility of design changes in the CAD-based flume section models. The *DOT*® (Design Optimization Tool) software with the includet *BigDOT*® tool for large numbers of design variables provided the optimization code for the procedure, while CAD software, e.g., *I-DEAS*®, *SolidWorks*®, and *Mathamatica*® were used for curve fitting and surface representations.

Among the many practical (water channel, water chutes) and not-so-practical (water slides, bobsled tracks) application of this work, water slides were used here as examples. For water slide design, safety and excitement of the ride are two common criteria. Of these, the excitement level of the ride can be increased by increasing the acceleration of the rider. The more important safety aspect is addressed by restricting the traveling object to stay within the physical boundaries of the slide during the entire time of the ride.

Various waterslide configurations were successfully optimized for these conflicting requirements.

CHAPTER 1

INTRODUCTION

Gravity driven open flow devices have been widely used in many application areas. The Roman Empire already built water channels in about A.D. 100 (Figure 1.1).

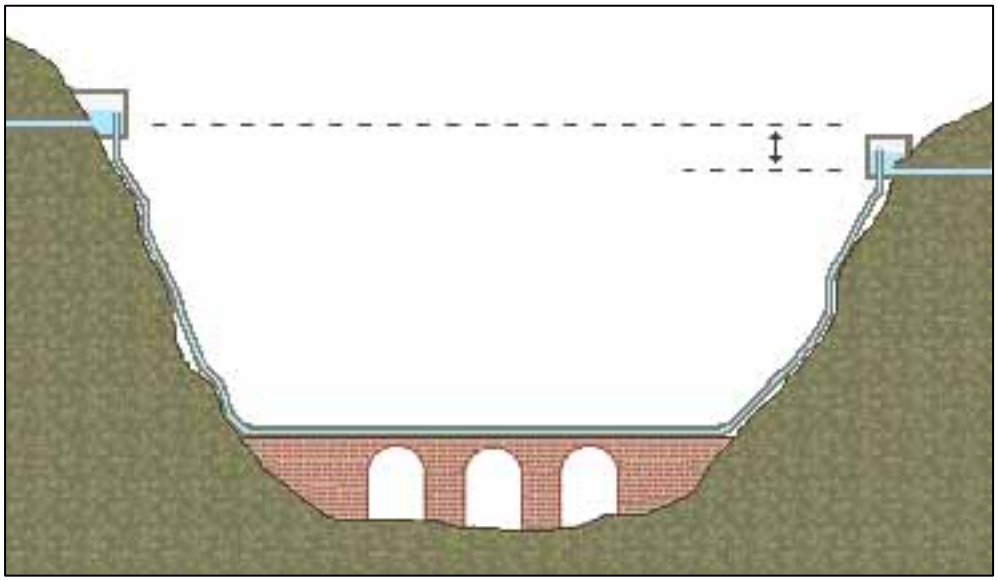


Figure 1.1 Roman Water Channel

In modern days, water chutes and sluices have been built for water delivery and control (Figure 1.2). For less practical purposes, water slides have been built for amusement parks around the world (Figure 1.3).



Figure 1.2 Water Sluice in Middle East Asia



Figure 1.3 Water Slide

In addition, flume configurations have been used in sports competition such as for bobsleds and luges (Figure 1.4).



Figure 1.4 Bobsled Track

Designing such flow channel models can require considerable resources and expertise. Especially, when a flow channel has to satisfy safety requirements (water slide, bobsled track) or has to be built on a low budget, designing a flow channel model in a Computer Aided Design (CAD) environment has advantages. Such flow channels can be represented by parametric surfaces such as cubic surfaces or B-Spline surfaces. Among the above applications, the water slide has been chosen as an example throughout this research because it is relatively easy to model and evaluate.

This chapter provides the reader with a general overview of the research. Section 1.2 contains the literature review. The objective and scope of the proposed research and the approaches developed for it are presented in Sections 1.3 and 1.4, respectively. The chapter closes with an outline of the remaining chapters in the dissertation.

1.1 Motivation and Literature Review

As mentioned in the introduction, designing water channels or flume sections in a CAD environment can save considerable resources. However, designing flume sections in a CAD environment also requires a certain level of knowledge about CAD applications, dynamics, numerical methods, and parametric surfaces. In addition, reliable optimization routines or software packages are required if optimization is desired. Thus, to date, few attempts have been made to design and optimize flume sections such as used in water slides. However, due to increasing competitiveness in the recreational equipment industry and stricter safety requirements from the government and the public, demands on computer tools that support modeling, analysis, and the optimized design of flume section for waterslides have increased as well. Therefore, developing flume section configurations in a CAD environment should allow for tremendous time and cost savings in the development and building of flume section configurations, not only for waters slides, but for other flow channel configurations as well.

In a literature search, very little information was found describing a mathematical model of a particle (human) moving in a gravity field, constrained within a given predefined cross section, such as in a waterslide. Several Mechanical Engineering students at the University of Oklahoma conducted the first work as a design project during the fall semester of 1993. Preliminary results showed that the path of a human rider could be determined using surface modeling techniques and dynamics analysis [1]. However, these results were not verified using real-world waterslide configurations. Following this preliminary work, research was conducted by Kondragunta for his M.S. Thesis in 1995 at the University of Oklahoma [2]. Again, accuracy of his work was not verified using real-world waterslide configurations.

Theories for designing flow channels haven been developed by several researcher like White [3] and have been commercially applied. However, designing flow channels using parametric surfaces is a relatively new concept. In addition, integrated tools which support the dynamic analysis and optimization are essentially non-existent.

In the area of computer aided parametric surface design, there has been much research done on parametric surfaces, especially splines, since the 1940s. Before computers came into play, numerical calculations were done by hand. Although piecewise-defined functions like the signum function or the step function were sometimes used, polynomials were generally preferred because they were easier to work with. Through the advent of computers, splines have gained importance. They were first used

as a replacement for polynomials in interpolation, then, as a tool to construct smooth and flexible shapes in computer graphics.

It is commonly accepted that the first mathematical reference to splines is a 1946 paper by Schoenberg [4], which first mentions the word "spline" in connection with smooth, piecewise polynomial approximations. However, these ideas have their roots in the aircraft and ship-building industries. In the foreword to Reference 5 (Bartels et al., 1987), Robin Forrest describes "lofting," a technique used in the British aircraft industry during World War II and ever since, to construct templates for airplanes by passing thin wooden strips (called "splines") through points laid out on the floor of a large design loft, a technique borrowed from ship-hull design. Lofting was replaced by what we call splines in the early 1960's, based on work by Ferguson at Boeing and by Sabin at British Aircraft Corporation.

The use of splines for modeling automobile bodies seems to have several independent beginnings. Credit is claimed on behalf of de Casteljau at Citroën, Bézier at Renault, and Birkhoff, Garabedian, and de Boor at General Motors (see Birkhoff and de Boor, 1965) [6], all for work occurring in the very early 1960s or late 1950s. Work was also being done at Pratt & Whitney Aircraft, where two of the authors of Reference 7 (Ahlberg, et al., 1967) — the first book-length treatment of splines — were employed, and at the David Taylor Model Basin by Theilheimer.

In the area of optimizing parametric surfaces, much research has been done, as well. e.g., by Sarkar, et al. [8], Speer, et al. [9], and Laurent-Gengoux [10]. However, the optimization of parametric surfaces has mostly been limited to developing better

parametric surface numerical algorithms. There has been little attempt made to develop an application tool to optimize parametric surfaces.

The research in this dissertation represents the continuation and conclusion of work performed by the author for his M.S. thesis at the University of Oklahoma [11, see also 12]. Important parts of the development leading to the optimization methodology have been included here again for clarity and continuity.

1.2 Objective and Scope

The objective of the research in this area is to develop an integrated modeling, analysis, and optimization methodology for the design of flume sections to address smoothness and speed of flow in general and safety and excitement in water slides in particular.

Another objective of the research is to parameterize and optimize a flow channel configuration in a CAD environment by defining control points or the geometric dimension as design variables.

Essentially, this research aims at solving the following design optimization problem:

$$\left.\begin{array}{ll} \text{Minimize:} & \phi(\boldsymbol{b}) \\ \text{Subject to:} & \psi_i(\boldsymbol{b}) \le \psi_i^u \\ & b_j^\ell \le b_j \le b_j^u \end{array}\right\} \qquad (1.1)$$

where $\phi(\boldsymbol{b})$ is the objective function; $\boldsymbol{b}$ is the vector of design variables defining the flume section surface model; $\psi_i(\boldsymbol{b})$ is the i^{th} dynamic performance with its corresponding upper bound ψ_i^u; and b_j^ℓ and b_j^u are the lower and upper bounds of the j^{th} design variable, respectively. To achieve this objective, an integrated tool environment that supports design parameterization, motion analysis, design sensitivity analysis, and optimization of flume sections will be developed.

1.3 Approach

1.3.1 Design Optimization of B-Spline-Based Flume Sections

In the first part of this research [11], the geometry of a flume section configuration is constructed from a set of discrete points. These discrete points or geometric points describe the shape of the flume section in a discrete form. Curve fitting and surface skinning techniques [14] are employed to construct a smooth, parametric B-Spline surface that best fits the given geometric points. The control points of the B-Spline surface that govern the shape of the flume section are chosen as shape design variables. The traveling object in this proposed method is assumed as a particle with concentrated mass. The interaction between the traveling object and the flume section surface with a thin water layer in between is simplified by a pre-assumed friction coefficient. With these assumptions, the ordinary differential equations that govern the motion of the traveling object are derived using Lagrange's equations of motion. These equations are solved

numerically using *Mathematica*® [4]. Analytic shape DSA expressions that describe the derivatives of the particle path, velocity, and acceleration with respect to control point perturbations of the flume section B-Spline surface are derived. These equations are again solved numerically using *Mathematica*®. A sensitivity display and what-if methodology developed for structural design optimization is employed to conduct interactive design for continuity and smoothness of flow in the flume section. As a final step, the optimization problem is defined and solved.

1.3.2 Design Optimization of CAD-Based Flume Sections

The objective of the second part of this research is to optimize a CAD-based flume section model. To accomplish this goal, such a model is parameterized, and analytical shape design sensitivity analysis for the CAD-based flume section is performed. In the first part of the research, it was shown that analytical shape DSA can be successfully used on the geometric model of a flume section constructed using a parametric B-spline surface. However, it is not always practical to use a perturbation of control points as a method to change the design model in real design cases because there are very few CAD tools, which support design change based on control points. Therefore, parameterization of a CAD-based flume section model and shape DSA with actual dimensions as design variables are much needed.

With parametric modeling techniques, designers are able to create parts using CAD tools such as *Pro/ENGINEER*®*, SolidWorks*®*, CATIA*®, and assemble these parts into a

product in the CAD environment. In addition, with parameterized product models, designers are able to define the dimensions as the design variables and make a design change simply by changing the design variable values. Also, these design variables can be used for analytical shape design sensitivity analysis (DSA) and design optimization.

In this research, several sets of CAD-based flume section models are first constructed in a CAD environment. Several key dimensions are implemented in the CAD model. The design variables, which are the dimensions of the CAD model, are defined for shape design sensitivity analysis and optimization. The same assumptions about the traveling object and about friction as used in the first part of the research are applied. The same ordinary differential equations that governed the motion of the traveling object in the first part of the research are used here, too. Analytic shape DSA expressions that describe the derivatives of the particle path, velocity, and acceleration with respect to the design variable perturbations of the CAD-based flume section shape are again derived and solved numerically using *Mathematica*®. A sensitivity analysis method again is employed, and the optimization problem is defined and solved.

1.4 Outline

In Chapters 2 and 3, B-Spline-based and CAD-based flume section geometries are introduced, respectively, and shape design sensitivity analysis is conducted. In Chapter 4, motion analysis of a particle down flume sections is introduced with a number of

examples. Design optimization of flume sections is presented in Chapter 5. In Chapter 6, present and future work are discussed.

CHAPTER 2

CONSTRUCTION OF B-SPLINE-BASED FLUME SECTION GEOMETRIES

2.1 Introduction

An open flow channel configuration such as a water slide is composed of basic building blocks, called flume sections. Each flume section is represented by a set of geometric points in a global x_1-, x_2-, x_3- coordinate system. These geometric points represent the shape of the basic building blocks in a discretized form. The geometric points of each flume section are transformed through translations and/or rotations to connect with other flume sections. In this research (see also Reference 11), bi-cubic B-Spline surfaces in parametric form are employed for representing the shape of the flow channel. Importantly, C^2-continuity of the bi-cubic B-Spline surfaces satisfies the regularity requirements of motion analysis. Thus, the transformed geometric points represent the geometric shape of the flow channel. In Section 2.2, the overall procedure for constructing the flow channel geometry is presented.

In Section 2.3, the geometric shapes and characteristics of basic flume sections are introduced. In Section 2.4, parametric representations of planar and spatial curves and surfaces are introduced. B-Spline curves and surfaces are introduced in Section 2.5. Finally, a number of real-world examples are shown in Section 2.6 to demonstrate the proposed geometric construction process for flume sections.

2.2 Flume Sections

Each flume section has its own unique shape. There are fifteen flume sections employed in this research, as listed in Table 2.1, serving as the basic building blocks for flow channel and water slide geometries. Each flume section was designed by the *Miracle Recreational Equipment Company,* a water slide company, and specific code names were designated by this company. These codes have been changed here for clarity. Since geometric shapes at the ends of each flume section are unique, it is important to choose compatible sections for connection, so that the junction between two flume sections is smooth. For example, the end section shape of *LC45* (Table 2.1c) and the beginning section shape of *CFL* (Table 2.1b) are compatible.

Straight Flume Sections

Five straight flume sections were used as basic sections. Code names have S (straight) + two-digit number format (total length in feet-inches) + D (if drop exists), e.g., *S30* means that it is a straight flume section with 3 feet 0 inches length. Flume sections are *S30, S60, S46, S58,* and *S68D.*

More detailed information is given in Table 2.1a. Note that the drawings are not to the same scale.

Table 2.1a Straight Flume Sections

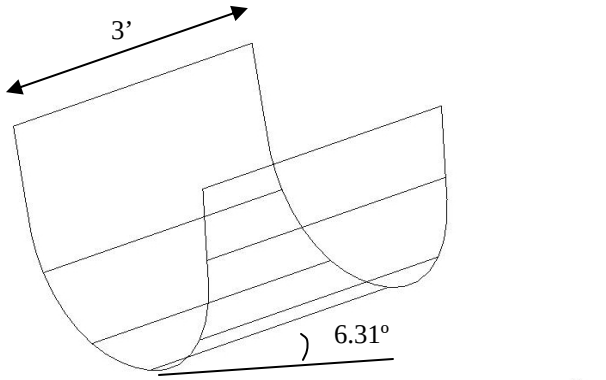
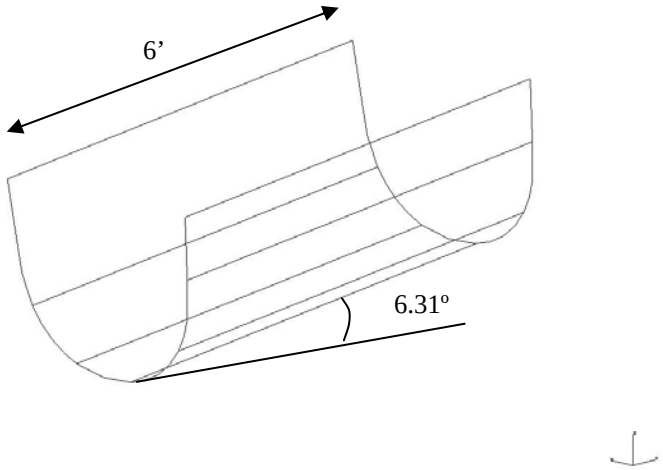
Code Name	Info.	Isometric View of Flume Section
S30	3’	
S60	6’	

Table 2.1a Straight Flume Sections (Cont'd)

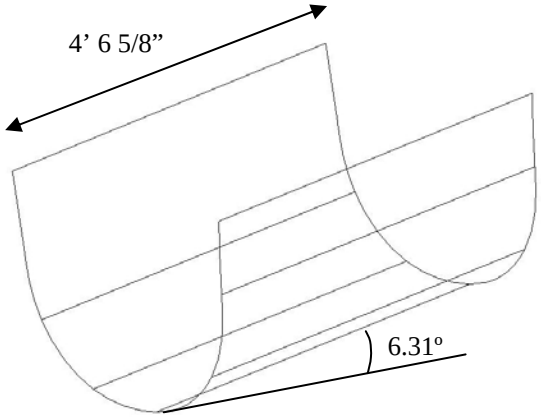
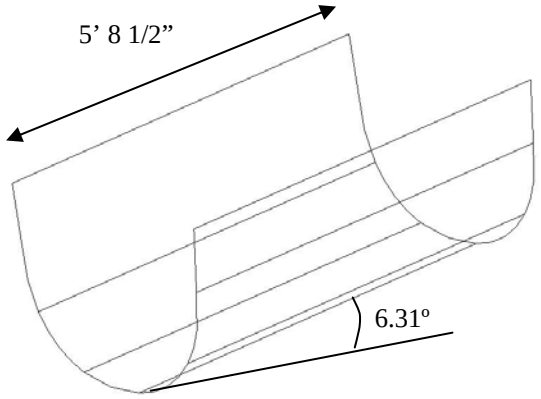
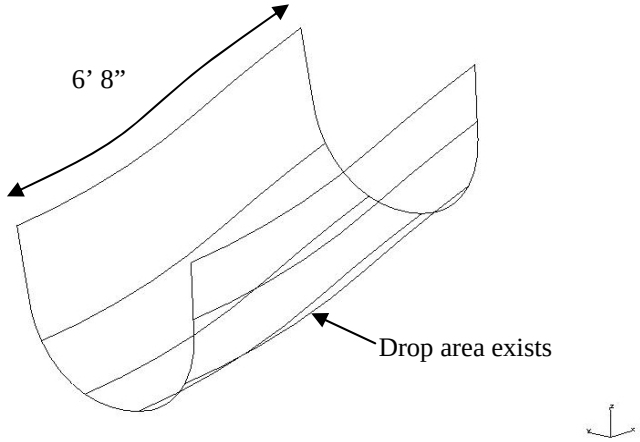
Code Name	Info.	Isometric View of Flume Section
S46	4'6 5/8"	
S58	5'8 1/2"	

Table 2.1a Straight Flume Sections (Cont'd)

Code Name	Info.	Isometric View of Flume Section
S68D	6' 8"	

Connection Flume Sections

Four connection flume sections were used as basic sections. Code names have C (connection) + T or F (to or from) + L or R (left or right), e.g., *CTL* means that it is a connection flume section to connect to a left-hand curved flume section from a straight flume section. All connection flume sections are used to connect curved flume sections with straight flume sections. Connection flume sections are *CTL*, *CTR*, *CFL*, and *CFR*. The length of each flume section is 3 ft.

More detailed information is given in Table 2.1b.

Table 2.1b Connection Flume Sections

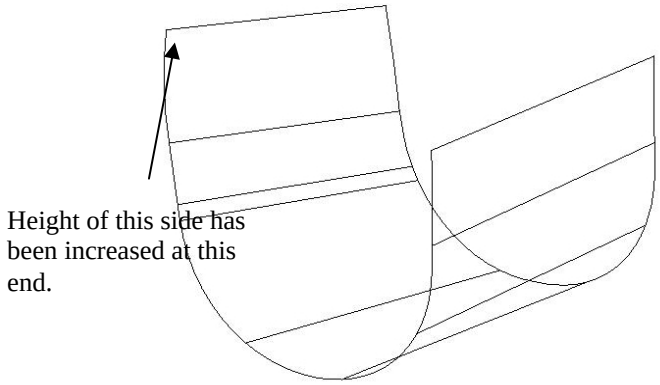
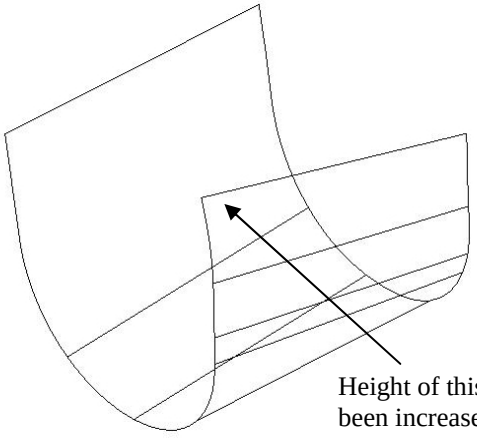
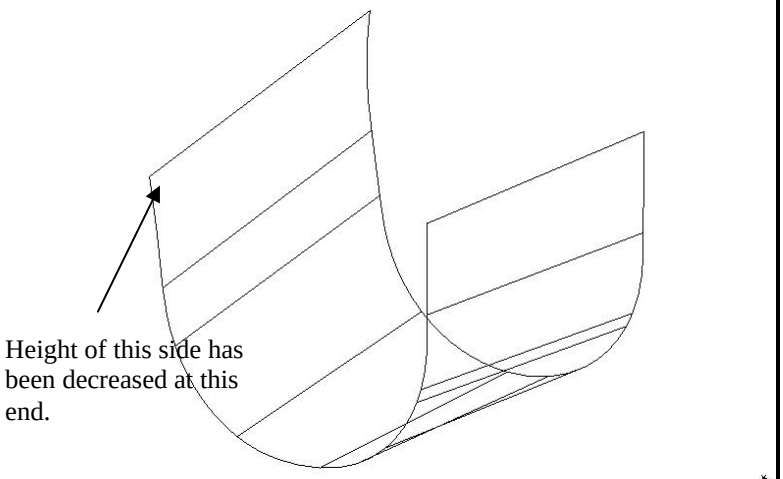
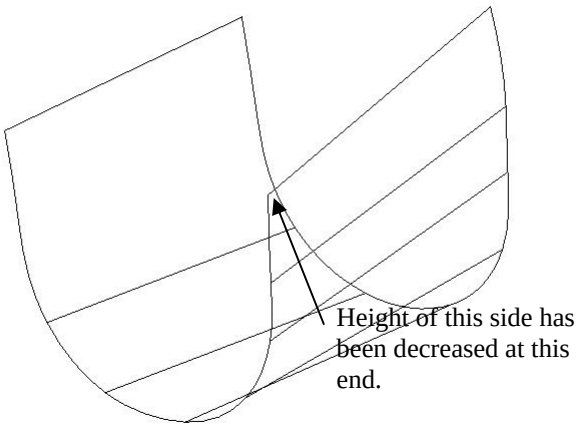
Code Name	Info.	Isometric View of Flume Section
CTL	End of straight flume section to Start of left-hand curved flume section	
CTR	End of straight flume section to Start of right-hand curved flume section	

Table 2.1b Connection Flume Sections (Cont'd)

Code Name	Info.	Isometric View of Flume Section
CFL	End of left-hand flume section to Start of straight flume section	
CFR	End of right-hand flume section to Start of straight flume section	

Curved Flume Sections

Four curved flume sections were used as basic sections. Code names have L or R (left or right) + C (curved) + two digit number format (45 or 90 in degree) + D (if drop exists), e.g., *LC90D* means that it is a left handed 90º curved flume section with drop. Note that a curved flume section's height on the outside wall is larger than on the inside wall. This is the reason why connection flume sections are needed. Curved flume sections are *LC45, LC90, LC90D, RC45, RC90,* and *RC90D*. More detailed information is given in Table 2.1c.

Table 2.1c Curved Flume Sections

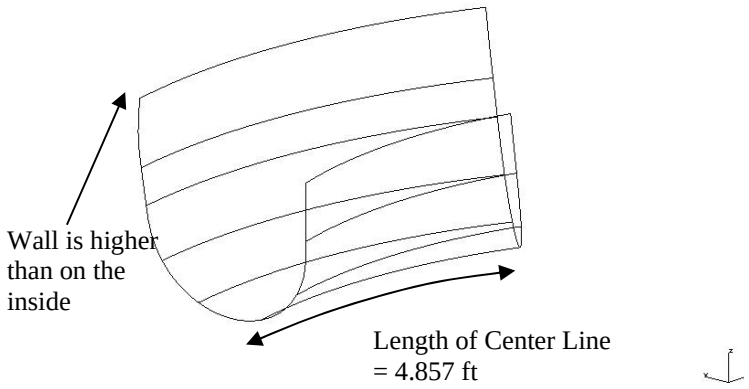
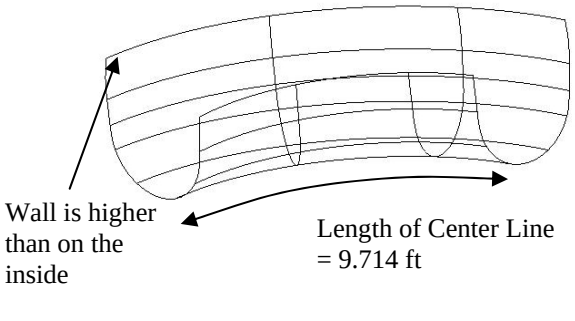
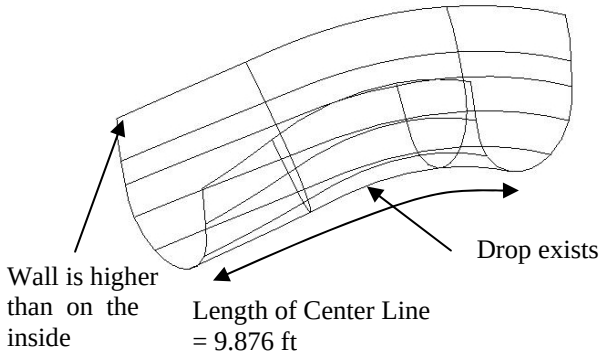
Code Name	Info.	Isometric View of Flume Section
LC45	45º Left-handed	

Table 2.1c Curved Flume Sections (Cont'd)

Code Name	Info.	Isometric View of Flume Section
LC90	90º Left-handed	
LC90D	90º Left-handed with Drop (Slope change)	

RC45, RC90, and *RC90D* are not shown in Figure 2.1c, since they are the exact same flume sections as *LC45, LC90,* and *LC90D*, respectively, except for the turn direction.

The following rules must be followed for connecting flume sections:

A left-hand or right-hand curved flume section cannot be connected to a straight flume section without a connection flume section. The following are examples of valid connections:

(Straight) + (To Left) + (Left-hand Curved) + (From Left) + (Straight),

(Straight) + (To Right) + (Right-hand Curved) + (From Right) + (Straight).

Identical flume sections can be connected directly without a connection flume section. The following are examples of valid connections:

(Straight) + (Straight),

(Left-hand Curved) + (Left-hand Curved),

(Right-hand Curved) + (Right-hand Curved).

As an example, the flow channel shown in Figure 2.1 is composed of five sections in the following order: *S30 + CTL + LC45 + CFL + S58*. Figure 2.2 shows the geometric points of the five flume sections before three-dimensional transformation. Figure 2.3 shows the geometric points of the flume sections after transformation. As shown in Figure 2.3, transformations convert individual flume sections to a well-connected flow channel configuration. Three-dimensional transformations are explained in Appendix A.

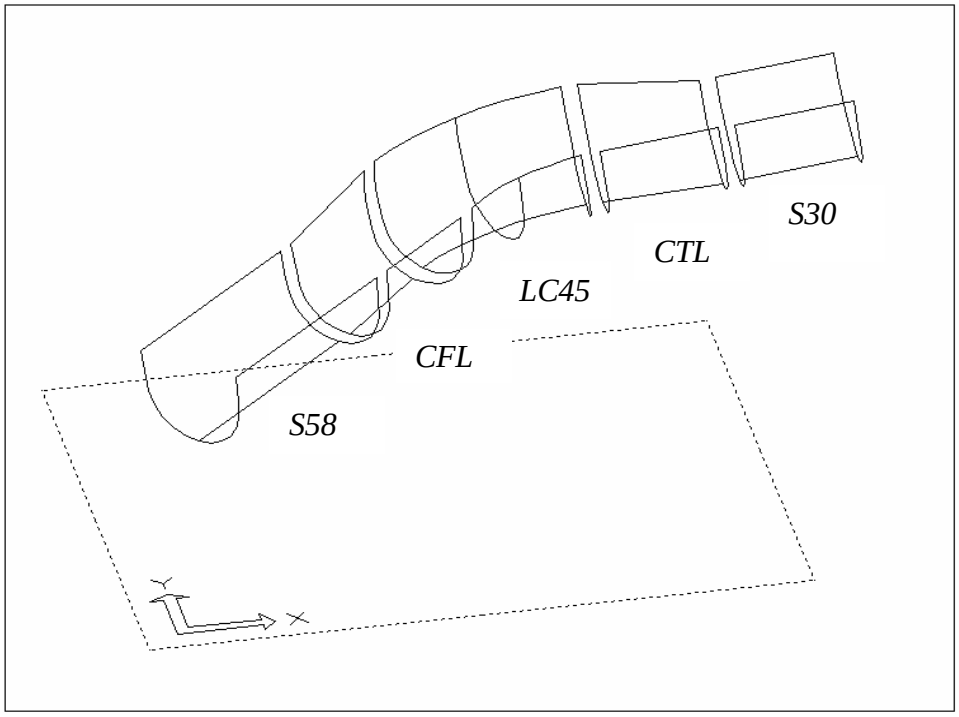


Figure 2.1 Flow Channel Composed of Five Flume Sections

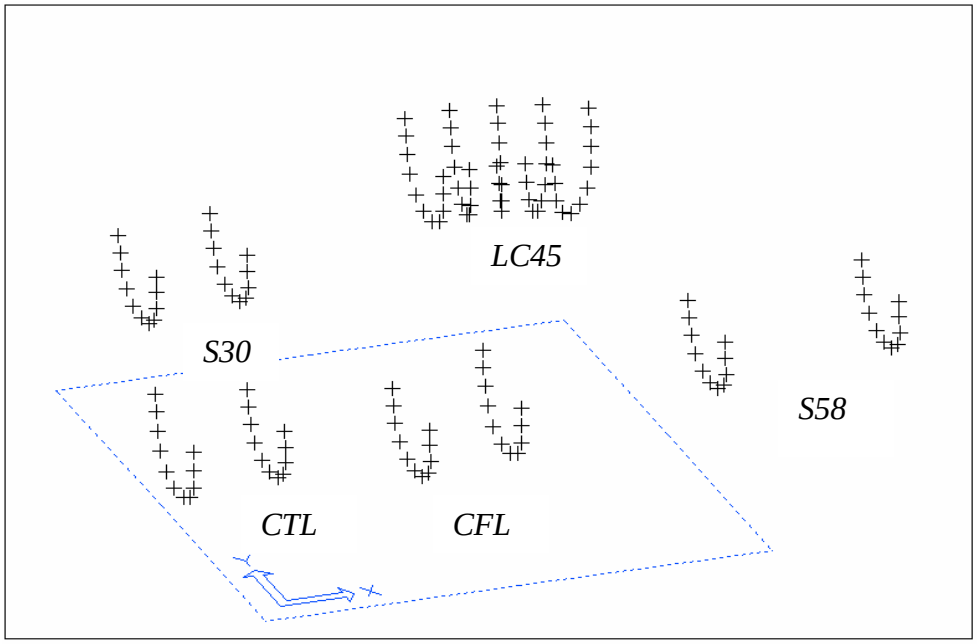


Figure 2.2 Flume Sections Before Transformation

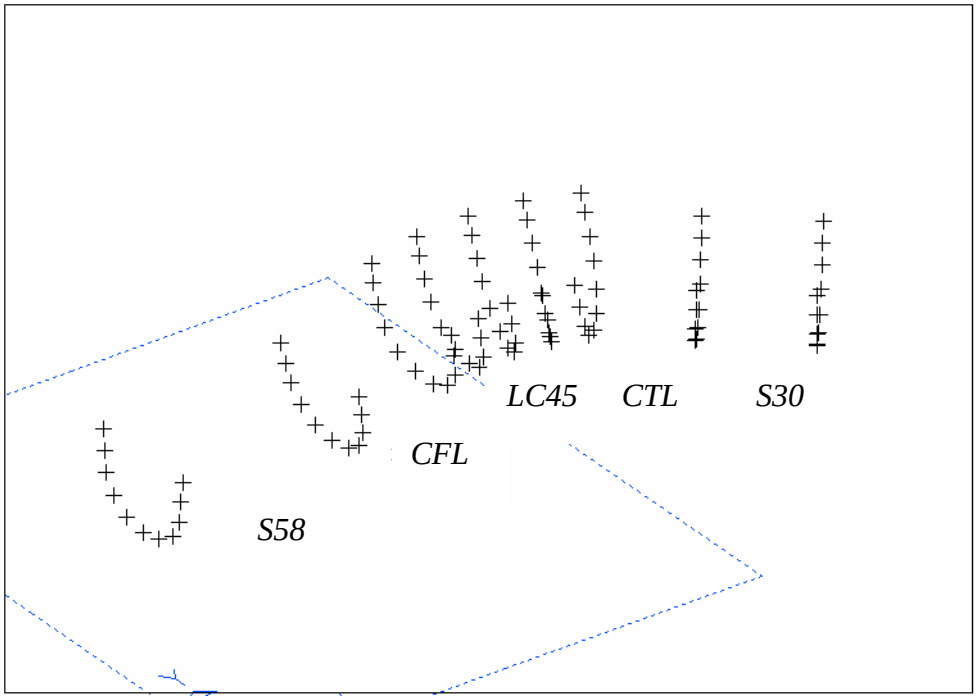


Figure 2.3 Transformed Flume Sections

2.3 General Procedure for Constructing Flume Section Geometry

The procedure starts with fifteen basic flume sections (Table 2.1), described by their corresponding sets of geometric points. Through three-dimensional transformations, the flume sections are connected, again using geometric points. A surface fitting process is conducted to generate bi-cubic B-Spline surfaces. The overall procedure is summerized in Figure 2.4.

An example of two flume sections is presented to illustrate the procedure. The two flume sections employed are *CTL* and *S68*, as shown in Figure 2.5. There are 5×11 and 2×11 geometric points in *CTL* and *S68*, respectively.

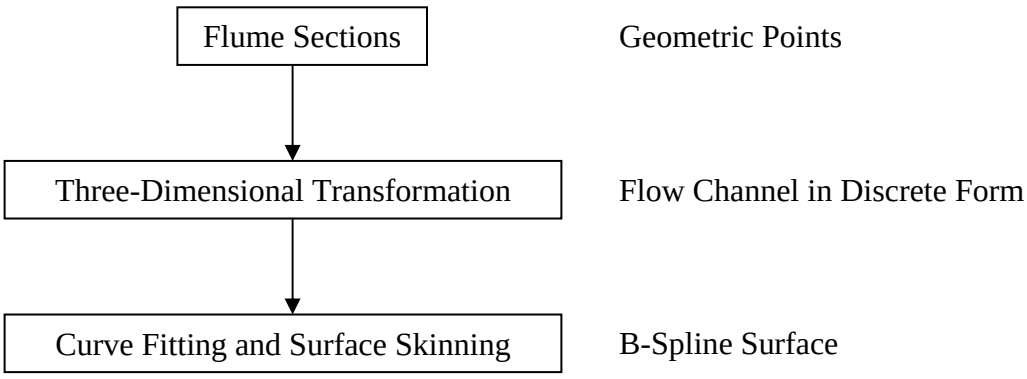


Figure 2.4 General Procedure for Constructing Flow Channel Geometries

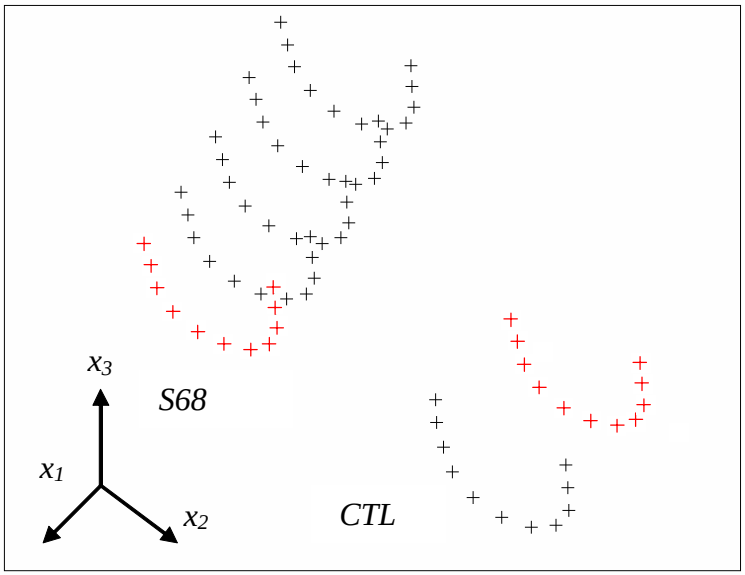


Figure 2.5 Geometric Points of *CTL* and *S68* Flume Sections

In this example, the red geometric points of flume section *S68* are translated and connected with those from *CTL* to form a desired flow channel, as shown in Figure 2.6.

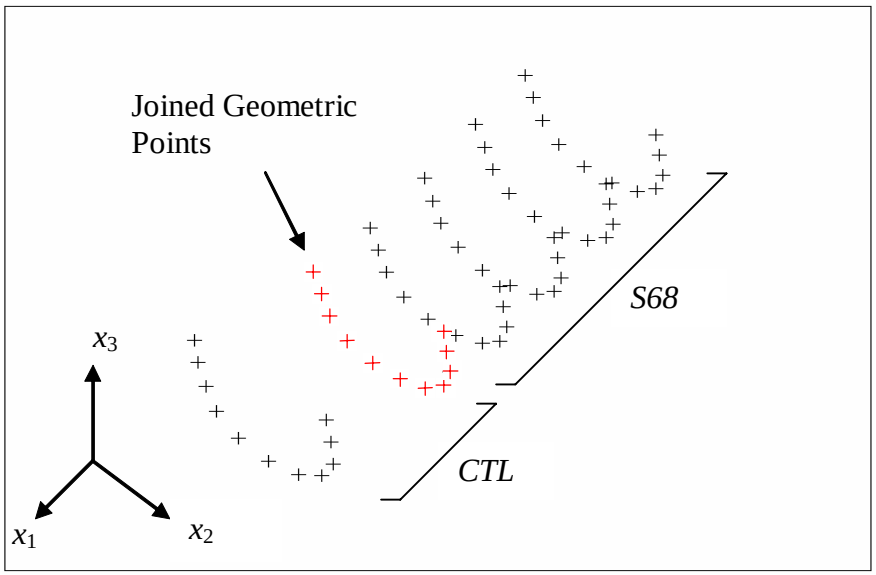


Figure 2.6 Completed Connection of *CTL* and *S68* Flume Sections

Surface fitting is then conducted to generate a bi-cubic parametric B-Spline surface with 13×7 red control points from the 11×6 blue geometric points, as shown in Figure 2.7. In this figure, *u* and *w* are the parametric coordinates of the B-Spline surface. In this example, $(u,w)\in[0,1]\times[0,1.3]$, which means the *u* parameter of the B-Spline surface has a range of [0,1] knot values, and the *w* parameter of the B-Spline surface has a range of [0,1.3] knot values. More detailed information about knot values is given in Section 2.4.

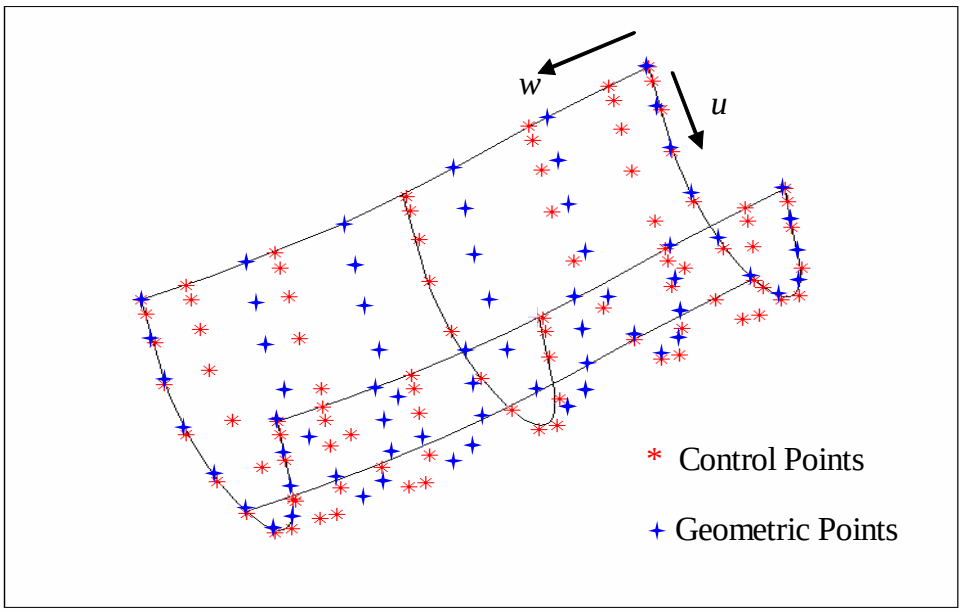


Figure 2.7 B-Spline Surface and Control/Geometric Points of Connected Flume Sections

2.4 Parametric B-Spline Representation

The parametric equation for a spatial curve as shown in Figure 2.8 can be expressed as

$$\boldsymbol{C}(u) = \left[x_1(u) \quad x_2(u) \quad x_3(u) \right] \tag{2.1}$$

where $x_1(u)$, $x_2(u)$, and $x_3(u)$ are functions of the parameter u bounded by $u = \left[u_{min}, u_{max} \right]$. Usually $u_{min} = 0$.

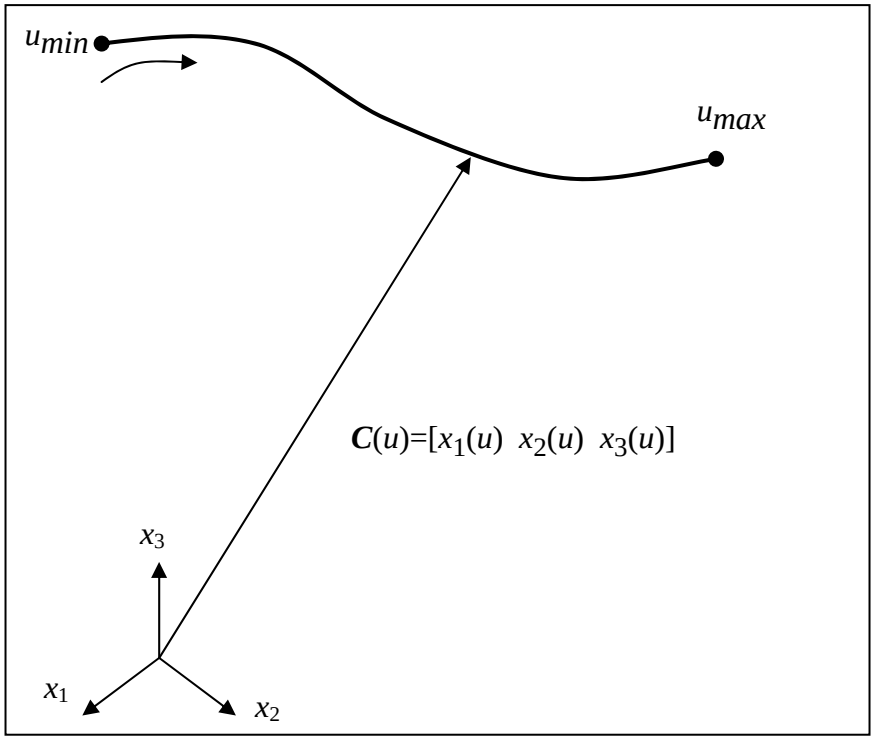


Figure 2.8 Parametric Curve in Space

Similarly, the parametric equation for a spatial surface as shown in Figure 2.9 can be expressed as

`

$$\boldsymbol{Q}(u,w)=[x_1(u,w)\quad x_2(u,w)\quad x_3(u,w)] \tag{2.2}$$

where $x_1(u, w)$, $x_2(u, w)$, and $x_3(u, w)$ are functions of the parameters u and w bounded by $u \in [u_{min}, u_{max}]$ and $w \in [w_{min}, w_{max}]$, respectively.

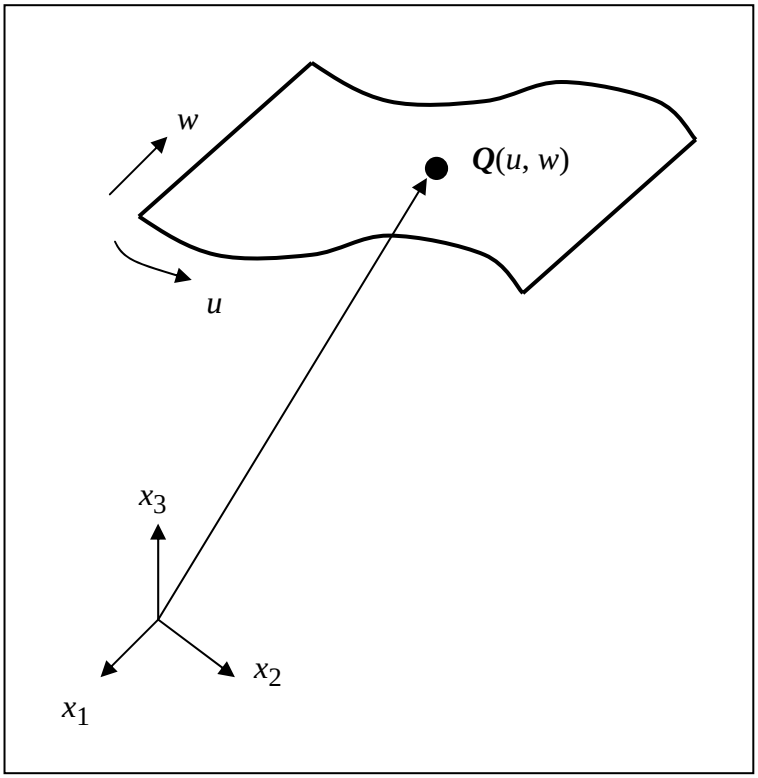


Figure 2.9 Parametric Surface in Space

2.4.1 B-Spline Curve

A parametric B-Spline curve as shown in Figure 2.10 can be defined mathematically as

$$\boldsymbol{C}(u) = \sum_{i=0}^{n} \boldsymbol{B}_i \cdot N_{i,k}(u) \qquad u_{min} \le u \le u_{max} \tag{2.3}$$

where $\boldsymbol{B}_i$ are the control points of the B-Spline curve, and $N_{i,k}(u)$ are basis functions of the curve.

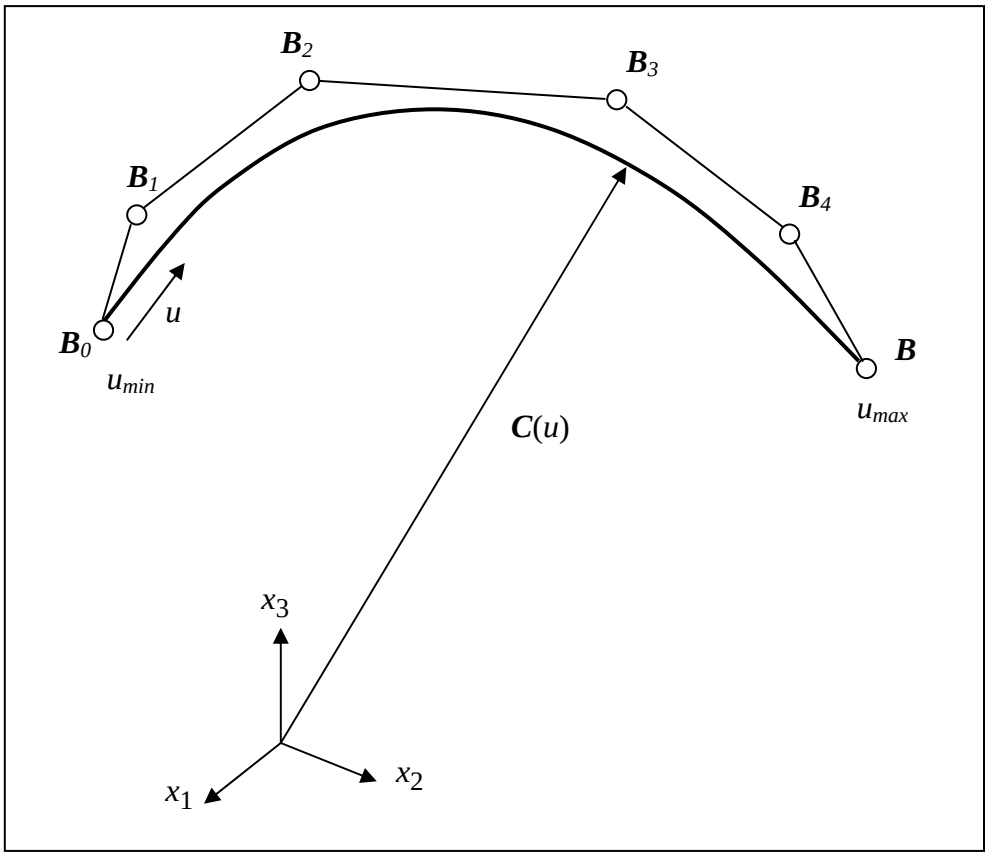


Figure 2.10 Parametric B-Spline Curve with Control Points and Control Polygon

A basis function $N_{i,k}(u)$ is a polynomial function of u, defined recursively by

$$N_{i,k}(u) = \frac{(u - x_i)N_{i,k-1}(u)}{x_{i+k-1} - x_i} + \frac{(x_{i+k} - u)N_{i+1,k-1}(u)}{x_{i+k} - x_{i+1}} \tag{2.4}$$

and

$$N_{i,1}(u) = 1, \quad \text{if } x_i \le u \le x_{i+1}$$
$$= 0, \quad \text{otherwise} \tag{2.5}$$

where k-1 represents the polynomial order of the basis functions with $2 \le k \le n+1$, and x_i's are so-called knots of the basis functions. A set of knots forms a knot vector $\boldsymbol{t}$. For an open B-Spline curve, the knots x_i are defined as

$$\begin{aligned} x_i &= 0 && \text{if} \quad i < k \\ x_i &= i - k + 1 && \text{if} \quad k \le i \le n \\ x_i &= n - k + 2 && \text{if} \quad i > n \end{aligned} \tag{2.6}$$

where $0 \le i \le n + k$.

According to Equation 2.6, a number of knots are repeated at the start and end of the curve for an open B-Spline. A B-Spline curve with nonevenly distributed knots along its parametric coordinate is called a non-uniform B-Spline curve. Usually, integer values are assigned to knots, as defined by Equation 2.6, although this is by no means a fixed requirement. According to Equation 2.6, the parametric coordinate u is

$$0 \le u \le n - k + 2 \tag{2.7}$$

In Equation 2.4, $0/0 \equiv 0$ is assumed.

For a cubic B-Spline curve, i.e., $k = 4$, C^2-continuity is ensured over the entire parametric coordinate u due to the fact that its basis functions $N_{i,k}(u)$ are continuous cubic functions.

The B-Spline curve reveals a local control property since each of its control points $\boldsymbol{B}_i$ is associated with a unique basis function $N_{i,k}(u)$ that governs the shape of the curve locally. When a control point $\boldsymbol{B}_i$ is moved, only a part of the curve segments is affected, thus, the term local control. In addition, when u or $w \neq [0,1]$, e.g. $u \in [0,2]$, there will be more than one curved segment to form the B-Spline curve. The polynomial order and number of control points can be changed independently so that the B-Spline curve fits the given geometric points properly. These properties are desirable for representing spatial curves and for supporting curve fitting.

2.4.2 B-Spline Surface

A B-Spline surface is represented mathematically by

$$\boldsymbol{Q}(u,w) = \sum_{i=0}^{n}\sum_{j=0}^{m} \boldsymbol{B}_{ij}\ N_{i,k}(u)\, M_{j,\ell}(w) \tag{2.8}$$

where $\boldsymbol{B}_{ij}$ are $(n+1)\times(m+1)$ control points, and $N_{i,k}(u)$ and $M_{i,\ell}(w)$ are basis functions of the B-Spline surface in the u and w parametric coordinates, respectively. Note that the functions $N_{i,k}(u)$ and $M_{i,\ell}(w)$ are identical to those of the B-Spline curve. In addition, a bi-cubic B-Spline surface is C^2-continuous, similar to the B-Spline curve.

2.5 Curve Fitting and Surface Skinning

The basic ideas for the proposed methodology of constructing flow channel geometries are improved least squares curves fitting and surface skinning, using B-Spline curves and surfaces, respectively. The improvement of the least squares fitting consists of (i) a robust knot vector construction that guarantees existence of a set of control points, and (ii) control of the curve fitting error with a minimum number of control points. These curve fitting and surface skinning methods were first proposed by DeBoor [16].

2.5.1 Least Squares Fitting Using B-Spline Curves

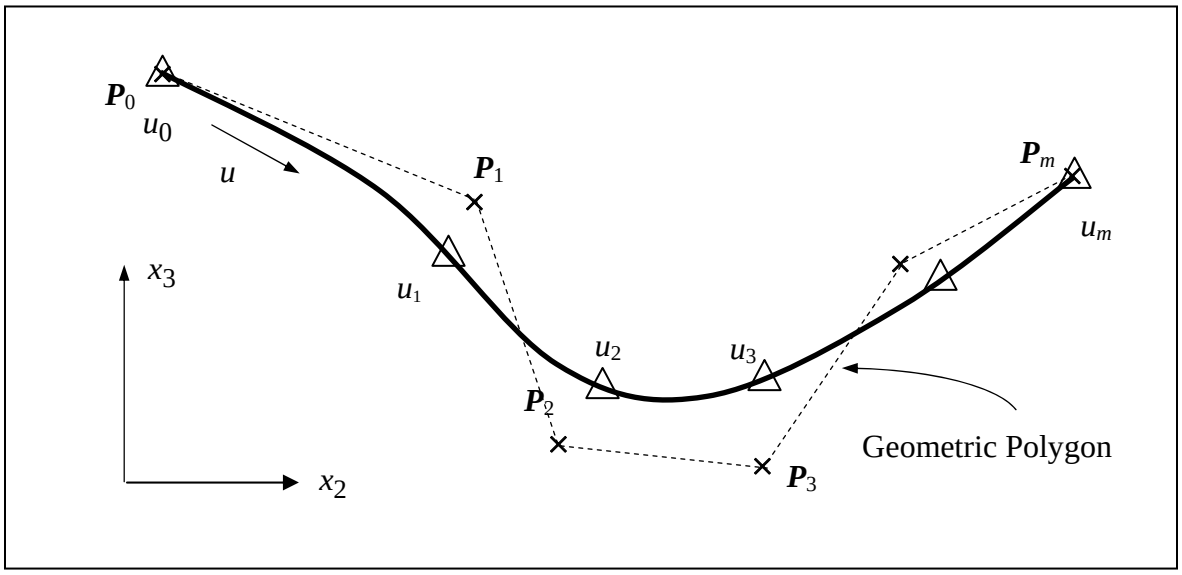
This method assumes that a set of geometric points describing each of the section contours of the flow channel are available. These points reside on serial sections that are normal to the centerline (along the longitudinal direction) of the flow channel. Using least squares fitting for geometric points on a plane, the best approximation curve is obtained by minimizing the distance sum f between the curve and the geometric points. The distance sum f is defined as

$$\mathrm{f} = \sum_{j=0}^{r} \left\| \boldsymbol{P}_j - \boldsymbol{C}(u_j) \right\|^2 \tag{2.9}$$

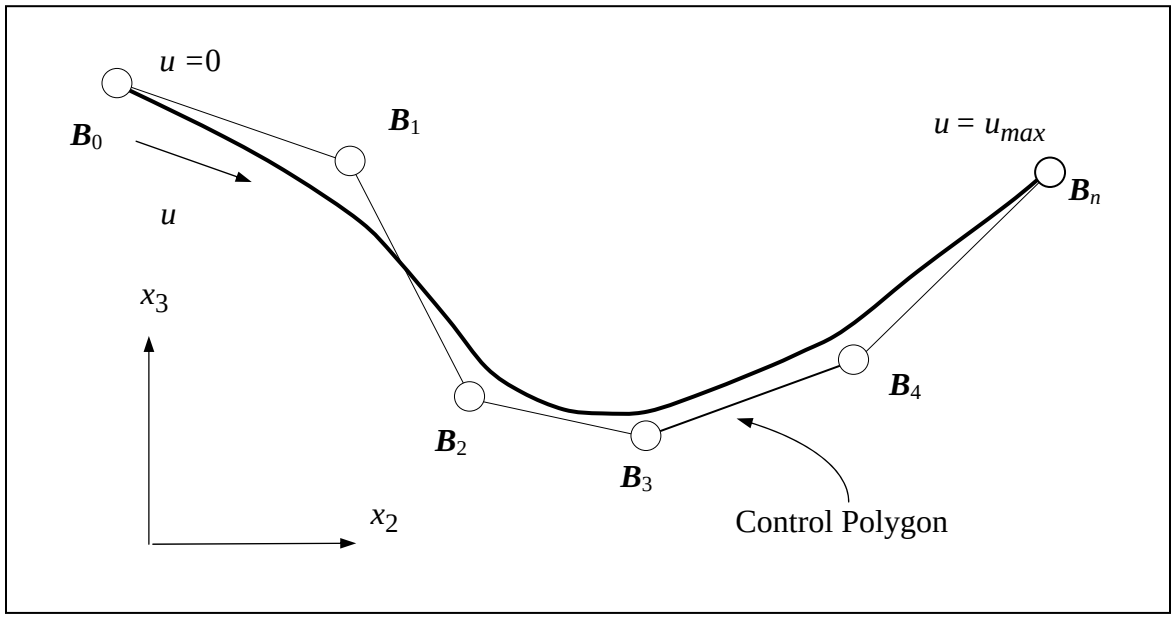
where $\boldsymbol{P}_j$ is the position vector of the j^{th} geometric point and r+1 is the total number of geometric points. In addition, $\boldsymbol{x}(u_j) = [x_1(u_j), x_2(u_j), x_3(u_j)]$ is the position vector of the fitting B-Spline curve at u_j, where u is the parametric coordinate of the curve. Note that u_j

is defined by the length ratio of the polygon formed by the geometric points $\boldsymbol{P}_j$, as illustrated in Figure 2.15a. Values of u_j are determined by

$$u_0 = 0,$$
$$u_j = (n+1)\left\{\sum_{k=0}^{j-1}\left|\boldsymbol{P}_{(k+1)\bmod(r+1)} - \boldsymbol{P}_k\right| / \sum_{k=0}^{m}\left|\boldsymbol{P}_{(k+1)\bmod(r+1)} - \boldsymbol{P}_k\right|\right\}, \quad j = 1,\ldots,r \tag{2.10}$$



(a) Curve Fitting for Geometric Points $\boldsymbol{P}_j$



(b) B-Spline Curve with Control Points $\boldsymbol{B}_i$

Figure 2.11 B-Spline Curve Fitting

The u_j can be further adjusted to reduce the curve fitting error [17]. In order to minimize f, the derivative of f with respect to the n+1 control points $\boldsymbol{B}_i$ is set to zero. For simplicity, considering only the ℓ^{th} control point, one has

$$\frac{df}{d\boldsymbol{B}_\ell} = \sum_{j=0}^{m} \left\| -2\boldsymbol{P}_j \sum_{i=0}^{n} N_{i,k}(u_j) + 2 \sum_{i=0}^{n} N_{i,k}(u_j)\left(\sum_{i=0}^{n} N_{i,k}(u_j)\boldsymbol{B}_\ell \right) \right\| = 0 \qquad (2.11)$$

Let ℓ = 0, …, n. Then, the above expression can be rewritten in matrix form as $\boldsymbol{N}^T\boldsymbol{N}\,\boldsymbol{B} = \boldsymbol{N}^T\boldsymbol{P}$. According to [6], $\boldsymbol{N}^T\boldsymbol{N}$ is invertible if $N_{i,k}(u_j) \neq 0$. This is true if and only if $x_{i-k+1} < u_j < x_{i+1}$, for i = 0, …, n, and j = 0, …, r. This implies that there must exist at least one u_j

in at least one knot span (e.g., $[x_{i-1}, x_i]$) so that $N_{i,k}(u_j) \neq 0$ for all basis functions. This requirement can be achieved by adjusting the knot values of the basis functions. As shown in the computational algorithm listed in Figure 2.12, the polynomial order and error of the approximate curve can be controlled.

1. Collect and sort geometric points
2. Smooth geometric points by averaging their positions with the two previous and two following nodes (optional)
3. Specify desired error bound ε
4. Determine polynomial order (if cubic B-Spline curve is employed, $k = 4$, and the curve is C^2-continuous)
5. Determine number of control points, $n+1$, as small as possible
6. Construct B-Spline curve, reduce fitting error by adjusting u_j values, calculate $e = f/(m+1)$, if $e < \varepsilon$, acquire control points $\boldsymbol{B}_i$ to construct B-Spline curve
7. Otherwise, increase k or n, repeat steps 4 to 6

Figure 2.12 Computational Algorithm for Curve Fitting

This curve fitting method allows for minimizing the number of control points, which avoids the difficulty of having a large number of design variables for design of the flow channel. The output of the curve fitting is a set of control points and basis functions that describe the smoothed section contour.

2.5.2 Surface Skinning

The fitting B-Spline curves discussed above are then connected across sections to form an open B-Spline surface, as shown in Figure 2.13, using the surface skinning technique. Note that, in this process, the number of control points of the B-Spline curves

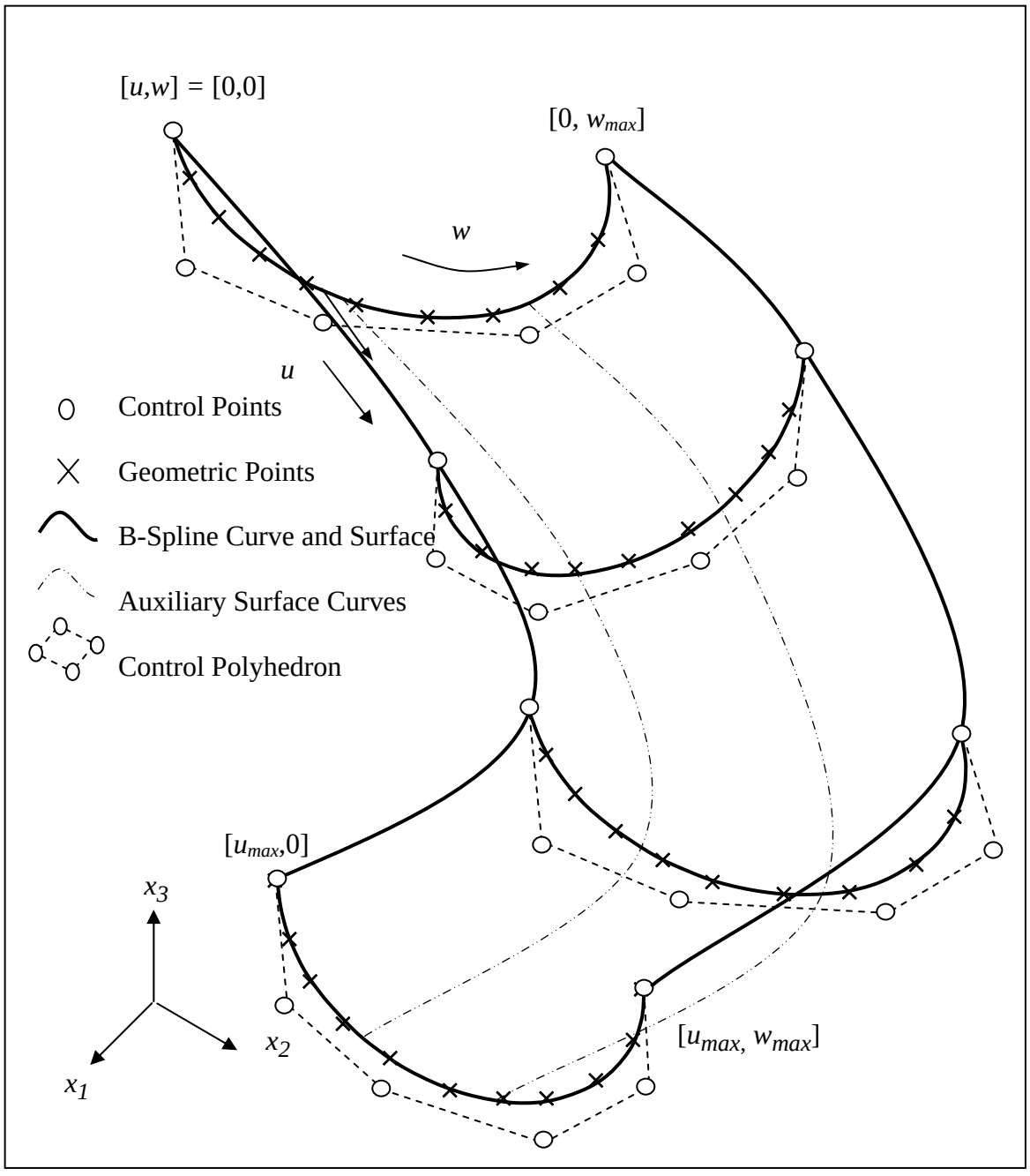


Figure 2.13 Spline Surface Skinning

must be kept identical across sections. In addition, the polynomial order of the basis functions and the knot values of the B-Spline curves must be identical on all sections. The control points are connected to their corresponding points across the sections, as shown in Figure 2.13, to form a control polyhedron. The enclosed B-Spline surface is then constructed by

$$\boldsymbol{Q}(u,w) = \sum_{i=0}^{n} \sum_{j=0}^{m} \boldsymbol{B}_{ij} N_{i,k}(u) M_{j,\ell}(w) \tag{2.12}$$

where n+1 and m+1 are the numbers of control points in the u and w parametric directions, respectively; and k-1 and l-1 are the polynomial orders of the basis functions $N_{i,k}(u)$ and $M_{j,\ell}(w)$, respectively. Note that the B-Spline surface constructed is C^2-continuous in the u and w parametric directions, if cubic basis functions are assumed. The control points and basis functions of the B-Spline surface can be imported into CAD tools to support visualization and other purposes, such as manufacturing of a flow channel. Note that, in this research, curve fitting and surface skinning are performed in *I-DEAS*® using the "sd tes ex ge" function.

2.6 Flume Section Configuration Examples

There were four real-world flow channel examples employed in this research to demonstrate the curve fitting and surface skinning methods. These examples are the Parker, McAllen, SAFbase, and Bloomfield configurations provided by the *Miracle Recreational Equipment, Company*. In this section, only the Parker configuration will be presented. The rest can be found in Reference [11].

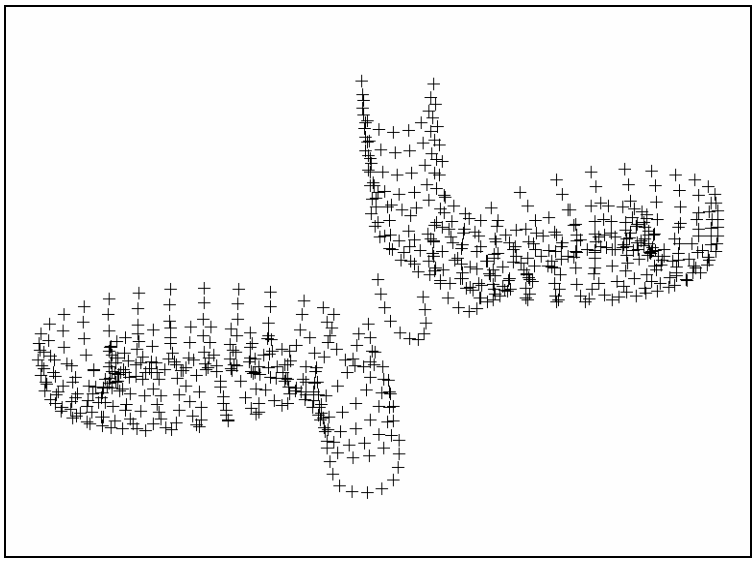


Figure 2.14 Geometric Points of Parker Water Slide after Three-Dimensional Transformation

The size of the water slide is W×L×H: 30.2'×83.9'×93'. Geometric points of the Parker configuration are shown in Figure 2.14. Note that this configuration is composed of the following flume sections:

S68+CTL+LC45+LC90+LC90+LC90D+CFL+S30+CTR+RC45+Rc90+RC90+RC90D RC90D+CFR.

After transforming the flume sections, there are 66×11 geometric points, as shown in Figure 2.14.

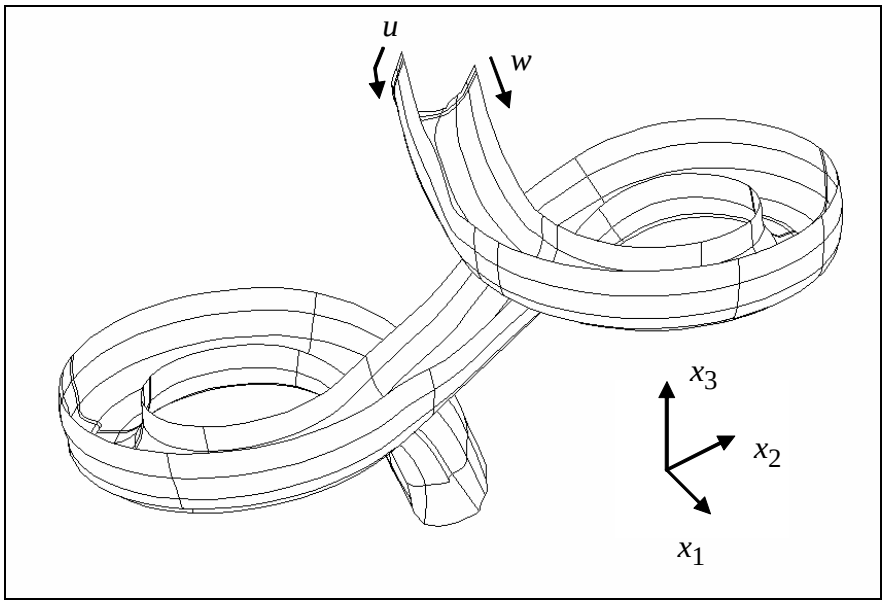


Figure 2.15 B-Spline Surface of Parker Water Slide

A bi-cubic open B-Spline surface that fits the geometric points given in Figure 2.14 is shown in Figure 2.15. Note that there are 68×13 control points in the B-Spline surface as shown in Figure 2.16. In addition, $[u, w] \in [0,1] \times [0, 11.2369]$, which means the *u* parameter of the B-Spline surface has a range of [0,1] knot values, and the *w* parameter of the B-Spline surface has a range of [0,11.2369] knot values.

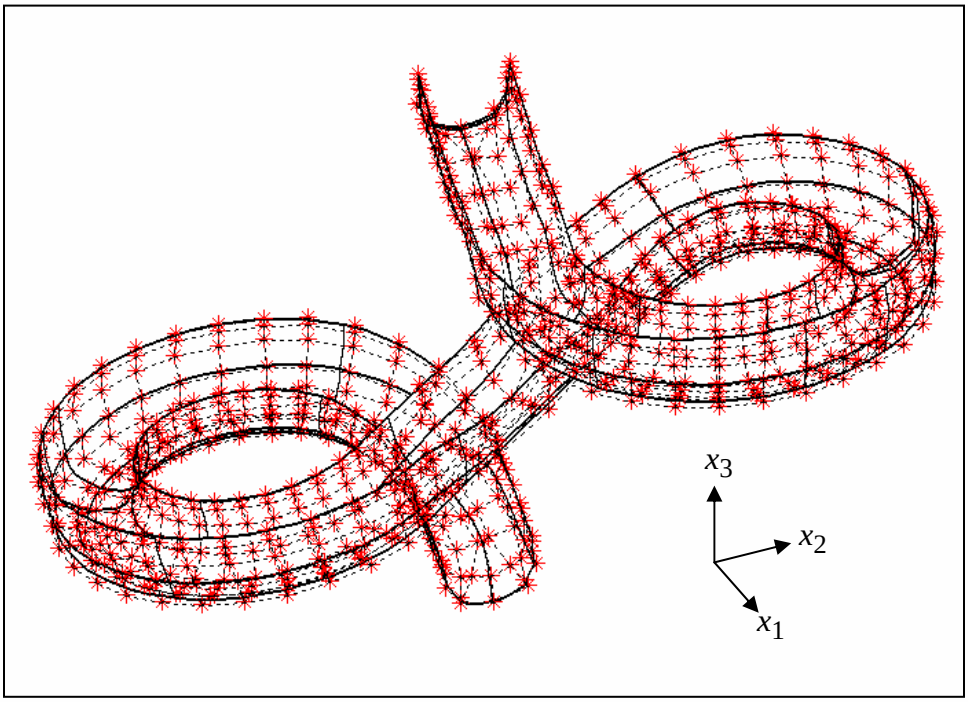


Figure 2.16 Control Points and Control Polygon of Parker Water Slide

CHAPTER 3

CONSTRUCTION OF CAD-BASED FLUME SECTION GEOMETRY

3.1 Introduction

In this chapter, the construction of CAD-based flume section configurations is presented. In Section 3.2, a mathematical representation of basic flume sections is introduced. In Section 3.4, continuity requirements and design parameterization are presented. The chapter closes with two numerical examples in Section 3.5.

3.2 Mathematic Representation of Basic Flume Sections

Three basic flume sections, straight, arced, and cubic-curve, are developed to serve as the building blocks for composing flow channel configurations. The geometries of all three flume sections are expressed in parametric surface form in terms of the parametric coordinates u and w, using CAD geometric dimensions. The general equations of a parametric surface can be expressed as

$$\boldsymbol{X}(u,w) = [X_1(u,w),\ X_2(u,w),\ X_3(u,w)]^T \tag{3.1}$$

where $X_i(u,w)$ is the i^{th} coordinate of any given point on the surface with prescribed parameters (u,w).

3.2.1 Equations of Straight Flume Section

The mathematical representation of a straight flume section as shown in Figure 3.1 can be given as

$$\boldsymbol{X}(u,w) = \boldsymbol{X}_0 \; + \; \boldsymbol{T}(\theta)\, \boldsymbol{x}(u,w) = \begin{bmatrix} X_{1_0} \\ X_{2_0} \\ X_{3_0} \end{bmatrix} + \begin{bmatrix} \cos\theta & \sin\theta & 0 \\ -\sin\theta & \cos\theta & 0 \\ 0 & 0 & 1 \end{bmatrix} \begin{bmatrix} x_1(u,w) \\ x_2(u,w) \\ x_3(u,w) \end{bmatrix} \tag{3.2}$$

where $\boldsymbol{T}(\theta)$ is the rotation matrix that orients the flume section by an orientation angle θ with respect to the X_3 axis, X_{i0} is the location of the local coordinate system of the flume section in the flow channel configuration, and $\boldsymbol{x}(u,w)$ is the surface function of the flume section referring to its local coordinate system. For a straight flume section,

$$\boldsymbol{x}(u,w) = [r \cos u \qquad \ell w \qquad r\,(1 + \sin u) - h\, w]^T,\ u \in [-\pi,\, 0]\ ,\ w \in [0,\, 1] \tag{3.3}$$

Note that, in Equation 3.3, h and l are the height and length of the straight flume section, respectively; r is the radius of the semicircular cross section of the flume section; and u and w are the parametric coordinates along the circumferential and longitudinal directions of the flume section, respectively.

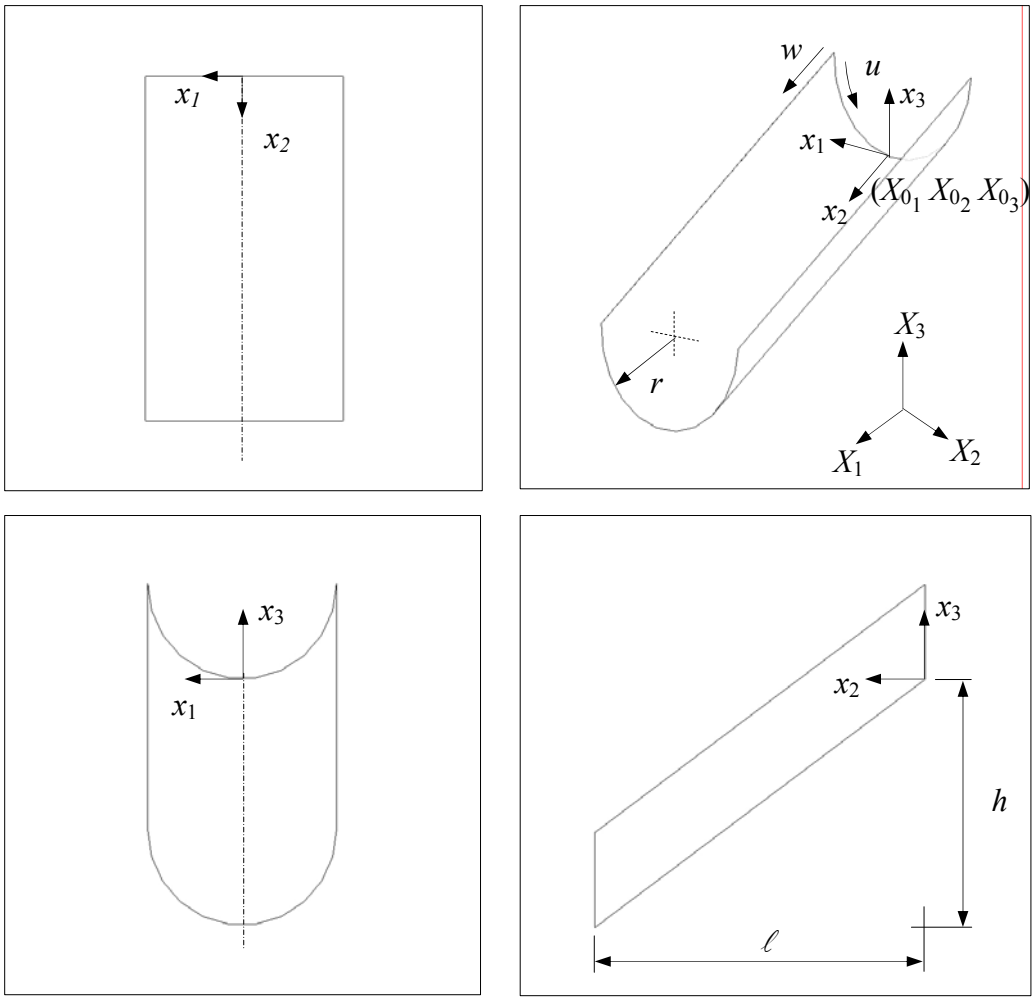


Figure 3.1 Straight Flume Section

3.2.2 Equations of Arced Flume Section

The mathematical representation of an arced flume section as shown in Figure 3.2 can be given using Equation 3.2, where

$$\boldsymbol{x}(u,w) = [\pm \cos w\phi\,(R + r\cos u) \mp R \qquad \sin w\phi\,(R + r\cos u) \qquad r(1 + \sin u) - h\,w]^T,$$

$$u \in [-\pi, 0],\ w \in [0,1] \tag{3.4}$$

Note that, in Equation 3.4, R is the radius of the arc of the flume section, and ϕ is the rotation angle measured about the X_3-axis. The signs in the first entry of Equation 3.4 are determined by the sign of the rotation angle ϕ of the flume section. An example of the arced flume section with $\phi = 90^o$ is shown in Figure 3.2.

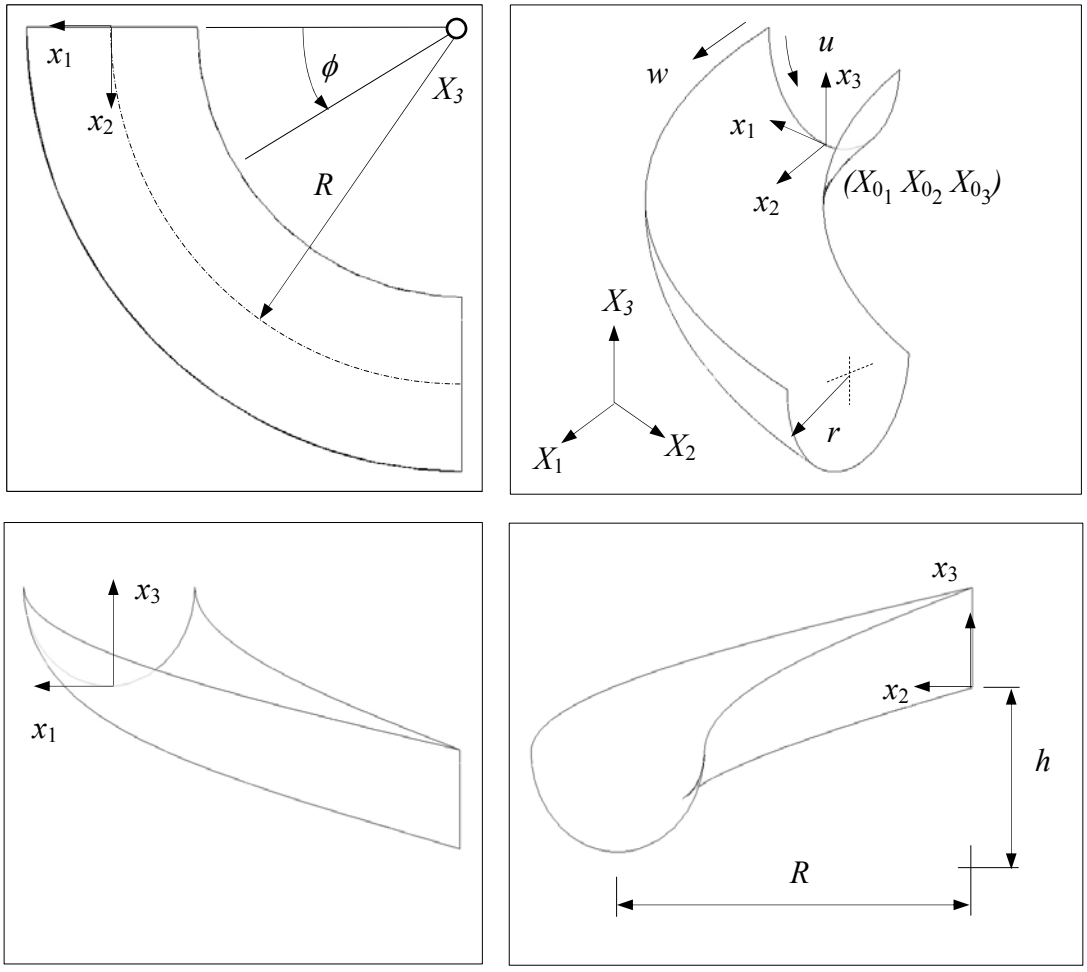


Figure 3.2 Arced Flume Section

3.2.3 Equations of Cubic-Curve Flume Section

A cubic-curve flume section is created by sweeping a semi-circle (cross sectional shape of the flume section) through a planar or spatial cubic curve. A spatial cubic curve can be expressed by its end points and tangent vectors at the end points, as shown in Figure 3.3.

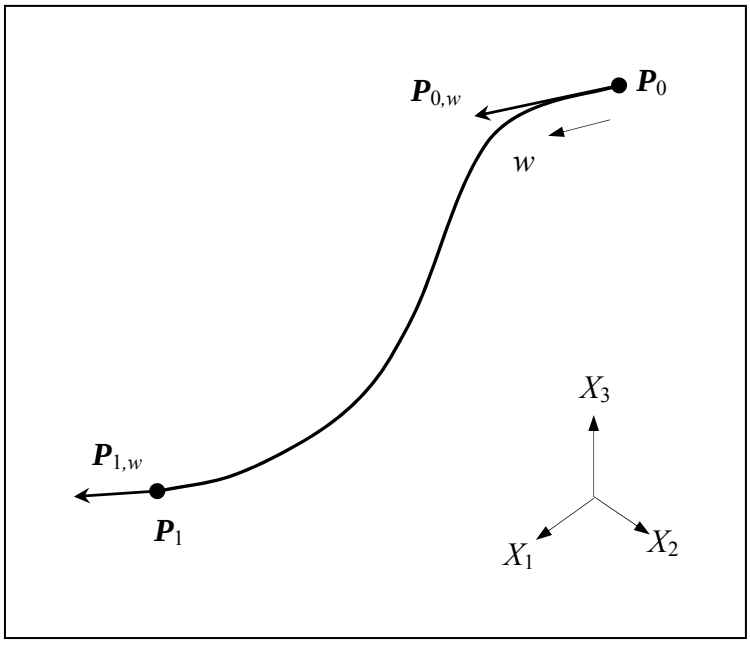


Figure 3.3 Spatial Cubic Curve

The parametric equations of the cubic curve are

$$\boldsymbol{P}(w) = \boldsymbol{W}^T \boldsymbol{M}\, \boldsymbol{G} = \begin{bmatrix} w^3 & w^2 & w & 1 \end{bmatrix} \begin{bmatrix} 2 & -2 & 1 & 1 \\ -3 & 3 & -2 & -1 \\ 0 & 0 & 1 & 0 \\ 1 & 0 & 0 & 0 \end{bmatrix} \begin{bmatrix} \boldsymbol{P}_0 \\ \boldsymbol{P}_1 \\ \boldsymbol{P}_{0,w} \\ \boldsymbol{P}_{1,w} \end{bmatrix}, \; w \in [0, 1] \tag{3.5}$$

where $\boldsymbol{M}$ is a constant 4×4 matrix, $\boldsymbol{P}_0$ and $\boldsymbol{P}_1$ are the start and end points of the curve, respectively, and $\boldsymbol{P}_{0,w}$ and $\boldsymbol{P}_{1,w}$ are the tangent vectors at the corresponding points.

With Equation 3.5, the mathematical representation of a cubic curve flume section as shown in Figure 3.4 can be given as

$$\boldsymbol{X}(u,w) = \boldsymbol{T}(\theta)\,\boldsymbol{x}(u) + \boldsymbol{P}(w) \tag{3.6}$$

where

$$\boldsymbol{x}(u) = [r\ cos\ u,\ \ 0,\ \ r\ (1 + sin\ u)]^T,\ \ u \in [-\pi,\ 0] \tag{3.7}$$

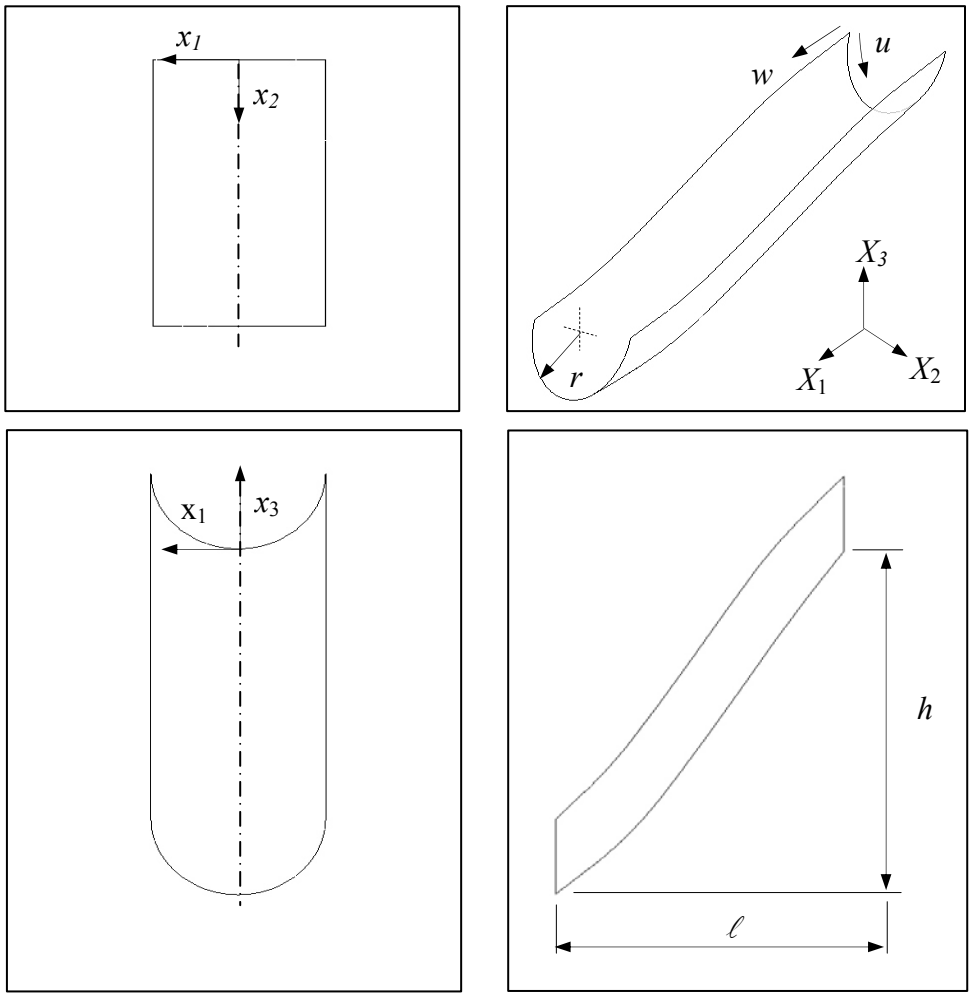


Figure 3.4 Cubic-Curve Flume Section

3.3 Continuity Requirements and Design Parameterization

From Equations 3.2, 3.4, and 3.6, $\boldsymbol{X}(u,w)$ must be at least second and third order differentiable with respect to u and w, respectively. It is obvious that this requirement is satisfied within individual flume sections. However, when joining two flume sections for, e.g., a waterslide configuration, the continuity requirements must be satisfied. Note that all continuity requirements are satisfied in the circumferential direction; i.e., in u-direction (referring to Equations. 3.3, 3.4, and 3.7), as long as the flume sections share an identical cross section radius r. However, in order to ensure that the geometry of the configuration is sufficiently differentiable, the first and second order derivatives of $\boldsymbol{X}(u,w)$ with respect to w must be continuous. Therefore, at the junction of two flume sections, for example flume sections A and B shown in Figure 3.5, the following conditions must hold,

$$\boldsymbol{X}^{A}(u,w)\Big|_{w_A=1} = \boldsymbol{X}^{B}(u,w)\Big|_{w_B=0} \tag{3.8a}$$

$$\frac{\partial \boldsymbol{X}^{A}(u,w)}{\partial w}\Bigg|_{w_A=1} = \frac{\partial \boldsymbol{X}^{B}(u,w)}{\partial w}\Bigg|_{w_B=0} \tag{3.8b}$$

$$\frac{\partial^2 \boldsymbol{X}^{A}(u,w)}{\partial w^2}\Bigg|_{w_A=1} = \frac{\partial^2 \boldsymbol{X}^{B}(u,w)}{\partial w^2}\Bigg|_{w_B=0} \tag{3.8c}$$

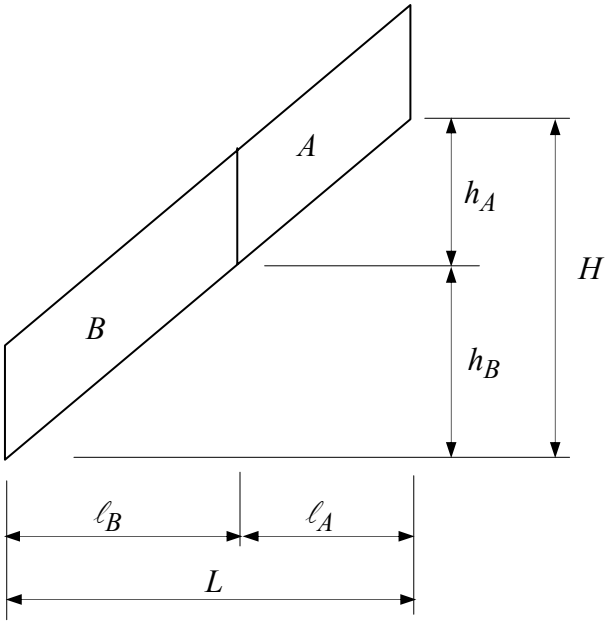
where $w_A = 1$ and $w_B = 0$ specify the end and start of the flume sections A and B, respectively. The continuity requirements not only restrict how flume sections can be joined but also dictate the changes of the configuration, hence, the design parameterization of the flow channel configurations. Note that not all flume sections can

be connected. Only straight-straight, arced-arced, straight-cubic, and cubic-straight sections can be connected under specific situations. Cubic-arced connections cannot be made due to the C^2-continuity problem. In addition, the dimension variables must be changed in certain ways in order to satisfy specific continuity requirements. A detailed discussion is given in Appendix B.

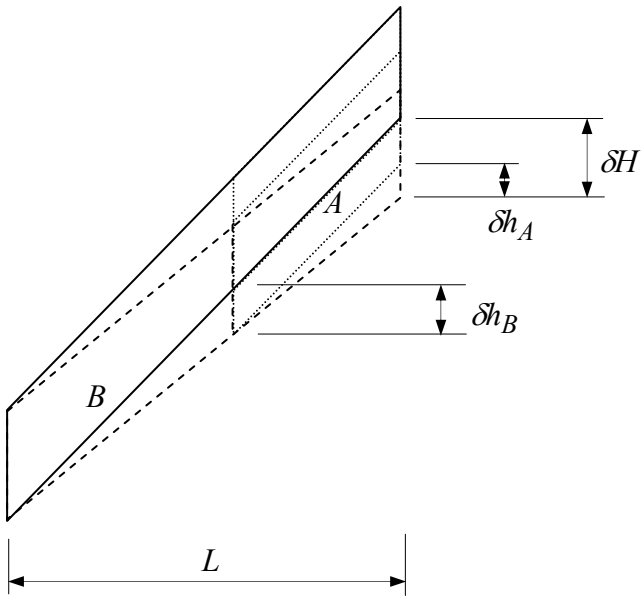
Due to the continuity requirements, two co-planar straight flume sections can be connected only when they share the same slope along the *w*-direction, as illustrated in Figure 3.5. When the height of the configuration is changed (δH), the change must be distributed to each section proportionally (δh_A and δh_B) in order to maintain the same slope along the *w*-direction. If the height of only one flume section is changed, each flume section will have a different slope and the continuity problem will arise. The mathematical arguments regarding continuity requirements can be seen in Appendix B.

Only two identical-direction (left-handed or right-handed) arced flume sections can be connected. When the height of the configuration is changed, the change must be distributed to each section proportionally in order to satisfy the continuity requirements along the *w*-direction. This requirement also can be seen in Appendix B. For both straight-cubic and cubic-straight connections, the slopes must be identical at the flume junction, and the tangent vectors of the cubic flume section must satisfy certain requirements, as described in Appendix B. For a straight-cubic-straight connection, more restrictions are imposed on the cubic curve. As a result, the slopes at both ends of the cubic curve must be identical, and the two straight flume sections must be in parallel. More detailed information is given in Appendix B.

Note that, when a dimension, e.g., the height, of a straight-cubic-straight configuration is changed, multiple conditions must be considered. As illustrated in Figure 3.6b, $\boldsymbol{P}_0$ can be changed with both straight flume sections kept unchanged. In addition, the slope of the straight flume sections can be adjusted according to an overall height change without changing the height of the cubic flume section, as illustrated in Figure 3.6c. Note that, in this case, $\boldsymbol{P}_{0,w}$ and $\boldsymbol{P}_{1,w}$ must be adjusted accordingly. Any combinations of the two cases are possible, as long as the continuity conditions are satisfied, as illustrated in Figure 3.6d. Note that C^1- and/or C^2-continuity cannot not be maintained when an arced flume section is connected to a straight or a cubic flume section. More detailed explanations are given in Appendix B.

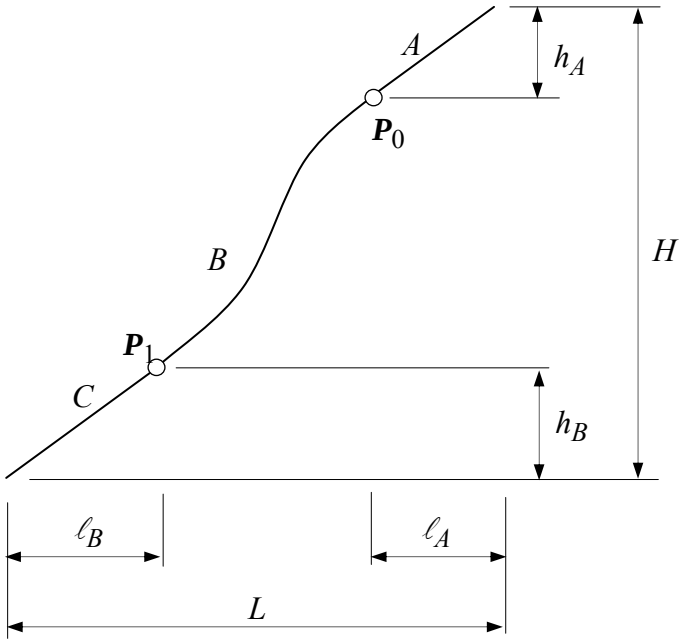


(a) Same Slope Along the *w*-Direction

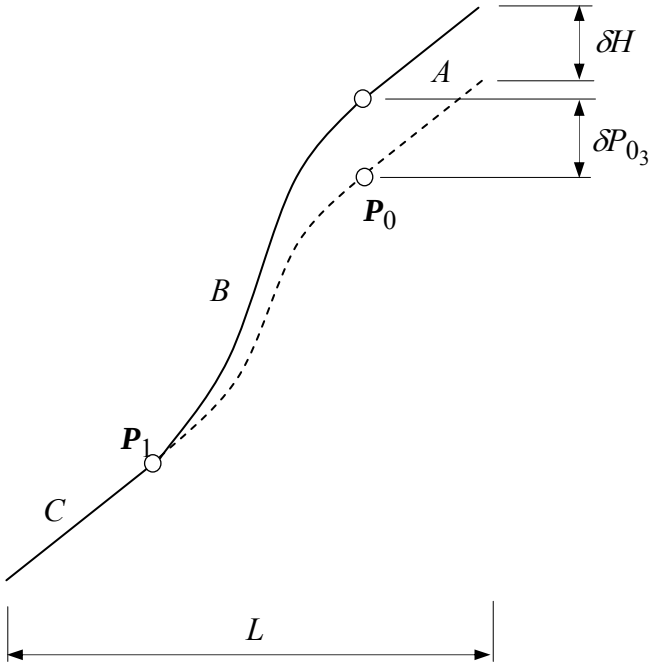


(b) Design Change in Height

Figure 3.5 Configuration of Two Straight Flume Sections

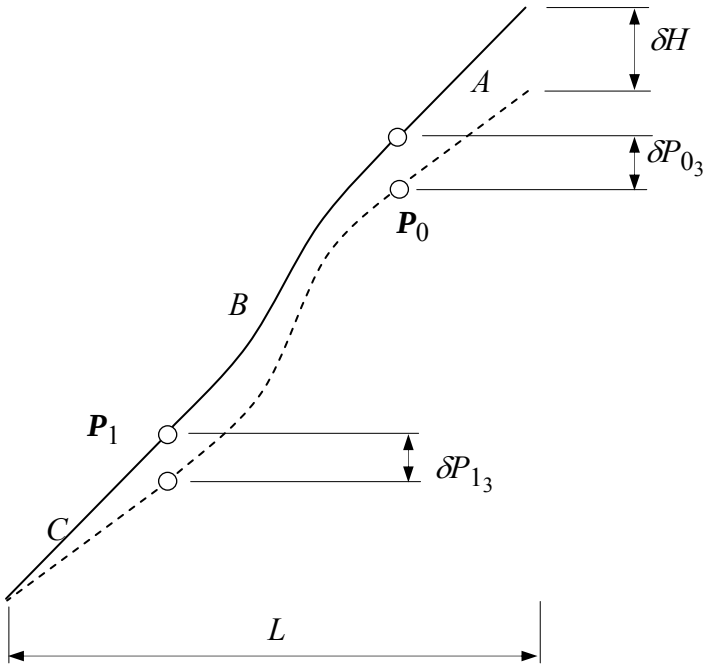


(a) Original Unchanged Configurations

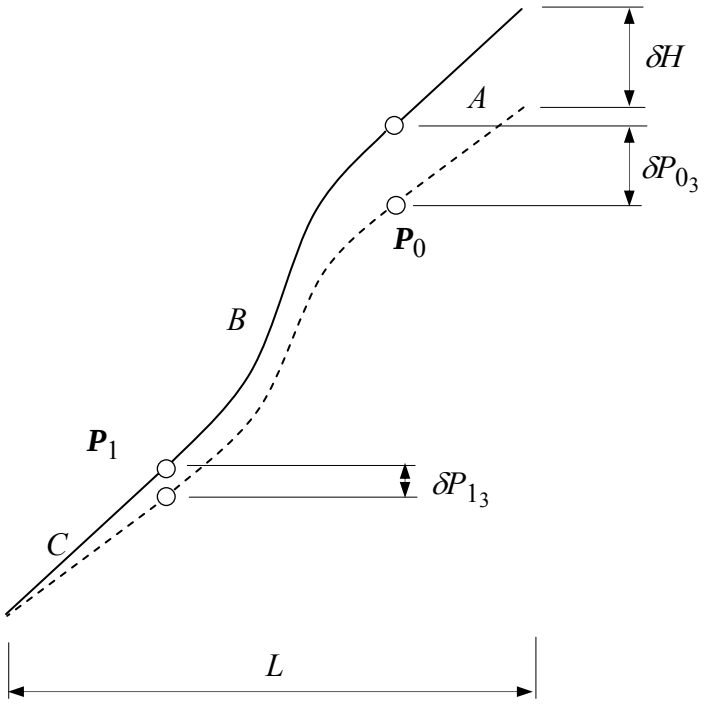


(b) Case 1: $\delta H = \delta P_{0_3}$ and $\delta P_{1_3} = 0$

Figure 3.6 Configuration of Straight-Cubic-Straight Flume Configuration



(c) Case 2: $\delta P_{0_3} = \delta P_{1_3}$



(d) Case 3: $\delta P_{0_3} \neq \delta P_{1_3} \neq 0$

Figure 3.6 Configuration of Straight-Cubic-Straight Flume Configuration (Cont'd)

CHAPTER 4

MOTION ANALYSIS ALONG FLUME SECTIONS

4.1 Introduction

This chapter describes the theory used to compute the particle path, velocity, and acceleration in a flow channel with and without friction forces (see also Reference 11). Lagrange's equations of motion are presented in Section 4.2, and the formulation of the coupled ordinary differential equations for motion analysis is presented in Section 4.3. Numerical methods are explained in Section 4.4.

4.2 Lagrange's Equations of Motion

According to Hamilton's Principle,

$$\int_{t_0}^{t_1} (\delta T + \delta W) dt = 0 \tag{4.1}$$

where δT is the variation of the kinetic energy and δW is the virtual work of the non-inertial forces. For a conservative system, $\delta W = -\delta V$, where V is the potential energy of the system. Consequently, Equation 4.1 may be written in the following form:

$$\delta A = 0, \quad A = \int_0^{t_1} L dt, \quad L = T - V \tag{4.2}$$

The quantity L is known as the "Lagrangian". Hamilton's Principle yields the conclusion that the Euler-Lagrange equations applied to the Lagrangian are the differential equations of motion. If the system has coordinates x_1, x_2, x_3, the differential equations of motion are accordingly

$$\frac{d}{dt}\frac{\partial L}{\partial \dot{x}_i} - \frac{\partial L}{\partial x_i} = 0 \qquad i=1,3 \tag{4.3}$$

Equations 4.3 are known as Lagrange's equations of motion.

If the coordinates of a mechanical system receive infinitesimal virtual displacements δx_i, the virtual work of all the forces that act on the system is represented by a linear differential expression

$$\delta W = \sum_{i=1}^{n} Q_i \delta x_i \tag{4.4}$$

where Q_i are the components of the generalized forces and n is the number of coordinate components. The components of Q_i are functions of (x_i, t). The variations δx_i are arbitrary functions of t.

Since the kinetic energy T is a function of $(x_i, \dot{x}_i, t)$, the theory of the first variation yields

$$\int_{t_0}^{t_1} \delta T dt = \int_{t_0}^{t_1} \sum_{i=1}^{n} \left(\frac{\partial T}{\partial x_i} - \frac{d}{dt}\frac{\partial T}{\partial \dot{x}_i} \right) \delta x_i dt \tag{4.5}$$

Consequently, Hamilton's Principle, Equation 4.1, yields

$$\int_{t_0}^{t_1} \sum_{i=1}^{n} \left(\frac{\partial T}{\partial x_i} - \frac{d}{dt} \frac{\partial T}{\partial \dot{x}_i} + Q_i \right) \delta x_i dt = 0 \tag{4.6}$$

This relation is true for all variations δx_i, that is,

$$\frac{d}{dt} \frac{\partial T}{\partial \dot{x}_i} - \frac{\partial T}{\partial x_i} = Q_i \tag{4.7}$$

Equation 4.7 is the general form of Lagrange's equations.

4.3 Generalized Equations of Motion

The position of a particle of mass *m* constrained to a parametric surface, represented in terms of parametric coordinates *u* and *w*, is

$$\boldsymbol{Q}(u,w) = \left[x_1(u,w), \quad x_2(u,w), \quad x_3(u,w) \right] \tag{4.8}$$

The potential energy of the particle at any position on the surface can be expressed as

$$U = mgx_3(u,w) \tag{4.9}$$

and the kinetic energy can be expressed as

$$T = \frac{m}{2}\sum_{i=1}^{3}\dot{x}_i^2 \tag{4.10}$$

with

$$\dot{x}_i = x_{i,u}\dot{u} + x_{i,w}\dot{w} \qquad i=1,3 \tag{4.11}$$

where

$$\dot{u} = \frac{\partial u}{\partial t} \qquad \text{and} \qquad \dot{w} = \frac{\partial w}{\partial t} \tag{4.12}$$

Substituting Equation 4.11 into Equation 4.10, one has

$$T = \frac{m}{2}\sum_{i=1}^{3}\left[x_{i,u}\,\dot{u} + x_{i,w}\dot{w}\right]^2 = \frac{m}{2}\sum_{i=1}^{3}\left[{x_{i,u}}^2\dot{u}^2 + 2x_{i,u}x_{i,w}\dot{u}\dot{w} + {x_{i,w}}^2\dot{w}^2\right]$$

$$= \frac{m}{2}\left(a\dot{u}^2 + 2b\dot{u}\dot{w} + c\dot{w}^2\right) \qquad i=1,3 \tag{4.13}$$

where

$$a = {x_{i,u}}^2 \tag{4.14}$$

$$b = x_{i,u} \cdot x_{i,w} \tag{4.15}$$

$$c = {x_{i,w}}^2 \tag{4.16}$$

The Lagrangian equations of motion can then be written as

$$\frac{d}{dt}\left(\frac{\partial T}{\partial \dot{u}}\right) - \frac{\partial T}{\partial u} = \sum_{i=1}^{3} F_i x_{i,u} \qquad i=1,3 \tag{4.17}$$

$$\frac{d}{dt}\left(\frac{\partial T}{\partial \dot{w}}\right) - \frac{\partial T}{\partial w} = \sum_{i=1}^{3} F_i x_{i,w} \qquad i=1,3 \tag{4.18}$$

or

$$\frac{d}{dt}\left(\frac{\partial T}{\partial \dot{u}}\right) - \frac{\partial T}{\partial u} = Q_u \tag{4.19}$$

$$\frac{d}{dt}\left(\frac{\partial T}{\partial \dot{w}}\right) - \frac{\partial T}{\partial w} = Q_w \tag{4.20}$$

where F_i are the components of the actual external forces in the x_i directions, respectively, acting on the particle in the Cartesian space. Q_u and Q_w represent the generalized forces acting in the u and w directions, respectively, in the parametric space. In this case, the external forces are friction and gravity forces. The friction forces are due to centrifugal forces and gravity, i.e., the weight of the particle.

The Lagrangian equations of motion with friction forces can be written as

$$\frac{d}{dt}\left(\frac{\partial L}{\partial \dot{u}}\right)-\frac{\partial L}{\partial u}=\left(\mu R+\frac{\mu m V^2}{\rho}\cos\phi\right)\left(-\hat{\boldsymbol{e}}_s\cdot\boldsymbol{P}_u\right) \tag{4.21}$$

and

$$\frac{d}{dt}\left(\frac{\partial L}{\partial \dot{w}}\right)-\frac{\partial L}{\partial w}=\left(\mu R+\frac{\mu m V^2}{\rho}\cos\phi\right)\left(-\hat{\boldsymbol{e}}_s\cdot\boldsymbol{P}_w\right) \tag{4.22}$$

Details of the friction forces are discussed in Appendix C.

Simplifying the above equations, one has

$$\begin{aligned} a\ddot{u}+b\ddot{w} &= -\frac{1}{2}a_{,u}\,\dot{u}^2+(\frac{1}{2}c_{,u}-b_{,w})\dot{w}^2-a_{,w}\,\dot{u}\dot{w}-gx_{3,u} \\ &+\frac{1}{m}\left(\mu R+\frac{\mu m V^2}{\rho}\cos\phi\right)\left(-\hat{\boldsymbol{e}}_s\cdot\boldsymbol{P}_u\right) \end{aligned} \tag{4.23}$$

and

$$\begin{aligned} b\ddot{u}+c\ddot{w} &= (\frac{1}{2}a_{,w}-b_{,u})\dot{u}^2-\frac{1}{2}c_{,w}\,\dot{w}^2-c_{,u}\,\dot{u}\dot{w}-gx_{3,w} \\ &+\frac{1}{m}\left(\mu R+\frac{\mu m V^2}{\rho}\cos\phi\right)\left(-\hat{\boldsymbol{e}}_s\cdot\boldsymbol{P}_w\right) \end{aligned} \tag{4.24}$$

Equations. 4.23 and 4.24 can be rewritten as

$$k_0\ddot{u} = k_1\dot{u}^2 + k_2\dot{w}^2 + k_3\dot{u}\dot{w} + k_4 + k_9 \tag{4.25}$$

$$k_0\ddot{w} = k_5\dot{u}^2 + k_6\dot{w}^2 + k_7\dot{u}\dot{w} + k_8 + k_{10} \tag{4.26}$$

where

$$\begin{aligned}
k_0 &= ac - b^2 \\
k_1 &= -0.5 \cdot c \cdot a_{,u} - 0.5 \cdot b \cdot a_{,w} + b \cdot b_{,u} \\
k_2 &= 0.5 \cdot c \cdot c_{,u} + 0.5 \cdot b \cdot c_{,w} - c \cdot b_{,w} \\
k_3 &= b \cdot c_{,u} - c \cdot a_{,w} \\
k_4 &= g \cdot (b \cdot x_{3,w} - c \cdot x_{3,u}) \\
k_5 &= 0.5 \cdot a \cdot a_{,w} + 0.5 \cdot b \cdot a_{,u} - a \cdot b_{,u} \\
k_6 &= -0.5 \cdot a \cdot c_{,w} - 0.5 \cdot b \cdot c_{,u} + b \cdot b_{,w} \\
k_7 &= b \cdot a_{,w} - a \cdot c_{,u} \\
k_7 &= g \cdot (b \cdot x_{3,u} - a \cdot x_{3,w}) \\
k_9, k_{10} &= \textit{friction forces}
\end{aligned} \tag{4.27}$$

Note that, for non-friction cases, k_9 and k_{10} are zero.

The system of differential equations can be solved if the four initial conditions are given, i.e.,

$$\begin{aligned}
u(0) &= u_0 \qquad w(0) = w_0 \\
\dot{u}(0) &= \dot{u}_0 \qquad \dot{w}(0) = \dot{w}_0
\end{aligned} \tag{4.28}$$

Note that the above initial conditions represent the position and velocity of the particle in the flow channel at time $t = 0$.

4.4 Numerical Calculations

The *Mathematica*® *NDSolve* function is employed in this dissertation to solve the system of ordinary differential equations for motion analysis. *NDSolve* is implemented using the *Adams-Bashforth-Moulton* method for non-stiff differential equations, as well as a backward difference formula (*Gear* method) [8]. *NDSolve* switches between these two algorithms based on an adaptively selected step size. Both methods are multi-step methods [18]. Multi-step methods, when applied to solve $y' = ay$, have more than one solution. In fact, the number of solutions is equal to the number of steps that the method uses. One of these solutions is an approximation to the solution of the differential equation. All explicit multi-step methods are, at most, conditionally stable, but many of them have regions in which they are truly stable. Implicit multi-step methods may be unconditionally stable.

The most general k step method is

$$\sum_{m=0}^{k} \alpha_m y_{n+1-m} + \sum_{m=0}^{k} \beta_m f(x_{n+1-m}, y_{n+1-m}) = 0 \tag{4.29}$$

A particular method is defined by the number of steps k and the parameters α_m and β_m.

If $\beta_0 = 0$, the method is explicit; otherwise it is implicit. Methods for $\alpha_0 = 1$, $\alpha_1 = -1$, and $\alpha_m = 0$ for $m > 1$ are called *Adams* methods. The explicit methods of this type are called *Adams-Bashforth* methods, and the implicit methods are called *Adams-Moulton* methods. These methods can be derived in a number of ways, one of which is from difference formulas. For the *Adams-Bashforth* methods, backward formulas are needed while, for the *Adams-Moulton* case, formulas with one forward point are required. They can be derived through the use of interpolation formulas. Fitting a Lagrange polynomial to the derivative y' at the points $x_{n-k+1}, x_{n-k}, \cdots, x_n$ and integrating the result from x_n to x_{n-1} yields the *Adams-Bashforth* formulas. Performing the same calculation with y'_{n+1} included in the interpolation yields the *Adams-Moulton* methods. The coefficients for the *Adams-Bashforth* methods are given in Table 4.1. Similarly, the coefficients for the *Adams-Moulton* methods are given in Table 4.2. For details on how they were chosen, see [19].

Adams-Bashforth methods are easy to use but not as stable as the *Adams-Moulton* methods, which are more difficult to use. Thus, a better approach is to construct a predictor-corrector method based on the *Adams* methods. Generally, such an approach consists of an *Adams-Bashforth* predictor followed by one or more corrector steps of the *Adams-Moulton* type. This method is called the *Adams-Bashforth-Moulton* method.

Also, stiffness is a special problem that can complicate the solution of ordinary differential equations. A number of approaches to the solution of stiff problems have been suggested. The *Gear* method is probably the most popular one in use today, and variations have been developed by various authors.

For a single equation, the Gear method gives

$$y_{n+1} = \sum_{i=1}^{k} \alpha_i y_{n+1-i} + h\beta_0 f(x_n, y_n) \tag{4.30}$$

The coefficients for this method are given in Table 4.3. For details on how they are chosen, see [18].

Table 4.1 Coefficients of *Adams-Bashforth* Methods

	$m=1$	$m=2$	$m=3$	$m=4$	$m=5$	$m=6$
β_{1m}	1					
$2\beta_{2m}$	3	-1				
$12\beta_{3m}$	23	-16	5			
$24\beta_{4m}$	55	-59	27	-9		
$720\beta_{5m}$	1901	-2774	2616	-1274	251	
$1440\beta_{6m}$	4277	-7923	9982	-7298	2877	-475

Table 4.2 Coefficients of *Adams-Moulton* Methods

	$m=0$	$m=1$	$m=2$	$m=3$	$m=4$	$m=5$
β_{1m}	1					
$2\beta_{2m}$	1	1				
$12\beta_{3m}$	5	8	-1			
$24\beta_{4m}$	9	19	-5	1		
$720\beta_{5m}$	251	646	-264	106	-19	
$1440\beta_{6m}$	475	1427	-798	482	-173	27

Table 4.3 Coefficients of *Gear* Methods

	$k=2$	$k=3$	$k=4$	$k=5$	$k=6$
β0	2/3	6/11	12/25	60/137	60/147
α1	4/3	18/11	48/25	300/137	360/147
α2	- 1/3	- 9/11	-36/25	300/137	450/147
α3		2/11	16/25	200/137	400/147
α4			- 3/25	- 75/137	- 75/49
α5				12/137	72/147
α6					- 10/147

Another important factor to affect the results is round-off error. In *NDSolve*, the round-off error can be controlled with the help of the *WorkingPrecision* option in *Mathematica*®. Specifically, the round-off error can be reduced by increasing the number of *WorkingPrecision*. High precision calculations normally require substantially more computational time and memory.

4.5 Numerical Examples

Again, water slides will be used as numerical examples to demonstrate the motion analysis for the two approaches.

4.5.1 Numerical Example of B-Spline-Based Flume Sections

The geometric shape of the Parker water slide configuration is shown in Figure 4.1. In this example, the particle weight is assumed to be 100 lbs. Particle traces of the friction and non-friction cases are shown in Figures 4.2 and 4.3, respectively. In the

friction case, the coefficient of the friction is assumed to be 0.03. Waterslide configuration and rider path are represented in the *I-DEAS*® CAD environment. Initial conditions for the rider are $u(0) = 0.5$ (i.e., the rider is at the center point), $w(0) = 0$, $\dot{u}(0) = 0$, and $\dot{w}(0) = 0$, respectively. The physical sizes of the configuration are described in Table 4.4. Note that some irregularities of the B-Spline surface are shown due to *I-DEAS*® software's limitations in representing the surface in Figures 4.3 and 4.5.

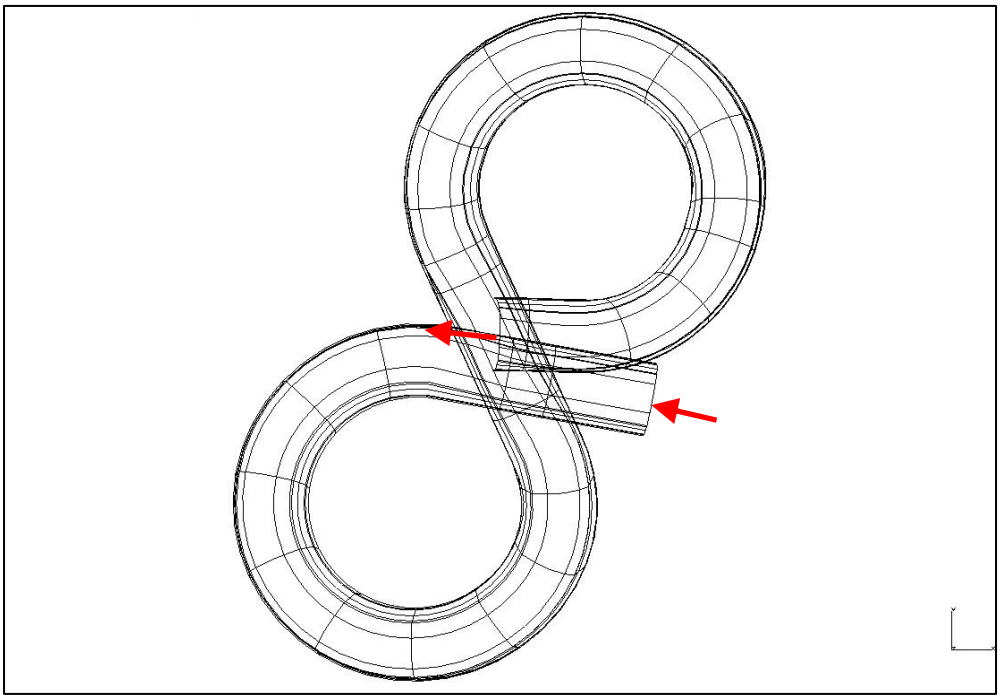


Figure 4.1 Geometric Shape of Parker Configuration

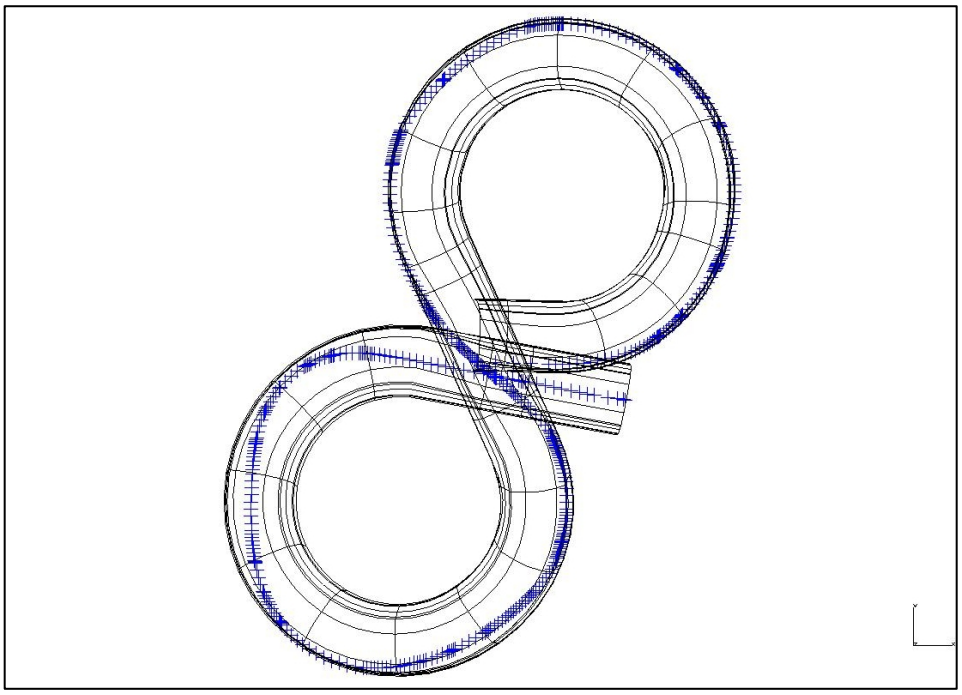


Figure 4.2 Top View of Particle Trace of Non-Friction Case (Parker)

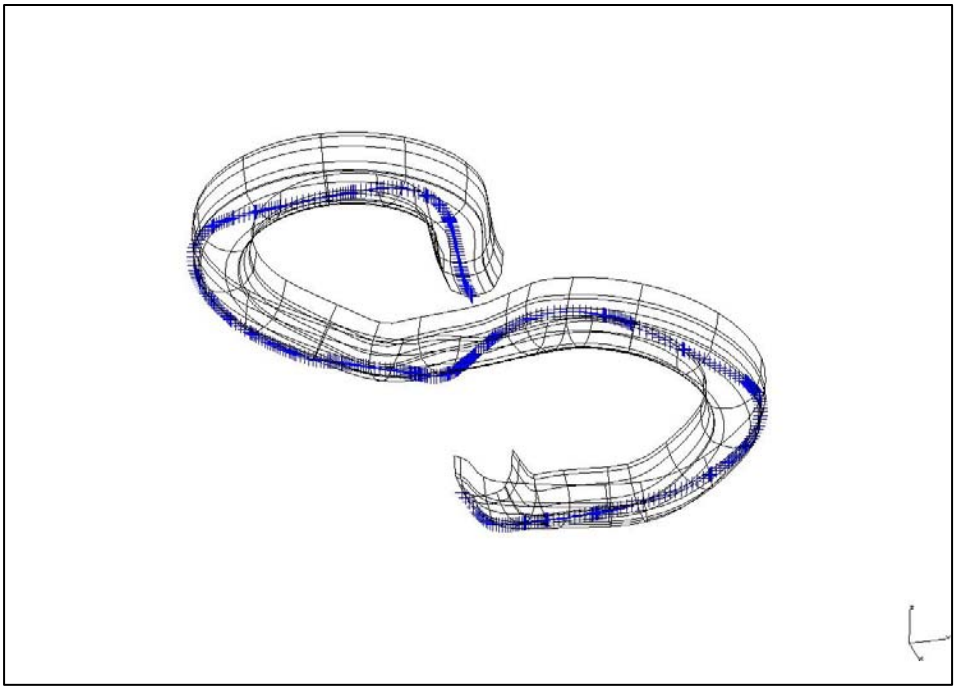


Figure 4.3 Isometric View of Particle Trace of Non-Friction Case (Parker)

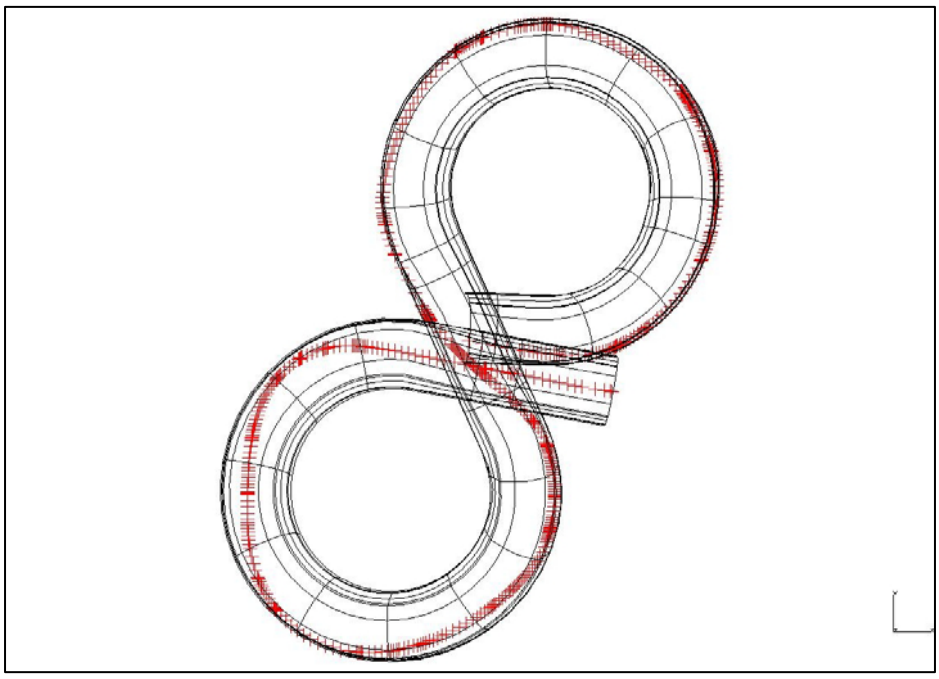


Figure 4.4 Top View of Particle Trace of Friction Case (Parker)

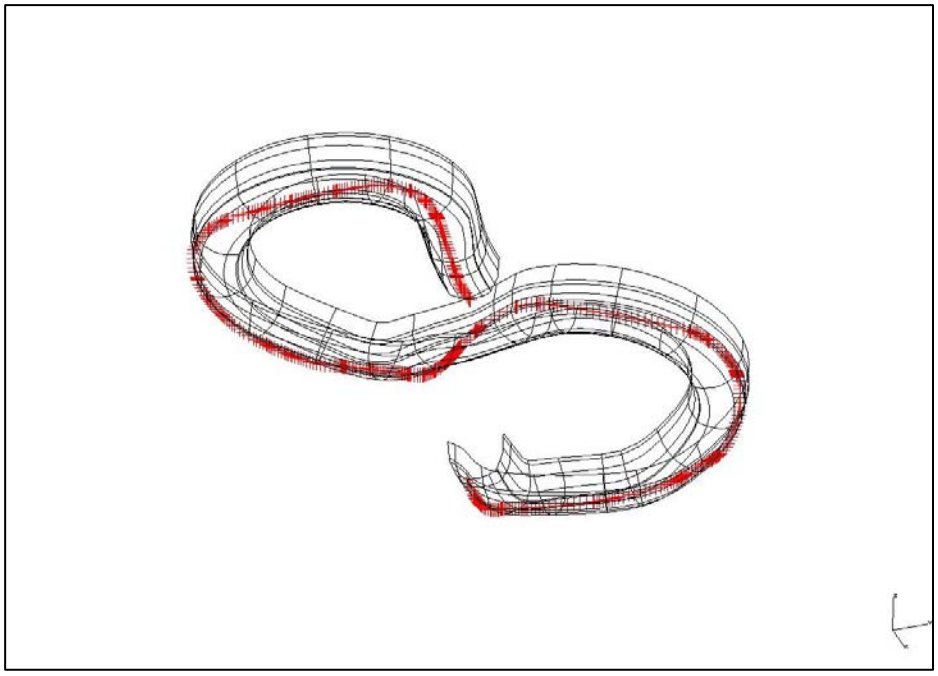


Figure 4.5 Isometric View of Particle Trace of Friction Case (Parker)

Table 4.4 Physical Sizes of Parker Configuration

Description	Size
W (Width of Flume Cross Section)	36.24 in. = 3.02 ft
L (Length of Flume Section)	1006.92 in. = 83.91 ft
H (Height of Configuration)	188.52 in. = 15.17 ft

4.5.2 Numerical Example of CAD-Based Flume Sections

Since the Parker water slide configuration was created using specific B-Spline-based basic flume sections, it would have been very difficult to create the same Parker water slide configuration for the CAD-based flume section example. Thus, two numerical examples are presented to demonstrate the feasibility of the motion analysis method, instead. The first example consists of arc flume sections. The second example is composed of both straight and cubic flume sections.

Weight examples of actual riders on water slide were not available. However, information about crash test dummies can be easily obtained [30]. According to Reference [30], automakers use dummies of 22.0, 34.2, 46.0, 108.0, and 172.0 lbs. This suggests that it is reasonable to use 40, 100, and 160 lbs for this research.

Example 1: Arced Flume Configuration

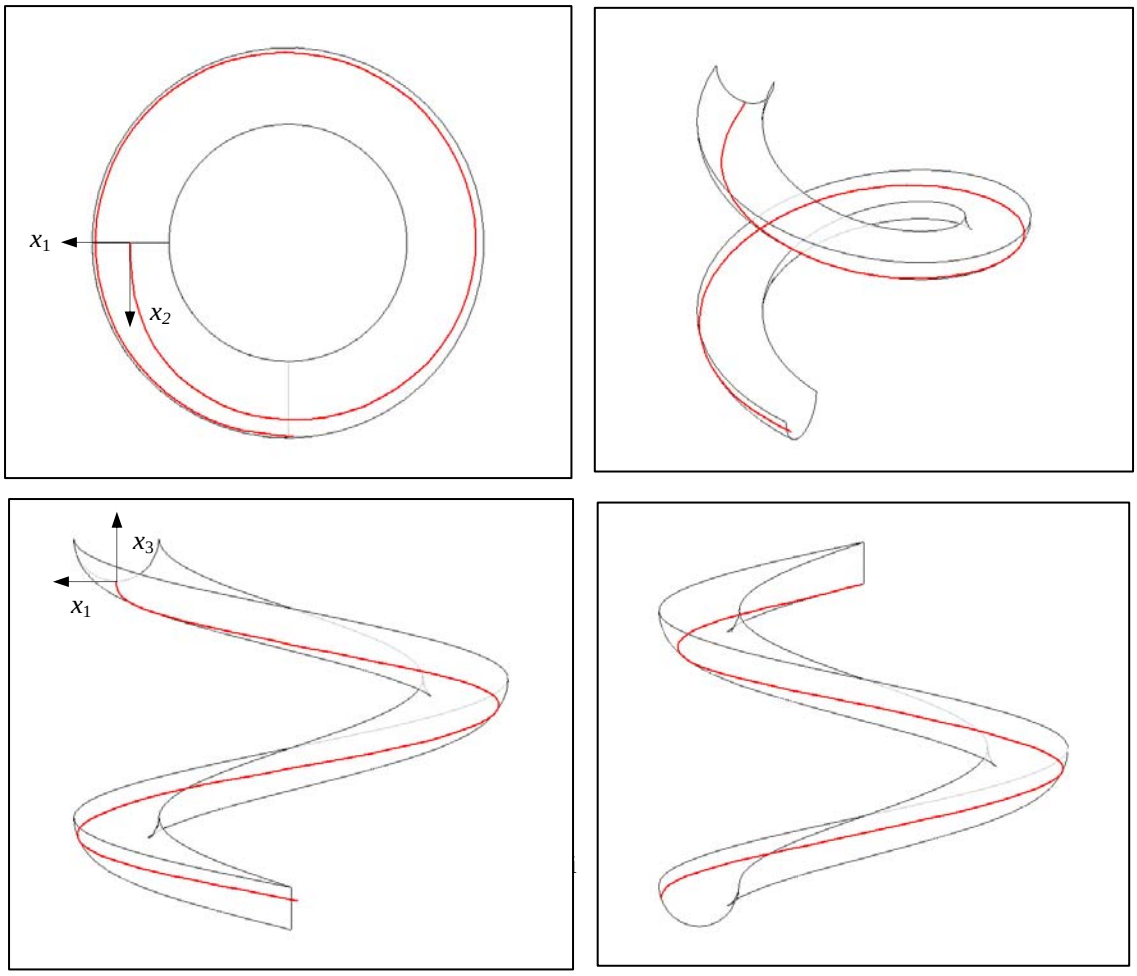


Figure 4.6 Particle Trace of Arced Flume Configuration

An arced waterslide configuration is analyzed first. The physical sizes of the configuration are given in Table 4.5. The path of the rider is displayed together with the waterslide configuration in Figure 4.6. The waterslide configuration is developed and the rider path is computed in the *SolidWorks*® environment, unlike the previous B-spline case, to show different code environments. The initial conditions of the rider are $u(0)$ = –1.5707 (–π/2; i.e., at the center), $w(0)$ = 0, $\dot{u}(0)$ = 0, and $\dot{w}(0)$ = 0, respectively. Note

that, if $u(t) \notin [-\pi, 0]$, the rider leaves the waterslide boundary, which is a severe safety violation. As shown in Figure 4.6, the rider stays in the water slide all the time for this particular case. The friction coefficient is 0.03 and the weight of the rider is 160 lbs.

Table 4.5 Physical Sizes of Arced Flume Configuration

Description	Size
R (Radius of Configuration)	71.56 in. = 5.6 ft
r (Radius of Flume Cross Section)	17.46 in. = 1.46 ft
h (Height of Configuration)	143.28 in. = 11.94 ft
ϕ (Total angle along X_3-axis)	450°

Example 2: Straight-Cubic-Straight Flume Configuration

A waterslide configuration composed of two straight end flume sections and one cubic middle flume section as shown in Figure 4.6 is defined with the physical dimensions given in Table 4.6.

Table 4.6 Physical Sizes of Straight and Cubic Mixed Flume Configuration

Description	Size
L (Length of Flume Configuration)	60 in. = 5.0 ft
R (Radius of Flume Cross Section)	17.46 in. = 1.46 ft
H (Height of Configuration)	45 in. = 3.75 ft
θ (Rotation along x_3 axis)	0°

Two particle paths are simulated with two different initial conditions, $u(0) = -2.5707$ (i.e, at a 31.8% off-center position) and $u(0) = -2.0707$ (i.e, at a 16% off-center position). For both cases, $w(0) = 0$, $\dot{u}(0) = 0$, and $\dot{w}(0) = 0$. Since the flume section configuration is relatively short and friction causes little difference, no friction is used. The weight of the rider is 160 lbs.

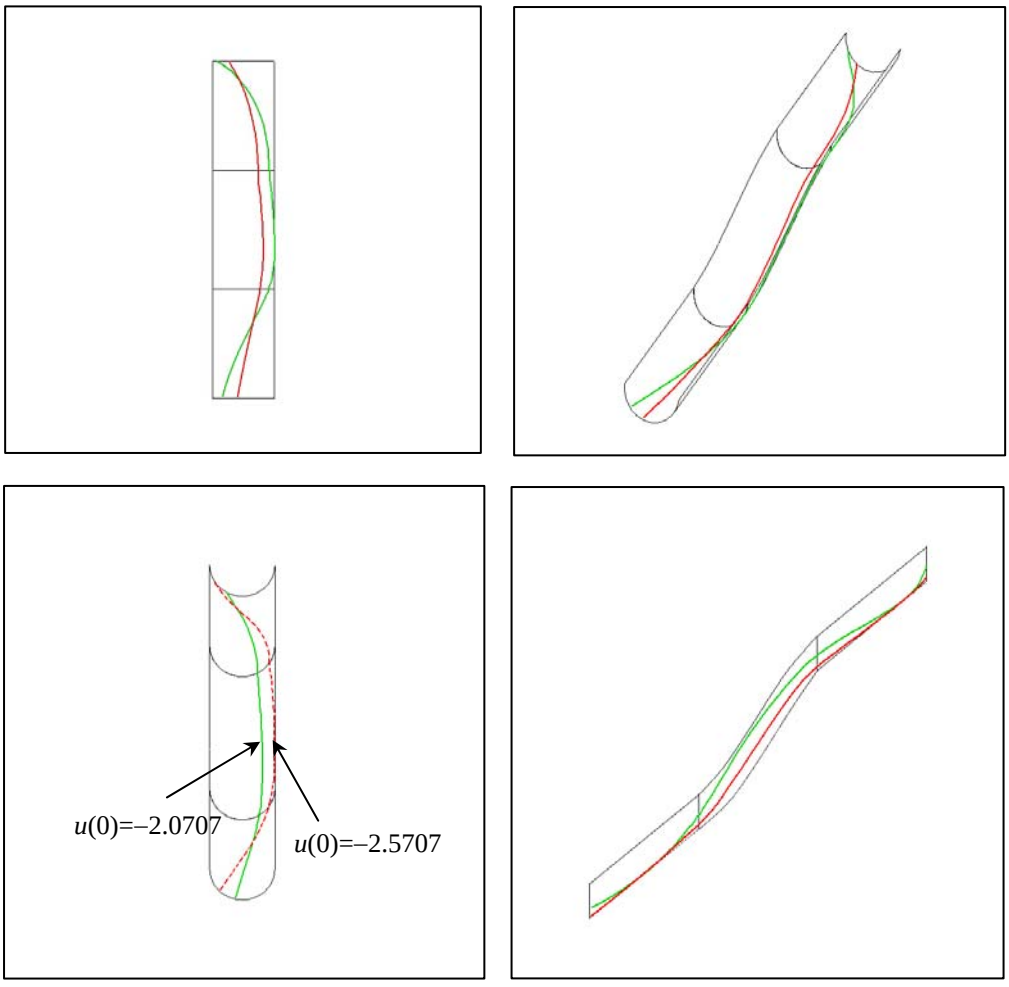


Figure 4.7 Particle Traces of Straight-Cubic-Straight Configuration

CHAPTER 5

SHAPE DESIGN SENSITIVITY ANALYSIS AND OPTIMIZATION OF FLUME SECTIONS

5.1 Introduction

In this chapter, shape design sensitivity analysis (DSA) and optimization are presented. The shape DSA calculates derivatives of position, velocity, and acceleration of the traveling particle with respect to the design variables, i.e., the control point positions of the B-Spline surface or the dimensions of the CAD-based flume section for the entire travel time (see also Reference 11). There are two methods to compute the design sensitivity coefficients, analytical and overall finite difference.

For this research, an analytical DSA method has been developed and employed for the design of flume sections. The overall finite difference method is used to verify the accuracy of the analytical DSA method. The overall finite difference method is first explained in Section 5.2. The analytical DSA method with its assumptions is presented in Section 5.3. Numerical methods to evaluate the shape design sensitivity coefficients are detailed in Section 5.4. A number of examples are given in Section 5.5 to verify the accuracy of the analytical DSA. In Section 5.6, optimization results for both flume sections are presented.

5.2 Overall Finite Difference Method

In this section, the friction forces are assumed to be zero. This is a conservative assumption, leading to higher accelerations. The equations of motion (Equations 4.25 and 4.26) are rewritten as

$$k_0\ddot{u} = k_1\dot{u}^2 + k_2\dot{w}^2 + k_3\dot{u}\dot{w} + k_4 \tag{5.1}$$

$$k_0\ddot{w} = k_5\dot{u}^2 + k_6\dot{w}^2 + k_7\dot{u}\dot{w} + k_8 \tag{5.2}$$

where

$$\begin{aligned}
k_0 &= ac - b^2 \\
k_1 &= -0.5\cdot c\cdot a_u - 0.5\cdot b\cdot a_w + b\cdot b_u \\
k_2 &= 0.5\cdot c\cdot c_u + 0.5\cdot b\cdot c_w - c\cdot b_w \\
k_3 &= b\cdot c_u - c\cdot a_w \\
k_4 &= g\cdot(b\cdot z_w - c\cdot z_u) \\
k_5 &= 0.5\cdot a\cdot a_w + 0.5\cdot b\cdot a_u - a\cdot b_u \\
k_6 &= -0.5\cdot a\cdot c_w - 0.5\cdot b\cdot c_u + b\cdot b_w \\
k_7 &= b\cdot a_w - a\cdot c_u \\
k_8 &= g\cdot(b\cdot z_u - a\cdot z_w)
\end{aligned} \tag{5.3}$$

Note that, in Equations. 5.1 and 5.2, $k_9 = k_{10} = 0$ is assumed for zero friction. The coefficients k_i in Equations 5.1 and 5.2 are functions of the design variables D. In this section, the control points $\boldsymbol{B}_{ij}$ have been used as the design variables throughout the equations. However, the dimensions of the surface can be used instead of the control points $\boldsymbol{B}_{ij}$ as design variables and the same sensitivity equations can be derived.

For example, for k_0, one has

$$\begin{aligned} k_0 &= ac - b^2 \\ &= (x_u{}^2 + y_u{}^2 + z_u{}^2)\cdot(x_u \cdot x_w + y_u \cdot y_w + z_u \cdot z_w) - (x_w{}^2 + y_w{}^2 + z_w{}^2)^2 \\ &= f(B_{ij}^k) \end{aligned} \tag{5.4}$$

since $x_u, x_w, y_u, y_w, z_u, z_w$ are functions of D. So, a control point movement ($\delta \boldsymbol{B}_{ij}$) or a change in dimension significantly affects the path, velocity, and acceleration of the traveling object. Hence, the $\delta \boldsymbol{B}_{ij}$ of the B-Spline surface or the dimensions of a CAD-based flume surface are defined as design variables for shape design sensitivity analysis (DSA) of the flume section configuration. The path, velocity, and acceleration of the traveling object depend on these shape design variables in two ways.

The first dependence is explicit, Here, the geometric shape of the surface of the flume section configuration varies due to design changes. This dependence is illustrated in Figure 5.1b and is characterized by

$$\delta \boldsymbol{x}(u,w) = \sum_{i=0}^{n}\sum_{j=0}^{m}\left(N_{i,k}(u)M_{j,\ell}(w)\right)\delta \boldsymbol{B}_{ij} \qquad \boldsymbol{x} = x, y, z \tag{5.5}$$

where $\delta \boldsymbol{x}$ represents the variation of the function $\boldsymbol{x}$ and $\delta \boldsymbol{B}_{ij}$ represents the movements of the control points. The dependence shows the variation of the position vector $\boldsymbol{x}$ due to $\delta \boldsymbol{B}_{ij}$, evaluated at the same parametric coordinates u and w. Note that, in this chapter, the control points of the B-Spline surface are used as design variables to explain the overall finite difference method.

The second dependence is implicit. Here, object path, velocity, and acceleration vary due to variations of $u(t)$ and $w(t)$, which are determined by Lagrange's equations of motion, reformulated based on a different flow channel geometry, as illustrated in Figure 5.1a. Using Taylor's series expansion, the object path in the parametric coordinate u (similar for w) at the perturbed design can be expressed as

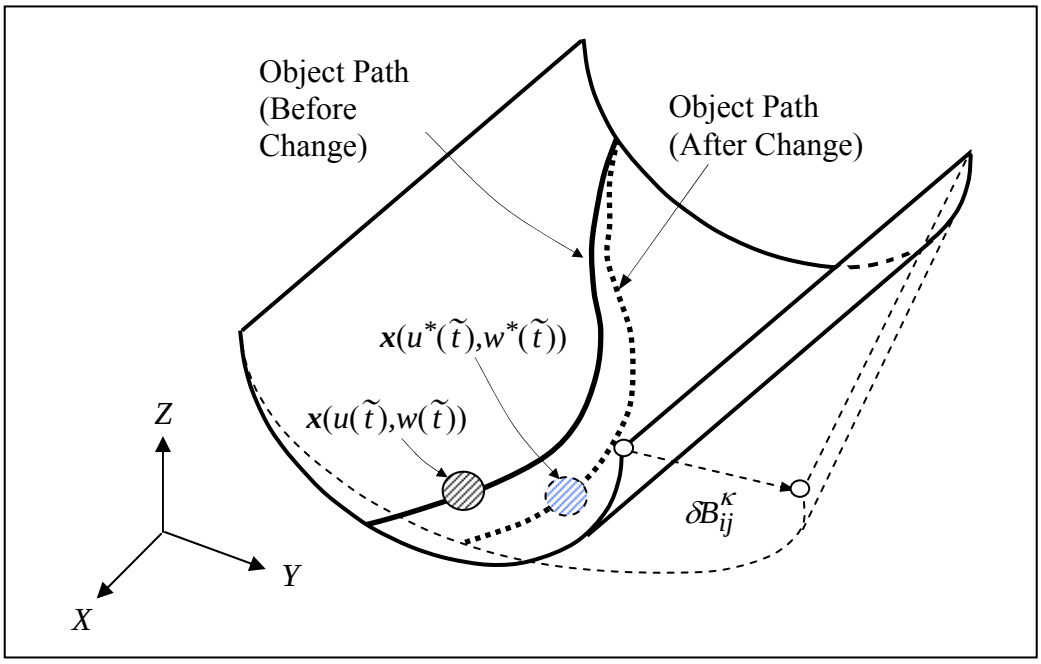
$$u^*(\tilde{t}) = u(\tilde{t}, \boldsymbol{B}_{ij} + \delta B_{ij}^k) = u(\tilde{t}, \boldsymbol{B}_{ij}) + \frac{\partial u}{\partial B_{ij}^k}\delta B_{ij}^k + \textit{Higher Order Terms} \tag{5.6}$$

where $\tilde{t}$ denotes that the time is kept constant and δB_{ij}^{κ} is the design perturbation of the control point $\boldsymbol{B}_{ij}$ in the k-direction, where k = 1, 2, and 3.

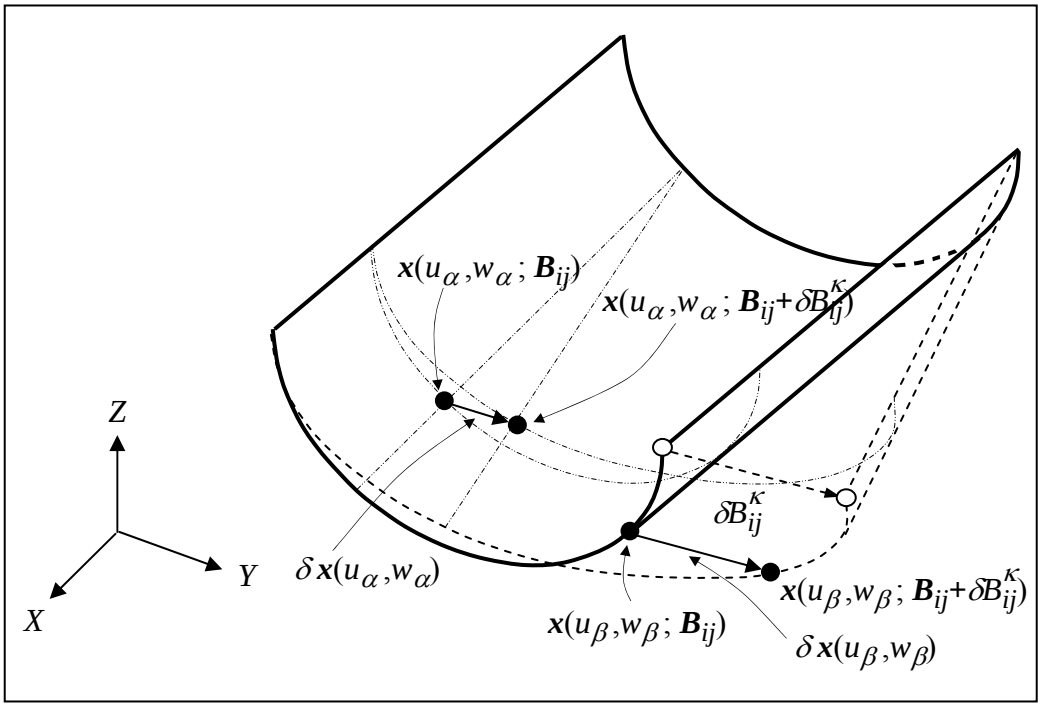
The simplest way for calculating sensitivity information is using the overall finite difference method, in which the sensitivity coefficients are approximated by

$$\frac{d\psi}{dB_{ij}^k} \approx \frac{\psi(u^*(\tilde{t}), w^*(\tilde{t}); \boldsymbol{B}_{ij} + \delta B_{ij}^k) - \psi(u(\tilde{t}), w(\tilde{t}); \boldsymbol{B}_{ij})}{\delta B_{ij}^k} \tag{5.7}$$

where ψ represents path, velocity, or acceleration of the traveling object obtained by solving the equations of motion and $u^*(\tilde{t}) = u(\tilde{t}, \boldsymbol{B}_{ij} + \delta B_{ij}^{\kappa})$ and $w^*(\tilde{t}) = w(\tilde{t}, \boldsymbol{B}_{ij} + \delta B_{ij}^{\kappa})$. Note that, when the design perturbation δB_{ij}^{κ} approaches zero, the results of the finite difference computation approach the true sensitivity information. The amount of design perturbation is usually difficult to determine. A small perturbation may result in an inaccurate sensitivity information due to numerical noise. On the other hand, a large



(a) Implicit Dependence through Geometry Variation



(b) Explicit Dependence through Equations of Motion

Figure 5.1 Dependence of Object Path on Design Changes

perturbation may also cause inaccuracy due to nonlinear effects of the function ψ. Moreover, a full motion analysis is required for every individual design variable perturbation, which is time consuming.

The analytical DSA does not require choosing a proper amount of δB_{ij}^{κ}. By taking derivatives of Equations 5.1 and 5.2 with respect to the design variable B_{ij}^{κ}, shape DSA of the motion problem can be obtained as follows

$$\frac{dk_0}{dB_{ij}^k}\ddot{u}+k_0\frac{d\ddot{u}}{dB_{ij}^k}=\frac{dk_1}{dB_{ij}^k}\dot{u}^2+2k_1\dot{u}\frac{d\dot{u}}{dB_{ij}^k}+\frac{dk_2}{dB_{ij}^k}\dot{w}^2+2k_2\dot{w}\frac{d\dot{w}}{dB_{ij}^k}+\frac{dk_3}{dB_{ij}^k}\dot{u}\dot{w}+k_3\frac{d\dot{u}}{dB_{ij}^k}\dot{w}+k_3\dot{u}\frac{d\dot{w}}{dB_{ij}^k}+\frac{dk_4}{dB_{ij}^k} \tag{5.8a}$$

$$\frac{dk_0}{dB_{ij}^k}\ddot{w}+k_0\frac{d\ddot{w}}{dB_{ij}^k}=\frac{dk_5}{dB_{ij}^k}\dot{u}^2+2k_5\dot{u}\frac{d\dot{u}}{dB_{ij}^k}+\frac{dk_6}{dB_{ij}^k}\dot{w}^2+2k_6\dot{w}\frac{d\dot{w}}{dB_{ij}^k}+\frac{dk_7}{dB_{ij}^k}\dot{u}\dot{w}+k_7\frac{d\dot{u}}{dB_{ij}^k}\dot{w}+k_7\dot{u}\frac{d\dot{w}}{dB_{ij}^k}+\frac{dk_8}{dB_{ij}^k} \tag{5.8b}$$

where

$$\frac{dk_0}{dB_{ij}^k}=\frac{da}{dB_{ij}^k}\cdot c+a\cdot\frac{dc}{dB_{ij}^k}-2b\cdot\frac{db}{dB_{ij}^k} \tag{5.9a}$$

$$\frac{dk_1}{dB_{ij}^k}=\frac{1}{2}\left(\frac{da}{dB_{ij}^k}\cdot a_{,w}+a\cdot\frac{da_{,w}}{dB_{ij}^k}\right)+\frac{1}{2}\left(\frac{db}{dB_{ij}^k}\cdot a_{,u}+b\cdot\frac{da_{,u}}{dB_{ij}^k}\right)-\left(\frac{da}{dB_{ij}^k}\cdot b_{,u}+a\cdot\frac{db_{,u}}{dB_{ij}^k}\right) \tag{5.9b}$$

$$\frac{dk_2}{dB_{ij}^k} = -\frac{1}{2}\left(\frac{da}{dB_{ij}^k}\cdot c_{,w} + a\cdot\frac{dc_{,w}}{dB_{ij}^k}\right) - \frac{1}{2}\left(\frac{db}{dB_{ij}^k}\cdot c_{,u} + b\cdot\frac{dc_{,u}}{dB_{ij}^k}\right) + \left(\frac{db}{dB_{ij}^k}\cdot b_{,w} + b\cdot\frac{db_{,w}}{dB_{ij}^k}\right) \tag{5.9c}$$

$$\frac{dk_3}{dB_{ij}^k} = \left(\frac{db}{dB_{ij}^k}\cdot a_{,w} + b\cdot\frac{da_{,w}}{dB_{ij}^k}\right) - \left(\frac{da}{dB_{ij}^k}\cdot c_{,u} + a\cdot\frac{dc_{,u}}{dB_{ij}^k}\right) \tag{5.9d}$$

$$\frac{dk_4}{dB_{ij}^k} = g\left(\frac{db}{dB_{ij}^k}\cdot z_{,u} + b\cdot\frac{dz_{,u}}{dB_{ij}^k} - \frac{da}{dB_{ij}^k}\cdot z_{,u} + a\cdot\frac{dz_{,u}}{dB_{ij}^k}\right) \tag{5.9e}$$

$$\frac{dk_5}{dB_{ij}^k} = -\frac{1}{2}\left(\frac{dc}{dB_{ij}^k}\cdot a_{,u} + c\cdot\frac{da_{,u}}{dB_{ij}^k}\right) - \frac{1}{2}\left(\frac{db}{dB_{ij}^k}\cdot a_{,w} + b\cdot\frac{da_{,w}}{dB_{ij}^k}\right) + \frac{db}{dB_{ij}^k}\cdot b_{,u} + b\cdot\frac{db_{,u}}{dB_{ij}^k} \tag{5.9f}$$

$$\frac{dk_6}{dB_{ij}^k} = \frac{1}{2}\left(\frac{dc}{dB_{ij}^k}\cdot c_{,u} + c\cdot\frac{dc_{,u}}{dB_{ij}^k}\right) + \frac{1}{2}\left(\frac{db}{dB_{ij}^k}\cdot c_{,w} + b\cdot\frac{dc_{,w}}{dB_{ij}^k}\right) - \frac{dc}{dB_{ij}^k}\cdot c_{,u} - c\cdot\frac{db_{,w}}{dB_{ij}^k} \tag{5.9g}$$

$$\frac{dk_7}{dB_{ij}^k} = \frac{db}{dB_{ij}^k}\cdot c_{,u} + b\cdot\frac{dc_{,u}}{dB_{ij}^k} - \frac{dc}{dB_{ij}^k}\cdot a_{,w} - c\cdot\frac{da_{,w}}{dB_{ij}^k} \tag{5.9h}$$

$$\frac{dk_8}{dB_{ij}^k} = g\left(\frac{db}{dB_{ij}^k}\cdot z_{,w} + b\cdot\frac{dz_{,w}}{dB_{ij}^k} - \frac{dc}{dB_{ij}^k}\cdot z_{,u} - c\cdot\frac{dz_{,u}}{dB_{ij}^k}\right). \tag{5.9i}$$

Note that, in Equations 5.9, friction forces are not included, a conservative assumption. Equation 5.9 contains derivatives of *a*, *b*, *c*, and their *u*- and *w*-derivatives with respect to the design variable B_{ij}^{κ}. Two typical terms in Equation 5.9 are presented in the following.

$$\frac{da_{,u}}{dB_{ij}^{k}} = 2\boldsymbol{x}_{,uu}\frac{d\boldsymbol{x}_{,uu}}{dB_{ij}^{k}} \tag{5.10}$$

where

$$\frac{d\boldsymbol{x}_{,uu}}{dB_{ij}^{k}} = \frac{\partial}{\partial u}\left(\frac{\partial \boldsymbol{x}_{,uu}}{\partial u}\right)\frac{\partial u}{\partial B_{ij}^{k}} + \frac{\partial}{\partial w}\left(\frac{\partial \boldsymbol{x}_{,uu}}{\partial w}\right)\frac{\partial w}{\partial B_{ij}^{k}} + \frac{\partial}{\partial t}\left(\frac{\partial \boldsymbol{x}_{,uu}}{\partial u} + \frac{\partial \boldsymbol{x}_{,uu}}{\partial w}\right)\frac{\partial t}{\partial B_{ij}^{k}} + \frac{\partial \boldsymbol{x}_{,uu}}{\partial B_{ij}^{k}} \tag{5.11}$$

Also,

$$\frac{dz}{dB_{ij}^{k}} = \frac{\partial}{\partial u}\left(\frac{\partial z}{\partial u}\right)\frac{\partial u}{\partial B_{ij}^{k}} + \frac{\partial}{\partial w}\left(\frac{\partial z}{\partial w}\right)\frac{\partial w}{\partial B_{ij}^{k}} + \frac{\partial}{\partial t}\left(\frac{\partial z}{\partial u} + \frac{\partial z}{\partial w}\right)\frac{\partial t}{\partial B_{ij}^{k}} + \frac{\partial z}{\partial B_{ij}^{k}} \tag{5.12}$$

The last terms on the right-hand side of Equations 5.11 and 5.12 represent the explicit dependence of $\boldsymbol{x}_{,uu}$ and z on the design variable B_{ij}^{κ}, respectively. The remaining terms describe the implicit dependence of $\boldsymbol{x}_{,uu}$ and z on the design variable B_{ij}^{κ}, through $u(t)$ and $w(t)$. As discussed earlier, t is kept unchanged to relate the object position before and after the design change. Therefore, $\partial t/\partial B_{ij}^{\kappa}$ vanishes from Equations 5.11 and 5.12. In fact, the shape DSA predicts the time dependent variables, i.e., position, velocity, and acceleration, of the object sliding on the surface of the perturbed flume section, assuming that the time steps are kept constant. This is further illustrated using the straight slide shown in Figure 5.2, where $u^*(\tilde{t}) < u(\tilde{t})$, since the distance that the object must travel on the perturbed design is longer. It takes a longer time for the object to slide on the

perturbed design down to the same parametric location *u* as the original one. In this paper, the DSA information will predict the time dependent variables of the perturbed design at the same time step.

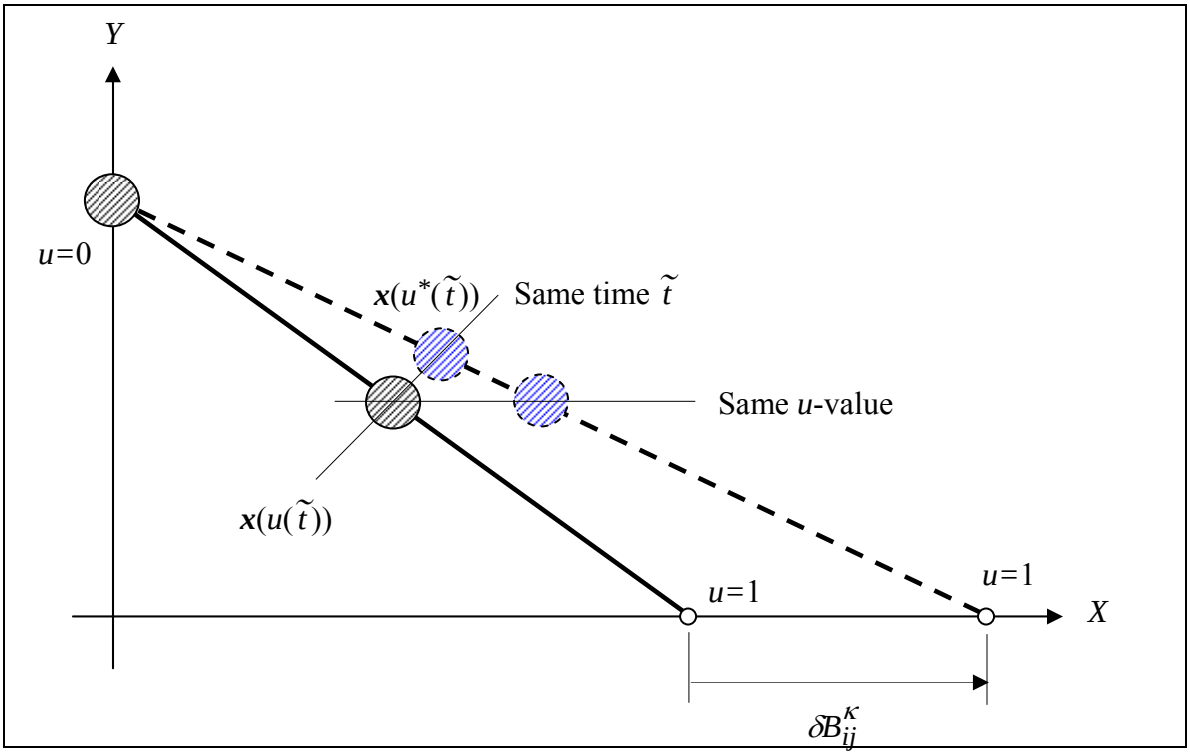


Figure 5.2 Illustration of DSA Predictions for Variables at Same Time Step

The initial conditions of the shape DSA equations are defined as follows

$$\frac{du(0)}{dB_{ij}^{k}} = 0,\ \frac{dw(0)}{dB_{ij}^{k}} = 0,\ \frac{d\dot{u}(0)}{dB_{ij}^{k}} = 0,\ \text{and}\ \frac{d\dot{w}(0)}{dB_{ij}^{k}} = 0 \tag{5.13}$$

which means that the initial position and velocity of the traveling object are assumed unchanged before and after the design changes. These assumptions are physically meaningful. A detailed derivation of the sensitivity equations is presented in Appendix D.

In this dissertation, the equations of motion (5.1 and 5.2) and the shape DSA equations (5.8) are solved simultaneously using *Mathematica*®. Note that the same design sensitivity equations can be derived by using the dimension instead of the control points. They were used for optimization of the CAD-based flume sections later.

5.3 Numerical Calculations

Before solving the sensitivity equations, the dynamic equations must be solved, since the sensitivity equations need $u(t)$, $\dot{u}(t)$, $w(t)$, and $\dot{w}(t)$. In the *Mathematica*® environment, two dynamics equations and two sensitivity equations are solved simultaneously as illustrated in Figure 5.3.

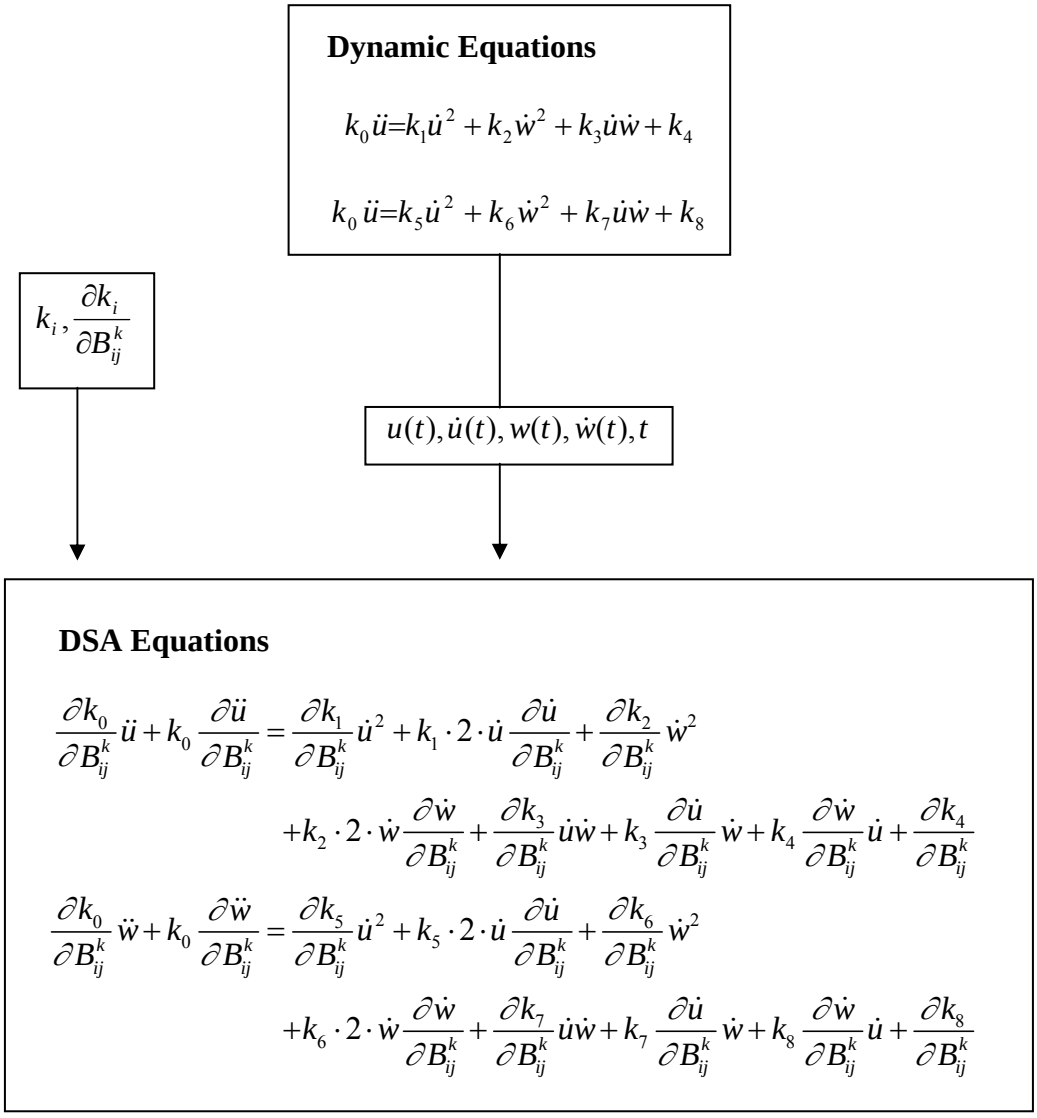


Figure 5.3 Procedure for Numerical Calculations

5.4 Design Sensitivity Verification

As an example, a Parker waterslide configuration is shown with a particle trace in Figure 5.4. In this example, the initial conditions are

$$u(0) = 0.0, \quad \dot{u}(0) = 0.0, \quad w(0) = 0.5, \quad \dot{w}(0) = 0.0$$

and

$$\frac{\partial u}{\partial B} = 0.0, \quad \frac{\partial \dot{u}}{\partial B} = 0.0, \quad \frac{\partial w}{\partial B} = 0.0, \quad \frac{\partial \dot{w}}{\partial B} = 0.0$$

The friction force is assumed to be zero, and the weight of the moving particle is 160 lbs.

The w-location of the particle during the entire ride is shown in Figure 5.5 Note that, if $u \notin [0,1]$, the traveling object leaves the waterslide. As shown in Figure 5.5, the object is close to sliding out of the boundary around t=15.2 (sec).

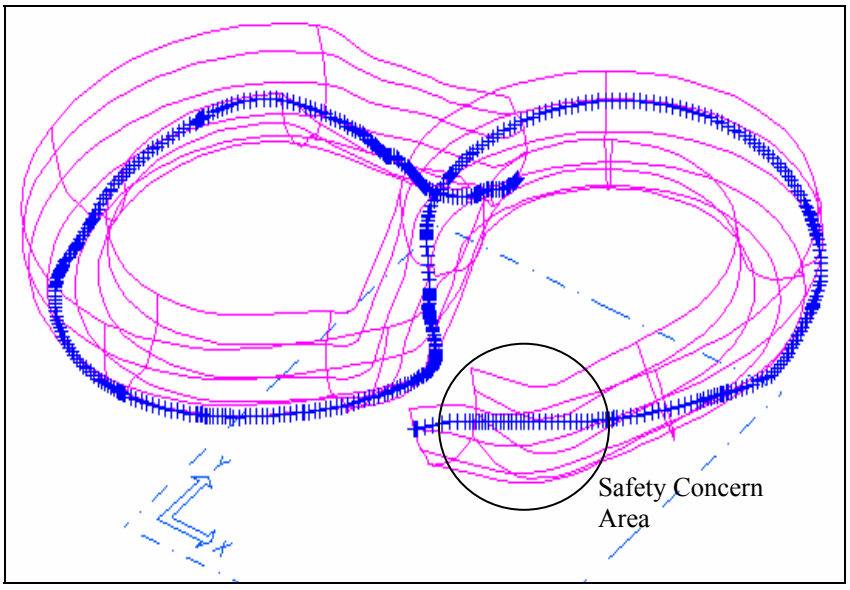


Figure 5.4 Parker Configuration with Particle Trace

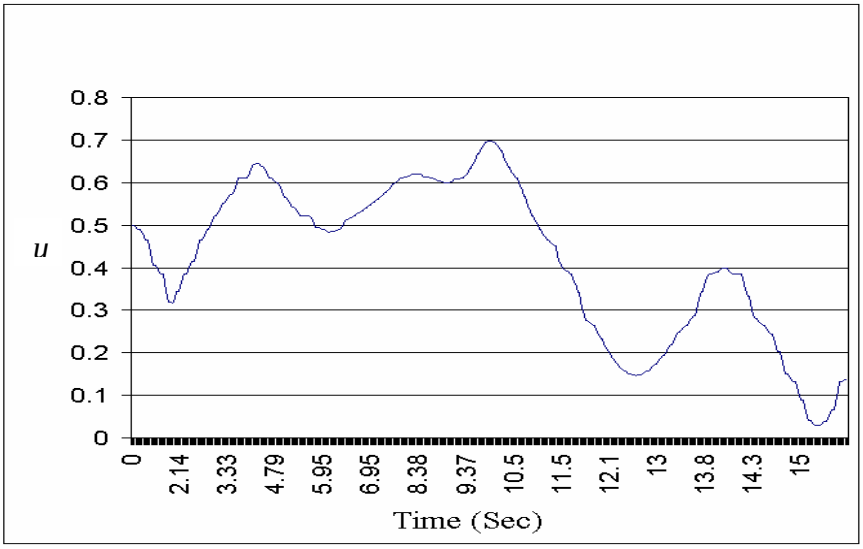


Figure 5.5 Location of Object $u(t)$ in Time Domain

Design sensitivity analysis is carried out for this example, with arbitrarily chosen design variables $B^z_{20,6}$, $B^y_{5,7}$, and $B^x_{8,8}$. It is shown in Figure 5.6, that the sensitivity coefficients of $u(t)$, $\dot{u}(t)$, $\ddot{u}(t)$, $w(t)$, $\dot{w}(t)$, and $\ddot{w}(t)$ are accurate compared to the overall finite difference results. In Figure 5.6, column B shows the time steps chosen arbitrarily from the results of the motion analyses. Columns C, D, and E list position, velocity, and acceleration of the object in the *u*- or *w*-direction at the selected time steps. Columns F, G, and H show the same information, but at the perturbed design. Note that columns C to H are obtained from the motion analyses. In this example, the design perturbation is $\delta B^z_{20,6} = \delta B^y_{5,7} = 0.1$, $\delta B^x_{8,8} = 1.0$ inch. Columns I, J, and K show the sensitivity of position, velocity, and acceleration obtained using the finite difference method, i.e., Column I = (Column F – Column C) / δB, Column J = (Column G – Column D) / δB, and Column K = (Column H – Column E) / δB. Columns L, M, and N list the sensitivity information obtained from the analytical shape DSA expressions. The last three columns show the accuracy of the analytical shape DSA by comparing data in Columns L, M, and N with

those in Columns I, J, and K, respectively. It is shown in columns O, P, and Q of Figure 5.6 that the sensitivity coefficients of $u(t)$, $\dot{u}(t)$, and $\ddot{u}(t)$ computed using the analytical shape DSA are accurate compared to the overall finite difference results.

B	C	D	E	F	G	H	I	J	K	L	M	N	O	P	Q
Time	Original Design			After Perturbation (+0.1)			Finite Difference			Sensitivity			Accuracy		
(Sec.)	w	$\dot{w}$	$\ddot{w}$	w	$\dot{w}$	$\ddot{w}$	w	$\dot{w}$	$\ddot{w}$	w	$\dot{w}$	$\ddot{w}$	w	$\dot{w}$	$\ddot{w}$
0.967	1.073E-01	5.535E-01	1.006E-01	1.073E-01	5.535E-01	1.006E-01	-2.225E-09	-2.202E-10	-6.369E-04	-2.225E-09	-2.201E-10	-6.480E-04	99.99	99.96	101.74
1.290	1.910E-01	7.421E-01	1.474E+00	1.910E-01	7.421E-01	1.474E+00	-1.106E-08	-2.268E-09	-2.410E-07	-1.106E-08	-2.268E-09	-2.476E-07	99.99	100.02	102.74
1.637	3.208E-01	9.635E-01	1.353E+00	3.208E-01	9.635E-01	1.353E+00	-1.145E-08	-2.010E-09	1.018E-06	-1.145E-08	-2.009E-09	1.017E-06	99.98	99.96	99.88
2.325	6.448E-01	1.401E+00	-4.105E-01	6.448E-01	1.401E+00	-4.105E-01	-7.598E-08	7.804E-08	6.091E-07	-7.594E-08	7.798E-08	6.082E-07	99.95	99.92	99.86
3.425	1.103E+00	1.438E+00	6.814E+00	1.103E+00	1.438E+00	6.814E+00	2.061E-08	1.563E-07	3.146E-05	2.060E-08	1.562E-07	3.140E-05	99.95	99.92	99.80
3.614	1.223E+00	1.623E+00	-3.625E+00	1.223E+00	1.623E+00	-3.625E+00	2.795E-08	-1.691E-09	3.708E-06	2.793E-08	-1.689E-09	3.744E-06	99.94	99.88	100.97
3.997	1.444E+00	1.299E+00	-6.937E-01	1.444E+00	1.299E+00	-6.937E-01	2.932E-08	2.242E-08	-1.778E-07	2.930E-08	2.241E-08	-1.792E-07	99.94	99.94	100.77
4.664	1.763E+00	1.220E+00	1.892E-01	1.763E+00	1.220E+00	1.892E-01	3.760E-08	4.658E-08	4.694E-08	3.757E-08	4.654E-08	4.692E-08	99.93	99.91	99.96
5.217	2.070E+00	1.416E+00	1.409E+00	2.070E+00	1.416E+00	1.409E+00	5.267E-08	8.734E-08	1.994E-07	5.263E-08	8.724E-08	1.956E-07	99.93	99.88	98.07
5.615	2.286E+00	1.605E+00	1.484E+00	2.286E+00	1.605E+00	1.484E+00	6.606E-08	1.073E-07	2.706E-06	6.601E-08	1.072E-07	2.629E-06	99.92	99.90	97.17
6.011	2.577E+00	1.712E+00	-4.889E-01	2.577E+00	1.712E+00	-4.889E-01	8.078E-08	5.140E-08	-5.405E-07	8.072E-08	5.134E-08	-5.535E-07	99.92	99.89	102.40
6.320	2.759E+00	1.587E+00	-1.669E+00	2.759E+00	1.587E+00	-1.669E+00	8.405E-08	1.358E-09	1.269E-07	8.397E-08	1.357E-09	1.325E-07	99.91	99.89	104.40
6.516	2.909E+00	1.459E+00	-1.261E+00	2.909E+00	1.459E+00	-1.261E+00	8.475E-08	-7.930E-10	-2.564E-07	8.467E-08	-7.914E-10	-2.791E-07	99.91	99.80	108.86
7.006	3.150E+00	1.256E+00	-8.074E-01	3.150E+00	1.256E+00	-8.074E-01	8.252E-08	-1.040E-08	-1.078E-08	8.245E-08	-1.038E-08	-1.072E-08	99.91	99.80	99.41
7.727	3.502E+00	1.281E+00	-9.296E-01	3.502E+00	1.281E+00	-9.296E-01	9.378E-08	8.979E-08	5.290E-07	9.370E-08	8.960E-08	5.296E-07	99.91	99.79	100.11
8.208	3.799E+00	1.585E+00	1.738E+00	3.799E+00	1.585E+00	1.738E+00	1.230E-07	1.809E-07	3.958E-07	1.229E-07	1.805E-07	3.951E-07	99.90	99.79	99.82
8.480	3.973E+00	1.781E+00	2.012E+00	3.973E+00	1.781E+00	2.012E+00	1.438E-07	2.215E-07	-5.469E-07	1.437E-07	2.210E-07	-5.466E-07	99.90	99.78	99.94
8.685	4.119E+00	1.906E+00	1.148E+00	4.119E+00	1.906E+00	1.148E+00	1.590E-07	1.680E-07	-8.773E-07	1.588E-07	1.676E-07	-8.654E-07	99.89	99.77	98.64
9.032	4.372E+00	1.890E+00	-1.838E+00	4.372E+00	1.890E+00	-1.838E+00	1.682E-07	-7.338E-08	-2.120E-06	1.680E-07	-7.318E-08	-2.100E-06	99.89	99.73	99.04
9.234	4.531E+00	1.887E+00	1.754E+00	4.531E+00	1.887E+00	1.754E+00	1.750E-07	2.276E-07	2.078E-05	1.748E-07	2.270E-07	2.117E-05	99.88	99.75	101.88
9.593	4.816E+00	1.830E+00	-1.844E+00	4.816E+00	1.830E+00	-1.844E+00	1.752E-07	-1.763E-07	3.833E-07	1.750E-07	-1.759E-07	3.844E-07	99.88	99.79	100.30
10.169	5.231E+00	1.853E+00	1.208E+00	5.231E+00	1.853E+00	1.208E+00	1.766E-07	1.052E-07	1.049E-06	1.764E-07	1.019E-07	1.048E-06	99.88	96.83	99.92
10.677	5.637E+00	2.167E+00	1.430E+00	5.637E+00	2.167E+00	1.430E+00	2.105E-07	-1.062E-06	2.526E-04	2.102E-07	-1.060E-06	2.500E-04	99.88	99.77	98.97
11.060	5.951E+00	1.838E+00	-3.831E+00	5.951E+00	1.838E+00	-3.831E+00	1.817E-07	-4.062E-07	7.554E-06	1.815E-07	-4.052E-07	7.494E-06	99.87	99.76	99.20
11.366	6.166E+00	1.739E+00	2.437E+00	6.166E+00	1.739E+00	2.437E+00	1.711E-07	2.221E-07	1.005E-04	1.709E-07	2.217E-07	1.006E-04	99.87	99.80	100.12
11.573	6.315E+00	1.905E+00	1.544E+00	6.315E+00	1.905E+00	1.544E+00	1.711E-07	1.620E-07	-2.098E-05	1.709E-07	1.617E-07	-2.109E-05	99.87	99.83	100.54
11.814	6.527E+00	1.891E+00	3.543E-01	6.527E+00	1.891E+00	3.543E-01	1.722E-07	5.837E-08	1.640E-05	1.720E-07	5.715E-08	1.692E-05	99.87	97.91	103.19
12.291	6.962E+00	2.769E+00	-2.197E+00	6.962E+00	2.769E+00	-2.197E+00	2.602E-07	-1.499E-07	1.143E-05	2.599E-07	-1.498E-07	1.139E-05	99.87	99.94	99.65
12.586	7.266E+00	2.874E+00	8.956E-01	7.266E+00	2.874E+00	8.956E-01	2.754E-07	1.404E-07	-1.056E-06	2.750E-07	1.403E-07	-1.055E-06	99.87	99.95	99.90
12.965	7.743E+00	3.130E+00	2.871E+00	7.743E+00	3.130E+00	2.871E+00	3.108E-07	3.954E-07	1.976E-06	3.104E-07	3.951E-07	1.978E-06	99.86	99.93	100.09
13.167	8.002E+00	3.324E+00	9.023E-01	8.002E+00	3.324E+00	9.023E-01	3.358E-07	8.251E-08	-8.198E-06	3.353E-07	8.248E-08	-8.200E-06	99.86	99.96	100.02
13.325	8.223E+00	3.270E+00	-1.985E+00	8.223E+00	3.270E+00	-1.985E+00	3.255E-07	-3.045E-09	-4.391E-07	3.250E-07	-3.044E-09	-4.387E-07	99.86	99.96	99.91
13.568	8.527E+00	3.166E+00	-1.092E-01	8.527E+00	3.166E+00	-1.092E-01	3.118E-07	1.533E-08	1.034E-05	3.113E-07	1.532E-08	1.034E-05	99.85	99.96	99.97
13.786	8.793E+00	3.165E+00	-6.624E-02	8.793E+00	3.165E+00	-6.624E-02	3.128E-07	-2.875E-08	2.390E-04	3.123E-07	-2.874E-08	2.389E-04	99.83	99.96	99.97
14.242	9.353E+00	3.145E+00	-7.601E-02	9.353E+00	3.145E+00	-7.601E-02	3.126E-07	8.921E-08	1.304E-06	3.120E-07	8.917E-08	1.303E-06	99.81	99.96	99.96
14.526	9.726E+00	3.143E+00	-1.737E-02	9.726E+00	3.143E+00	-1.737E-02	3.373E-07	1.596E-09	6.373E-08	3.366E-07	1.595E-09	6.366E-08	99.78	99.96	99.89
14.876	1.018E+01	3.216E+00	6.730E+00	1.018E+01	3.216E+00	6.730E+00	3.854E-07	1.476E-06	5.072E-05	3.844E-07	1.475E-06	5.077E-05	99.74	99.96	100.10
15.170	6.527E+00	1.890E+00	-3.543E-01	6.527E+00	1.890E+00	-3.543E-01	1.722E-07	5.837E-08	1.640E-05	1.716E-07	5.835E-08	1.641E-05	99.68	99.96	100.06
15.373	1.090E+01	3.401E+00	-5.891E+00	1.090E+01	3.401E+00	-5.891E+00	3.997E-07	-2.081E-06	2.381E-05	3.980E-07	-2.080E-06	2.382E-05	99.57	99.96	100.04
15.559	1.112E+01	3.261E+00	1.882E+00	1.112E+01	3.261E+00	1.882E+00	3.260E-07	-2.282E-07	2.675E-04	3.239E-07	-2.281E-07	2.676E-04	99.35	99.95	100.02
15.796	1.146E+01	3.594E+00	-1.346E+00	1.146E+01	3.594E+00	-1.346E+00	3.399E-07	-5.595E-07	-2.432E-04	3.377E-07	-5.592E-07	-2.432E-04	99.35	99.95	99.98
16.119	1.181E+01	2.327E+00	-4.513E+00	1.181E+01	2.327E+00	-4.513E+00	1.395E-07	-1.328E-06	4.578E-06	1.377E-07	-1.327E-06	4.578E-06	98.73	99.95	99.99

Figure 5.6a Sensitivity Verification for $w(t)$ due to Change of $\boldsymbol{B}^{z}_{20,6}$

B	C	D	E	F	G	H	I	J	K	L	M	N	O	P	Q
Time	Original Design			After Perturbation (+0.1)			Finite Difference			Sensitivity			Accuracy		
(Sec.)	u	$\dot{u}$	$\ddot{u}$	u	$\dot{u}$	$\ddot{u}$	u	$\dot{u}$	$\ddot{u}$	u	$\dot{u}$	$\ddot{u}$	u	$\dot{u}$	$\ddot{u}$
0.290	4.996E-01	-5.342E-03	-4.723E-02	4.996E-01	-5.342E-03	-4.723E-02	1.904E-13	1.380E-10	3.303E-08	1.904E-13	1.380E-10	3.300E-08	100.00	100.00	99.91
1.064	4.947E-01	-4.172E-02	-1.723E-01	4.947E-01	-4.172E-02	-1.723E-01	1.506E-10	-1.308E-11	4.188E-08	1.506E-10	-1.308E-11	4.182E-08	100.00	100.00	99.85
1.614	4.969E-01	9.164E-02	-2.353E+00	4.969E-01	9.164E-02	-2.353E+00	-3.395E-10	1.445E-09	-1.993E-04	-3.395E-10	1.445E-09	-1.993E-04	100.00	100.00	100.02
1.964	4.997E-01	-4.050E-02	-1.903E-01	4.997E-01	-4.050E-02	-1.903E-01	1.978E-10	1.116E-10	-4.383E-08	1.978E-10	1.116E-10	-4.383E-08	100.00	100.00	99.99
2.574	4.927E-01	-1.229E-01	-1.132E+00	4.927E-01	-1.229E-01	-1.132E+00	-5.117E-10	1.338E-09	5.427E-08	-5.117E-10	1.337E-09	5.425E-08	99.99	99.99	99.96
3.614	1.223E+00	1.623E+00	-3.625E+00	1.223E+00	1.623E+00	-3.625E+00	2.795E-09	-1.691E-10	3.708E-07	2.794E-09	-1.690E-10	3.701E-07	99.99	99.97	99.81
3.631	5.358E-01	4.947E-01	-3.648E+00	5.358E-01	4.947E-01	-3.648E+00	1.039E-09	-4.210E-09	5.295E-08	1.039E-09	-4.207E-09	5.295E-08	99.98	99.95	99.99
3.631	5.358E-01	4.947E-01	-3.648E+00	5.358E-01	4.947E-01	-3.648E+00	1.039E-09	-4.210E-09	5.295E-08	1.039E-09	-4.207E-09	5.335E-08	99.97	99.94	100.75
4.030	6.062E-01	4.974E-01	1.514E+00	6.062E-01	4.974E-01	1.514E+00	1.652E-09	8.999E-09	-4.998E-08	1.652E-09	8.993E-09	-4.992E-08	99.97	99.94	99.88
5.016	6.172E-01	-5.330E-01	8.896E-01	6.172E-01	-5.330E-01	8.896E-01	-9.412E-10	-3.241E-09	2.389E-07	-9.409E-10	-3.239E-09	2.387E-07	99.97	99.93	99.90
6.011	2.577E+00	1.712E+00	-4.889E-01	2.577E+00	1.712E+00	-4.889E-01	8.078E-09	5.140E-09	-5.405E-08	8.076E-09	5.136E-09	-5.399E-08	99.97	99.93	99.89
5.504	5.268E-01	-5.682E-01	-5.702E+00	5.268E-01	-5.682E-01	-5.702E+00	-1.686E-09	-1.938E-08	-7.046E-07	-1.685E-09	-1.936E-08	-7.038E-07	99.96	99.92	99.89
5.616	4.972E-01	-5.932E-01	1.163E+01	4.972E-01	-5.932E-01	1.163E+01	-1.833E-09	3.405E-08	1.472E-06	-1.832E-09	3.402E-08	1.471E-06	99.96	99.91	99.87
5.744	4.736E-01	-2.270E-01	3.302E+00	4.736E-01	-2.270E-01	3.302E+00	-7.422E-10	1.023E-08	-6.124E-08	-7.419E-10	1.022E-08	-6.114E-08	99.95	99.89	99.84
6.147	4.754E-01	2.470E-01	3.282E+00	4.754E-01	2.470E-01	3.282E+00	7.628E-10	1.326E-08	-4.450E-07	7.623E-10	1.325E-08	-4.441E-07	99.94	99.88	99.79
7.233	6.470E-01	1.292E-01	-3.385E+00	6.470E-01	1.292E-01	-3.385E+00	2.002E-09	-1.714E-08	-9.489E-08	2.001E-09	-1.711E-08	-9.467E-08	99.94	99.87	99.76
7.755	6.137E-01	-3.836E-01	-2.562E-01	6.137E-01	-3.836E-01	-2.562E-01	-1.498E-09	-9.628E-09	3.645E-07	-1.497E-09	-9.615E-09	3.631E-07	99.93	99.86	99.61
8.361	5.108E-01	-6.565E-01	-2.594E+00	5.108E-01	-6.565E-01	-2.594E+00	-4.859E-09	-2.533E-08	3.328E-06	-4.855E-09	-2.530E-08	3.305E-06	99.93	99.85	99.32
8.911	4.759E-01	2.480E-01	4.055E+00	4.759E-01	2.480E-01	4.055E+00	1.610E-09	3.187E-08	5.720E-07	1.609E-09	3.182E-08	5.990E-07	99.92	99.84	104.71
9.265	5.437E-01	5.054E-01	-1.418E+00	5.437E-01	5.054E-01	-1.418E+00	4.285E-09	8.313E-10	1.333E-06	4.281E-09	8.298E-10	1.338E-06	99.92	99.82	100.38
9.623	6.344E-01	7.739E-01	1.299E+00	6.344E-01	7.739E-01	1.299E+00	8.841E-09	2.646E-08	-1.386E-06	8.833E-09	2.641E-08	-1.388E-06	99.91	99.80	100.16
10.483	7.718E-01	-1.435E-01	-5.848E+00	7.718E-01	-1.435E-01	-5.848E+00	2.011E-09	-6.170E-08	-1.377E-08	2.009E-09	-6.156E-08	-1.378E-08	99.90	99.78	100.07
10.769	7.238E-01	-7.878E-01	-8.939E+00	7.238E-01	-7.878E-01	-8.939E+00	-4.910E-09	-9.659E-08	1.524E-04	-4.905E-09	-9.635E-08	1.524E-04	99.90	99.74	100.03
11.510	4.088E-01	-1.376E+00	-5.951E+00	4.088E-01	-1.376E+00	-5.951E+00	-7.251E-09	-2.498E-08	3.771E-05	-7.242E-09	-2.461E-08	3.769E-05	99.88	98.52	99.94
11.814	2.736E-01	-3.761E-01	9.423E+00	2.736E-01	-3.761E-01	9.423E+00	6.287E-10	7.021E-08	-2.255E-05	6.277E-10	7.039E-08	-2.253E-05	99.85	100.25	99.92
12.044	2.647E-01	1.758E-02	-1.677E+00	2.647E-01	1.758E-02	-1.677E+00	3.294E-09	-2.948E-08	-4.384E-06	3.288E-09	-2.951E-08	-4.380E-06	99.81	100.08	99.91
12.323	2.516E-01	3.895E-02	4.607E+00	2.516E-01	3.895E-02	4.607E+00	3.315E-09	4.356E-08	-7.698E-07	3.306E-09	4.357E-08	-7.688E-07	99.74	100.03	99.88
12.512	2.620E-01	2.373E-01	2.961E+00	2.620E-01	2.373E-01	2.961E+00	5.349E-09	2.312E-08	-4.458E-06	5.327E-09	2.312E-08	-4.451E-06	99.59	100.00	99.83
12.586	7.266E+00	2.874E+00	8.956E-01	7.266E+00	2.874E+00	8.956E-01	2.754E-08	1.404E-08	-1.056E-07	2.723E-08	1.404E-08	-1.052E-07	98.86	99.98	99.62
12.735	2.928E-01	5.252E-01	3.562E+00	2.928E-01	5.252E-01	3.562E+00	8.514E-09	4.151E-08	-5.736E-08	8.617E-09	4.149E-08	-5.762E-08	101.20	99.97	100.45
13.117	3.876E-01	2.621E-01	-9.210E+00	3.876E-01	2.621E-01	-9.210E+00	3.007E-09	-1.348E-07	-1.504E-07	3.018E-09	-1.347E-07	-1.506E-07	100.37	99.95	100.13
13.299	3.796E-01	-4.735E-01	-9.341E+00	3.796E-01	-4.735E-01	-9.341E+00	-7.474E-09	-1.290E-07	8.608E-07	-7.490E-09	-1.289E-07	8.613E-07	100.21	99.93	100.06
13.568	8.527E+00	3.166E+00	-1.092E-01	8.527E+00	3.166E+00	-1.092E-01	3.118E-08	1.533E-09	1.034E-06	3.123E-08	1.531E-09	1.035E-06	100.14	99.90	100.05
13.596	2.948E-01	-6.077E-01	3.635E+00	2.948E-01	-6.077E-01	3.635E+00	-7.672E-09	7.167E-08	-7.304E-06	-7.680E-09	7.157E-08	-7.307E-06	100.10	99.86	100.04
13.843	2.517E-01	-3.065E-01	2.596E+00	2.517E-01	-3.065E-01	2.596E+00	-1.597E-09	4.889E-08	-2.782E-05	-1.598E-09	4.880E-08	-2.783E-05	100.07	99.80	100.04
14.284	2.355E-01	1.193E-01	2.375E+00	2.355E-01	1.193E-01	2.375E+00	9.984E-09	9.777E-08	-4.967E-08	9.989E-09	9.745E-08	-4.969E-08	100.05	99.68	100.04
14.876	1.018E+01	3.216E+00	6.730E+00	1.018E+01	3.216E+00	6.730E+00	3.854E-08	1.476E-07	5.072E-06	3.855E-08	1.467E-07	5.074E-06	100.03	99.38	100.04
14.808	3.203E-01	7.556E-01	3.338E+00	3.203E-01	7.556E-01	3.338E+00	3.798E-08	1.662E-07	7.589E-05	3.798E-08	1.625E-07	7.592E-05	100.01	97.74	100.04
15.629	2.420E-01	-4.824E-01	8.098E+00	2.420E-01	-4.824E-01	8.098E+00	-4.409E-08	-6.443E-08	-2.666E-06	-4.408E-08	-6.619E-08	-2.668E-06	99.99	102.74	100.07
15.850	2.314E-01	1.917E-01	1.581E+00	2.314E-01	1.917E-01	1.581E+00	-5.322E-08	-2.179E-07	-5.445E-06	-5.321E-08	-2.202E-07	-5.450E-06	99.97	101.06	100.09
15.961	2.444E-01	3.168E-01	4.929E+00	2.444E-01	3.168E-01	4.929E+00	-7.118E-08	-4.086E-07	-3.768E-06	-7.114E-08	-4.114E-07	-3.771E-06	99.95	100.69	100.07
16.119	2.654E-01	6.463E-01	9.166E+00	2.654E-01	6.463E-01	9.166E+00	-9.259E-08	-4.812E-07	1.714E-05	-9.251E-08	-4.837E-07	1.715E-05	99.92	100.52	100.09

Figure 5.6b Sensitivity Verification for $u(t)$ due to Change of $\boldsymbol{B}^{z}_{20,6}$

B	C	D	E	F	G	H	I	J	K	L	M	N	O	P	Q
Time	Original Design			After Perturbation (+0.1)			Finite Difference			Sensitivity			Accuracy		
(Sec.)	w	$\dot{w}$	$\ddot{w}$	w	$\dot{w}$	$\ddot{w}$	w	$\dot{w}$	$\ddot{w}$	w	$\dot{w}$	$\ddot{w}$	w	$\dot{w}$	$\ddot{w}$
0.097	6.735E-03	1.393E-01	1.438E+00	6.735E-03	1.393E-01	1.438E+00	0.000E+00	0.000E+00	0.000E+00	0.000E+00	0.000E+00	0.000E+00	N/A	N/A	N/A
1.290	1.910E-01	7.421E-01	1.474E+00	1.910E-01	7.421E-01	1.474E+00	0.000E+00	0.000E+00	0.000E+00	0.000E+00	0.000E+00	0.000E+00	N/A	N/A	N/A
1.978	5.305E-01	1.227E+00	2.143E+00	4.646E-01	1.129E+00	1.453E+00	-6.593E-01	-9.783E-01	-6.903E+00	-6.588E-01	-9.771E-01	-6.770E+00	99.93	99.88	98.07
2.373	9.183E-01	8.989E-01	3.361E-01	6.895E-01	1.344E+00	-2.802E+00	-2.288E+00	4.455E+00	-3.138E+01	-2.285E+00	4.445E+00	-3.106E+01	99.88	99.77	98.97
2.990	1.204E+00	1.655E+00	-1.830E+00	9.145E-01	8.973E-01	2.640E-01	-2.895E+00	-7.577E+00	2.094E+01	-2.889E+00	-7.574E+00	2.093E+01	99.81	99.96	99.96
3.574	1.458E+00	1.291E+00	-7.284E-01	1.212E+00	1.732E+00	-3.413E+00	-2.457E+00	4.409E+00	-2.685E+01	-2.465E+00	4.389E+00	-2.684E+01	100.34	99.55	99.97
3.756	1.806E+00	1.228E+00	2.783E-01	1.331E+00	1.433E+00	-1.950E+00	-4.751E+00	2.054E+00	-2.228E+01	-4.773E+00	2.055E+00	-2.228E+01	100.47	100.04	99.99
4.275	2.111E+00	1.456E+00	1.396E+00	1.589E+00	1.218E+00	-8.520E-01	-5.218E+00	-2.377E+00	-2.248E+01	-5.216E+00	-2.379E+00	-2.245E+01	99.96	100.08	99.86
5.049	2.286E+00	1.606E+00	1.486E+00	1.975E+00	1.241E+00	8.687E-01	-3.112E+00	-3.652E+00	-6.173E+00	-3.114E+00	-3.640E+00	-6.174E+00	100.05	99.67	100.02
5.553	2.498E+00	1.721E+00	1.105E-01	2.243E+00	1.526E+00	1.433E+00	-2.554E+00	-1.951E+00	1.322E+01	-2.532E+00	-1.950E+00	1.322E+01	99.14	99.97	100.02
5.777	2.759E+00	1.588E+00	-1.669E+00	2.378E+00	1.668E+00	1.475E+00	-3.809E+00	7.979E-01	3.144E+01	-3.804E+00	7.966E-01	3.147E+01	99.87	99.84	100.10
6.220	2.759E+00	1.588E+00	-1.669E+00	2.378E+00	1.668E+00	1.475E+00	-3.809E+00	7.979E-01	3.144E+01	-3.861E+00	7.920E-01	3.146E+01	101.36	99.26	100.06
7.066	3.637E+00	1.408E+00	1.504E+00	3.208E+00	1.393E+00	-1.193E+00	-4.290E+00	-1.479E-01	-2.697E+01	-4.213E+00	-1.462E-01	-2.699E+01	98.21	98.85	100.08
7.723	3.868E+00	1.659E+00	1.712E+00	3.534E+00	1.226E+00	6.120E-01	-3.342E+00	-4.334E+00	-1.100E+01	-3.298E+00	-4.310E+00	-1.101E+01	98.67	99.45	100.12
8.421	4.198E+00	1.943E+00	6.696E-01	3.902E+00	1.629E+00	1.992E+00	-2.961E+00	-3.143E+00	1.322E+01	-2.935E+00	-3.121E+00	1.312E+01	99.13	99.31	99.22
8.775	4.468E+00	1.849E+00	5.345E-01	4.172E+00	1.943E+00	1.609E+00	-2.962E+00	9.384E-01	1.074E+01	-2.945E+00	9.750E-01	1.062E+01	99.42	103.90	98.87
9.261	4.787E+00	1.859E+00	-1.910E+00	4.540E+00	2.001E+00	1.856E+00	-2.475E+00	1.421E+00	3.766E+01	-2.469E+00	1.158E+00	3.859E+01	99.74	81.51	102.46
9.427	5.116E+00	1.794E+00	7.461E-01	4.692E+00	2.064E+00	-1.125E+00	-4.239E+00	2.695E+00	-1.871E+01	-4.236E+00	2.692E+00	-1.889E+01	99.94	99.88	100.97
9.733	5.477E+00	2.101E+00	1.890E+00	4.944E+00	1.795E+00	-1.607E+00	-5.326E+00	-3.061E+00	-3.497E+01	-5.320E+00	-3.053E+00	-3.463E+01	99.89	99.73	99.04
10.163	5.729E+00	2.271E+00	3.453E+00	5.239E+00	1.800E+00	9.330E-01	-4.901E+00	-4.714E+00	-2.520E+01	-4.894E+00	-4.712E+00	-2.521E+01	99.86	99.96	100.02
10.739	6.082E+00	1.700E+00	-3.865E-01	5.706E+00	2.239E+00	3.725E+00	-3.761E+00	5.389E+00	4.111E+01	-3.781E+00	5.384E+00	4.110E+01	100.54	99.91	99.97
11.056	6.188E+00	1.772E+00	2.421E+00	5.992E+00	1.703E+00	-2.458E+00	-1.961E+00	-6.948E-01	-4.879E+01	-1.968E+00	-6.952E-01	-4.879E+01	100.36	100.06	99.99
11.424	6.460E+00	1.914E+00	-1.656E+00	6.204E+00	1.761E+00	2.396E+00	-2.565E+00	-1.531E+00	4.052E+01	-2.562E+00	-1.532E+00	4.078E+01	99.89	100.06	100.63
11.644	6.918E+00	2.819E+00	-4.077E+00	6.366E+00	1.883E+00	7.470E-01	-5.523E+00	-9.360E+00	4.824E+01	-5.525E+00	-9.248E+00	4.825E+01	100.04	98.80	100.03
12.179	7.352E+00	2.904E+00	1.133E+00	6.827E+00	2.692E+00	7.323E+00	-5.247E+00	-2.118E+00	6.190E+01	-5.232E+00	-2.117E+00	6.192E+01	99.71	99.97	100.03
12.503	7.700E+00	3.092E+00	2.553E+00	7.178E+00	2.749E+00	1.359E+00	-5.216E+00	-3.435E+00	-1.194E+01	-5.209E+00	-3.430E+00	-1.195E+01	99.87	99.84	100.10
12.919	7.962E+00	3.309E+00	1.093E+01	7.614E+00	2.914E+00	8.458E+00	-3.481E+00	-3.950E+00	-2.472E+01	-3.474E+00	-4.018E+00	-2.483E+01	99.79	101.72	100.44
13.066	8.122E+00	3.320E+00	-1.068E+00	7.788E+00	2.987E+00	1.252E+00	-3.342E+00	-3.329E+00	2.320E+01	-3.333E+00	-3.364E+00	2.334E+01	99.73	101.06	100.61
13.546	8.753E+00	3.166E+00	-3.529E-02	8.389E+00	3.349E+00	3.196E+00	-3.641E+00	1.833E+00	3.231E+01	-3.575E+00	1.811E+00	3.230E+01	98.20	98.78	99.98
13.756	9.093E+00	3.154E+00	-1.289E-01	8.689E+00	3.402E+00	-2.308E+00	-4.039E+00	2.475E+00	-2.179E+01	-3.980E+00	2.459E+00	-2.179E+01	98.53	99.37	100.02
14.006	9.528E+00	3.143E+00	7.198E-02	9.006E+00	3.146E+00	-5.746E+00	-5.218E+00	3.491E-02	-5.818E+01	-5.171E+00	3.468E-02	-5.751E+01	99.10	99.35	98.84
14.240	9.856E+00	3.151E+00	4.220E-01	9.321E+00	3.130E+00	-5.356E-01	-5.355E+00	-2.082E-01	-9.576E+00	-5.308E+00	-2.061E-01	-9.532E+00	99.12	99.01	99.54
14.648	1.035E+01	3.678E+00	6.294E+00	9.832E+00	3.615E+00	-1.570E-01	-5.184E+00	-6.292E-01	-6.451E+01	-5.157E+00	-6.435E-01	-6.399E+01	99.48	102.28	99.20
15.072	1.060E+01	3.751E+00	-2.278E+00	1.035E+01	3.699E+00	3.280E-01	-2.506E+00	-5.221E-01	2.606E+01	-2.500E+00	-4.986E-01	2.666E+01	99.75	95.49	102.31
15.421	1.099E+01	3.277E+00	-3.063E+00	1.081E+01	3.234E+00	9.700E-02	-1.816E+00	-4.341E-01	3.160E+01	-1.815E+00	-4.336E-01	3.191E+01	99.94	99.88	100.97
15.806	1.131E+01	3.367E+00	2.548E+00	1.131E+01	3.391E+00	8.120E-01	9.092E-04	2.388E-01	-1.736E+01	9.081E-04	2.383E-01	-1.741E+01	99.88	99.79	100.30
15.986	1.164E+01	2.844E+00	-1.222E+01	1.154E+01	3.269E+00	-1.701E+01	-9.786E-01	4.245E+00	-4.792E+01	-9.772E-01	4.243E+00	-4.793E+01	99.86	99.96	100.02
16.213	1.185E+01	2.253E+00	-3.457E+00	1.178E+01	2.384E+00	-3.741E+00	-7.238E-01	1.305E+00	-2.841E+00	-7.207E-01	1.304E+00	-2.842E+00	99.57	99.96	100.04

Figure 5.6c Sensitivity Verification for $w(t)$ due to Change of $\boldsymbol{B}^{y}_{5,7}$

B	C	D	E	F	G	H	I	J	K	L	M	N	O	P	Q
Time	Original Design			After Perturbation (+0.1)			Finite Difference			Sensitivity			Accuracy		
(Sec.)	w	$\dot{w}$	$\ddot{w}$	w	$\dot{w}$	$\ddot{w}$	w	$\dot{w}$	$\ddot{w}$	w	$\dot{w}$	$\ddot{w}$	w	$\dot{w}$	$\ddot{w}$
0.097	6.735E-03	1.393E-01	1.438E+00	6.735E-03	1.393E-01	1.438E+00	0.000E+00	0.000E+00	0.000E+00	0.000E+00	0.000E+00	0.000E+00	N/A	N/A	N/A
1.290	1.910E-01	7.421E-01	1.474E+00	1.910E-01	7.421E-01	1.474E+00	0.000E+00	0.000E+00	0.000E+00	0.000E+00	0.000E+00	0.000E+00	N/A	N/A	N/A
1.978	5.305E-01	1.227E+00	2.143E+00	4.646E-01	1.129E+00	1.453E+00	-6.593E-01	-9.783E-01	-6.903E+00	-6.588E-01	-9.771E-01	-6.770E+00	99.93	99.88	98.07
2.373	9.183E-01	8.989E-01	3.361E-01	6.895E-01	1.344E+00	-2.802E+00	-2.288E+00	4.455E+00	-3.138E+01	-2.285E+00	4.445E+00	-3.106E+01	99.88	99.77	98.97
2.990	1.204E+00	1.655E+00	-1.830E+00	9.145E-01	8.973E-01	2.640E-01	-2.895E+00	-7.577E+00	2.094E+01	-2.889E+00	-7.574E+00	2.093E+01	99.81	99.96	99.96
3.574	1.458E+00	1.291E+00	-7.284E-01	1.212E+00	1.732E+00	-3.413E+00	-2.457E+00	4.409E+00	-2.685E+01	-2.465E+00	4.389E+00	-2.684E+01	100.34	99.55	99.97
3.756	1.806E+00	1.228E+00	2.783E-01	1.331E+00	1.433E+00	-1.950E+00	-4.751E+00	2.054E+00	-2.228E+01	-4.773E+00	2.055E+00	-2.228E+01	100.47	100.04	99.99
4.275	2.111E+00	1.456E+00	1.396E+00	1.589E+00	1.218E+00	-8.520E-01	-5.218E+00	-2.377E+00	-2.248E+01	-5.216E+00	-2.379E+00	-2.245E+01	99.96	100.08	99.86
5.049	2.286E+00	1.606E+00	1.486E+00	1.975E+00	1.241E+00	8.687E-01	-3.112E+00	-3.652E+00	-6.173E+00	-3.114E+00	-3.640E+00	-6.174E+00	100.05	99.67	100.02
5.553	2.498E+00	1.721E+00	1.105E-01	2.243E+00	1.526E+00	1.433E+00	-2.554E+00	-1.951E+00	1.322E+01	-2.532E+00	-1.950E+00	1.322E+01	99.14	99.97	100.02
5.777	2.759E+00	1.588E+00	-1.669E+00	2.378E+00	1.668E+00	1.475E+00	-3.809E+00	7.979E-01	3.144E+01	-3.804E+00	7.966E-01	3.147E+01	99.87	99.84	100.10
6.220	2.759E+00	1.588E+00	-1.669E+00	2.378E+00	1.668E+00	1.475E+00	-3.809E+00	7.979E-01	3.144E+01	-3.861E+00	7.920E-01	3.146E+01	101.36	99.26	100.06
7.066	3.637E+00	1.408E+00	1.504E+00	3.208E+00	1.393E+00	-1.193E+00	-4.290E+00	-1.479E-01	-2.697E+01	-4.213E+00	-1.462E-01	-2.699E+01	98.21	98.85	100.08
7.723	3.868E+00	1.659E+00	1.712E+00	3.534E+00	1.226E+00	6.120E-01	-3.342E+00	-4.334E+00	-1.100E+01	-3.298E+00	-4.310E+00	-1.101E+01	98.67	99.45	100.12
8.421	4.198E+00	1.943E+00	6.696E-01	3.902E+00	1.629E+00	1.992E+00	-2.961E+00	-3.143E+00	1.322E+01	-2.935E+00	-3.121E+00	1.312E+01	99.13	99.31	99.22
8.775	4.468E+00	1.849E+00	5.345E-01	4.172E+00	1.943E+00	1.609E+00	-2.962E+00	9.384E-01	1.074E+01	-2.945E+00	9.750E-01	1.062E+01	99.42	103.90	98.87
9.261	4.787E+00	1.859E+00	-1.910E+00	4.540E+00	2.001E+00	1.856E+00	-2.475E+00	1.421E+00	3.766E+01	-2.469E+00	1.158E+00	3.859E+01	99.74	81.51	102.46
9.427	5.116E+00	1.794E+00	7.461E-01	4.692E+00	2.064E+00	-1.125E+00	-4.239E+00	2.695E+00	-1.871E+01	-4.236E+00	2.692E+00	-1.889E+01	99.94	99.88	100.97
9.733	5.477E+00	2.101E+00	1.890E+00	4.944E+00	1.795E+00	-1.607E+00	-5.326E+00	-3.061E+00	-3.497E+01	-5.320E+00	-3.053E+00	-3.463E+01	99.89	99.73	99.04
10.163	5.729E+00	2.271E+00	3.453E+00	5.239E+00	1.800E+00	9.330E-01	-4.901E+00	-4.714E+00	-2.520E+01	-4.894E+00	-4.712E+00	-2.521E+01	99.86	99.96	100.02
10.739	6.082E+00	1.700E+00	-3.865E-01	5.706E+00	2.239E+00	3.725E+00	-3.761E+00	5.389E+00	4.111E+01	-3.781E+00	5.384E+00	4.110E+01	100.54	99.91	99.97
11.056	6.188E+00	1.772E+00	2.421E+00	5.992E+00	1.703E+00	-2.458E+00	-1.961E+00	-6.948E-01	-4.879E+01	-1.968E+00	-6.952E-01	-4.879E+01	100.36	100.06	99.99
11.424	6.460E+00	1.914E+00	-1.656E+00	6.204E+00	1.761E+00	2.396E+00	-2.565E+00	-1.531E+00	4.052E+01	-2.562E+00	-1.532E+00	4.078E+01	99.89	100.06	100.63
11.644	6.918E+00	2.819E+00	-4.077E+00	6.366E+00	1.883E+00	7.470E-01	-5.523E+00	-9.360E+00	4.824E+01	-5.525E+00	-9.248E+00	4.825E+01	100.04	98.80	100.03
12.179	7.352E+00	2.904E+00	1.133E+00	6.827E+00	2.692E+00	7.323E+00	-5.247E+00	-2.118E+00	6.190E+01	-5.232E+00	-2.117E+00	6.192E+01	99.71	99.97	100.03
12.503	7.700E+00	3.092E+00	2.553E+00	7.178E+00	2.749E+00	1.359E+00	-5.216E+00	-3.435E+00	-1.194E+01	-5.209E+00	-3.430E+00	-1.195E+01	99.87	99.84	100.10
12.919	7.962E+00	3.309E+00	1.093E+01	7.614E+00	2.914E+00	8.458E+00	-3.481E+00	-3.950E+00	-2.472E+01	-3.474E+00	-4.018E+00	-2.483E+01	99.79	101.72	100.44
13.066	8.122E+00	3.320E+00	-1.068E+00	7.788E+00	2.987E+00	1.252E+00	-3.342E+00	-3.329E+00	2.320E+01	-3.333E+00	-3.364E+00	2.334E+01	99.73	101.06	100.61
13.546	8.753E+00	3.166E+00	-3.529E-02	8.389E+00	3.349E+00	3.196E+00	-3.641E+00	1.833E+00	3.231E+01	-3.575E+00	1.811E+00	3.230E+01	98.20	98.78	99.98
13.756	9.093E+00	3.154E+00	-1.289E-01	8.689E+00	3.402E+00	-2.308E+00	-4.039E+00	2.475E+00	-2.179E+01	-3.980E+00	2.459E+00	-2.179E+01	98.53	99.37	100.02
14.006	9.528E+00	3.143E+00	7.198E-02	9.006E+00	3.146E+00	-5.746E+00	-5.218E+00	3.491E-02	-5.818E+01	-5.171E+00	3.468E-02	-5.751E+01	99.10	99.35	98.84
14.240	9.856E+00	3.151E+00	4.220E-01	9.321E+00	3.130E+00	-5.356E-01	-5.355E+00	-2.082E-01	-9.576E+00	-5.308E+00	-2.061E-01	-9.532E+00	99.12	99.01	99.54
14.648	1.035E+01	3.678E+00	6.294E+00	9.832E+00	3.615E+00	-1.570E-01	-5.184E+00	-6.292E-01	-6.451E+01	-5.157E+00	-6.435E-01	-6.399E+01	99.48	102.28	99.20
15.072	1.060E+01	3.751E+00	-2.278E+00	1.035E+01	3.699E+00	3.280E-01	-2.506E+00	-5.221E-01	2.606E+01	-2.500E+00	-4.986E-01	2.666E+01	99.75	95.49	102.31
15.421	1.099E+01	3.277E+00	-3.063E+00	1.081E+01	3.234E+00	9.700E-02	-1.816E+00	-4.341E-01	3.160E+01	-1.815E+00	-4.336E-01	3.191E+01	99.94	99.88	100.97
15.806	1.131E+01	3.367E+00	2.548E+00	1.131E+01	3.391E+00	8.120E-01	9.092E-04	2.388E-01	-1.736E+01	9.081E-04	2.383E-01	-1.741E+01	99.88	99.79	100.30
15.986	1.164E+01	2.844E+00	-1.222E+01	1.154E+01	3.269E+00	-1.701E+01	-9.786E-01	4.245E+00	-4.792E+01	-9.772E-01	4.243E+00	-4.793E+01	99.86	99.96	100.02
16.213	1.185E+01	2.253E+00	-3.457E+00	1.178E+01	2.384E+00	-3.741E+00	-7.238E-01	1.305E+00	-2.841E+00	-7.207E-01	1.304E+00	-2.842E+00	99.57	99.96	100.04

Figure 5.6d Sensitivity Verification for w (t) due to change of $\boldsymbol{B}^{y}_{5,7}$

B	C	D	E	F	G	H	I	J	K	L	M	N	O	P	Q
Time	Original Design			After Perturbation (+1.0)			Finite Difference			Sensitivity			Accuracy		
(Sec.)	w	$\dot{w}$	$\ddot{w}$	w	$\dot{w}$	$\ddot{w}$	w	$\dot{w}$	$\ddot{w}$	w	$\dot{w}$	$\ddot{w}$	w	$\dot{w}$	$\ddot{w}$
0.097	6.735E-03	1.393E-01	1.438E+00	6.735E-03	1.393E-01	1.438E+00	0.000E+00	0.000E+00	0.000E+00	0.000E+00	0.000E+00	0.000E+00	N/A	N/A	N/A
1.290	1.910E-01	7.421E-01	1.474E+00	1.910E-01	7.421E-01	1.474E+00	0.000E+00	0.000E+00	0.000E+00	0.000E+00	0.000E+00	0.000E+00	N/A	N/A	N/A
1.963	4.803E-01	1.149E+00	1.577E+00	4.803E-01	1.149E+00	1.577E+00	0.000E+00	0.000E+00	0.000E+00	0.000E+00	0.000E+00	0.000E+00	N/A	N/A	N/A
2.373	4.744E-01	-4.644E-02	1.156E+00	5.041E-01	4.251E-02	-3.238E+00	2.971E-02	8.895E-02	-4.394E+00	2.971E-02	8.896E-02	-4.395E+00	100.00	100.00	100.02
2.857	9.183E-01	8.989E-01	3.361E-01	9.183E-01	8.989E-01	3.361E-01	1.155E-07	-1.052E-06	4.553E-05	1.155E-07	-1.052E-06	4.557E-05	100.00	100.00	100.11
3.540	1.182E+00	1.663E+00	5.994E-01	1.183E+00	1.764E+00	3.071E-02	9.487E-04	1.006E-01	-5.686E-01	9.479E-04	1.005E-01	-5.638E-01	99.92	99.88	99.14
3.740	1.332E+00	1.385E+00	-1.829E+00	1.332E+00	1.340E+00	-1.830E+00	5.841E-04	-4.490E-02	-5.864E-04	5.834E-04	-4.522E-02	-5.859E-04	99.88	100.70	99.91
4.307	1.589E+00	1.227E+00	-4.097E-01	1.589E+00	1.226E+00	-4.004E-01	-2.540E-05	-9.178E-04	9.238E-03	-2.520E-05	-9.170E-04	9.239E-03	99.19	99.92	100.01
5.044	1.954E+00	1.304E+00	7.786E+00	1.953E+00	1.303E+00	7.804E+00	-1.266E-03	-2.954E-04	1.810E-02	-1.262E-03	-2.967E-04	1.804E-02	99.67	100.45	99.70
5.568	2.267E+00	1.589E+00	1.339E+00	2.267E+00	1.590E+00	1.361E+00	-3.600E-04	1.254E-03	2.198E-02	-3.594E-04	1.316E-03	2.193E-02	99.83	104.92	99.77
5.739	2.287E+00	1.606E+00	1.488E+00	2.389E+00	1.688E+00	9.428E-01	1.022E-01	8.153E-02	-5.455E-01	1.021E-01	8.036E-02	-5.455E-01	99.94	98.57	100.00
6.241	2.629E+00	1.692E+00	-8.714E-01	2.727E+00	1.618E+00	-1.544E+00	9.897E-02	-7.359E-02	-6.722E-01	9.997E-02	-6.820E-02	-6.751E-01	101.01	92.67	100.43
7.055	3.141E+00	1.262E+00	-8.579E-01	3.199E+00	1.229E+00	-4.948E-01	5.746E-02	-3.290E-02	3.632E-01	5.838E-02	-3.360E-02	3.654E-01	101.60	102.12	100.63
7.770	3.502E+00	1.281E+00	9.292E-01	3.525E+00	1.299E+00	1.073E+00	2.292E-02	1.852E-02	1.435E-01	2.333E-02	1.716E-02	1.457E-01	101.79	92.63	101.52
8.045	3.527E+00	1.300E+00	7.504E+00	3.677E+00	1.452E+00	1.114E+01	1.495E-01	1.516E-01	3.639E+00	1.523E-01	1.493E-01	3.681E+00	101.87	98.51	101.14
8.747	4.076E+00	1.876E+00	1.402E+00	4.170E+00	1.933E+00	8.256E-01	9.426E-02	5.642E-02	-5.765E-01	9.608E-02	5.708E-02	-5.846E-01	101.93	101.16	101.41
9.284	4.502E+00	1.865E+00	1.157E+00	4.589E+00	1.937E+00	1.237E+00	8.648E-02	7.260E-02	8.060E-02	8.829E-02	7.583E-02	8.223E-02	102.09	104.45	102.02
9.492	4.589E+00	1.940E+00	1.254E+00	4.735E+00	1.907E+00	-1.749E+00	1.463E-01	-3.273E-02	-3.003E+00	1.495E-01	-3.426E-02	-3.092E+00	102.23	104.68	102.97
9.728	4.788E+00	1.859E+00	-1.337E+01	4.898E+00	1.762E+00	-5.940E+00	1.105E-01	-9.734E-02	7.435E+00	1.132E-01	-1.027E-01	7.801E+00	102.40	105.53	104.92
10.241	5.128E+00	1.799E+00	7.737E-01	5.266E+00	1.877E+00	1.423E+00	1.373E-01	7.851E-02	6.493E-01	1.372E-01	7.843E-02	6.482E-01	99.93	99.90	99.83
10.743	5.593E+00	2.150E+00	1.438E-01	5.680E+00	2.205E+00	2.494E+00	8.666E-02	5.441E-02	2.350E+00	8.651E-02	5.442E-02	2.345E+00	99.84	100.02	99.79
11.055	5.894E+00	2.005E+00	-5.596E+01	5.949E+00	1.842E+00	-2.728E+01	5.545E-02	-1.627E-01	2.868E+01	5.513E-02	-1.631E-01	2.878E+01	99.41	100.25	100.32
11.427	6.183E+00	1.764E+00	2.542E+00	6.226E+00	1.819E+00	2.120E+00	4.321E-02	5.488E-02	-4.214E-01	4.314E-02	5.758E-02	-4.204E-01	99.83	104.92	99.77
11.682	6.285E+00	1.880E+00	1.696E+00	6.424E+00	1.937E+00	-7.447E-01	1.386E-01	5.764E-02	-2.441E+00	1.386E-01	5.708E-02	-2.443E+00	99.98	99.02	100.10
12.127	6.629E+00	1.997E+00	3.904E+00	6.784E+00	2.593E+00	1.162E+01	1.548E-01	5.961E-01	7.715E+00	1.557E-01	5.896E-01	7.747E+00	100.54	98.91	100.42
12.505	7.048E+00	2.751E+00	8.973E-01	7.199E+00	2.848E+00	1.420E+00	1.505E-01	9.720E-02	5.224E-01	1.528E-01	9.912E-02	5.252E-01	101.51	101.97	100.53
12.919	7.526E+00	2.982E+00	1.468E+00	7.700E+00	3.095E+00	2.590E+00	1.737E-01	1.125E-01	1.122E+00	1.765E-01	1.147E-01	1.126E+00	101.58	101.90	100.38
13.220	7.948E+00	3.302E+00	1.784E+00	8.078E+00	3.328E+00	-4.610E-01	1.298E-01	2.598E-02	-2.245E+00	1.322E-01	2.474E-02	-2.276E+00	101.81	95.25	101.39
13.591	8.397E+00	3.183E+00	-8.776E-01	8.571E+00	3.165E+00	-4.235E-03	1.734E-01	-1.833E-02	8.733E-01	1.772E-01	-1.906E-02	8.738E-01	102.19	103.98	100.05
13.779	8.706E+00	3.166E+00	3.941E-04	8.791E+00	3.165E+00	-6.334E-02	8.510E-02	-8.648E-04	-6.373E-02	8.688E-02	-8.734E-04	-6.415E-02	102.09	100.99	100.66
14.113	9.049E+00	3.156E+00	-1.331E-01	9.223E+00	3.149E+00	-1.064E-01	1.741E-01	-6.235E-03	2.670E-02	1.770E-01	-6.383E-03	2.705E-02	101.66	102.38	101.33
14.582	9.701E+00	3.143E+00	-4.108E-02	9.788E+00	3.146E+00	1.919E-01	8.660E-02	3.231E-03	2.330E-01	8.841E-02	3.375E-03	2.377E-01	102.09	104.45	102.02
14.692	9.837E+00	3.149E+00	3.518E-01	9.962E+00	3.156E+00	-4.644E-01	1.256E-01	7.399E-03	-8.162E-01	1.284E-01	7.781E-03	-8.366E-01	102.29	105.17	102.50
15.066	1.040E+01	3.740E+00	2.790E+00	1.045E+01	3.774E+00	1.500E+00	4.917E-02	3.460E-02	-1.289E+00	4.914E-02	3.457E-02	-1.288E+00	99.94	99.91	99.86
15.421	1.076E+01	3.622E+00	-2.587E+01	1.094E+01	3.319E+00	-3.330E+01	1.857E-01	-3.032E-01	-7.433E+00	1.852E-01	-3.032E-01	-7.437E+00	99.73	99.98	100.05
15.790	1.131E+01	3.367E+00	2.548E+00	1.146E+01	3.594E+00	-1.379E+00	1.526E-01	2.273E-01	-3.927E+00	1.521E-01	2.283E-01	-3.915E+00	99.67	100.45	99.70
16.039	1.154E+01	3.383E+00	-1.630E+01	1.178E+01	2.395E+00	-5.571E+00	2.425E-01	-9.877E-01	1.073E+01	2.418E-01	-9.945E-01	1.071E+01	99.73	100.69	99.79
16.160	1.181E+01	2.327E+00	-4.516E+00	1.185E+01	2.248E+00	-3.438E+00	4.295E-02	-7.900E-02	1.079E+00	4.288E-02	-8.289E-02	1.076E+00	99.83	104.92	99.77

Figure 5.6e Sensitivity Verification for $w(t)$ due to Change of $\boldsymbol{B}^{x}_{8,8}$

B	C	D	E	F	G	H	I	J	K	L	M	N	O	P	Q
Time	Original Design			After Perturbation (+1.0)			Finite Difference			Sensitivity			Accuracy		
(Sec.)	u	$\dot{u}$	$\ddot{u}$	u	$\dot{u}$	$\ddot{u}$	u	$\dot{u}$	$\ddot{u}$	u	$\dot{u}$	$\ddot{u}$	u	$\dot{u}$	$\ddot{u}$
0.097	4.999E-01	-2.035E-03	-2.496E-02	4.999E-01	-2.035E-03	-2.496E-02	0.000E+00	0.000E+00	0.000E+00	0.000E+00	0.000E+00	0.000E+00	N/A	N/A	N/A
1.290	4.920E-01	-3.380E-02	6.157E-01	4.920E-01	-3.380E-02	6.157E-01	0.000E+00	0.000E+00	0.000E+00	0.000E+00	0.000E+00	0.000E+00	N/A	N/A	N/A
1.963	4.997E-01	-4.049E-02	-1.908E-01	4.997E-01	-4.049E-02	-1.908E-01	0.000E+00	0.000E+00	0.000E+00	0.000E+00	0.000E+00	0.000E+00	N/A	N/A	N/A
2.390	4.975E-01	-9.235E-03	-1.441E+00	4.975E-01	-9.235E-03	-1.441E+00	0.000E+00	0.000E+00	0.000E+00	0.000E+00	0.000E+00	0.000E+00	N/A	N/A	N/A
2.857	4.744E-01	-4.644E-02	1.156E+00	4.744E-01	-4.644E-02	1.156E+00	1.879E-07	4.715E-06	3.941E-05	1.879E-07	4.716E-06	3.937E-05	100.00	100.00	99.91
3.591	5.267E-01	5.615E-01	-3.979E+00	5.267E-01	5.888E-01	-4.868E+00	-1.569E-05	2.727E-02	-8.894E-01	-1.568E-05	2.724E-02	-8.882E-01	99.96	99.91	99.87
3.740	5.645E-01	3.978E-01	1.752E-01	5.649E-01	3.906E-01	7.939E-02	3.317E-04	-7.196E-03	-9.580E-02	3.314E-04	-7.182E-03	-9.596E-02	99.91	99.80	100.16
4.213	6.477E-01	4.640E-01	-2.752E+00	6.482E-01	4.626E-01	-2.789E+00	4.743E-04	-1.341E-03	-3.744E-02	4.753E-04	-1.340E-03	-3.746E-02	100.21	99.93	100.06
5.044	6.119E-01	-5.214E-01	1.433E+00	6.119E-01	-5.224E-01	1.443E+00	-1.890E-05	-1.008E-03	9.602E-03	-1.883E-05	-1.011E-03	9.618E-03	99.63	100.30	100.17
5.568	5.052E-01	-6.936E-01	3.328E+00	5.044E-01	-6.911E-01	4.370E+00	-7.948E-04	2.440E-03	1.042E+00	-8.113E-04	2.447E-03	1.041E+00	102.07	100.29	99.84
5.823	4.969E-01	-5.886E-01	1.173E+01	4.696E-01	-1.636E-01	3.026E+00	-2.738E-02	4.250E-01	-8.703E+00	-2.759E-02	4.265E-01	-8.725E+00	100.78	100.36	100.25
6.241	4.708E-01	1.798E-01	2.953E+00	4.877E-01	4.115E-01	6.055E+00	1.690E-02	2.317E-01	3.101E+00	1.718E-02	2.327E-01	3.120E+00	101.61	100.46	100.61
7.055	6.132E-01	3.829E-01	-1.908E-01	6.306E-01	3.302E-01	-2.045E+00	1.742E-02	-5.267E-02	-1.854E+00	1.746E-02	-5.293E-02	-1.878E+00	100.24	100.50	101.30
7.752	6.315E-01	-3.229E-01	-2.155E+00	6.135E-01	-3.850E-01	-2.358E-01	-1.799E-02	-6.202E-02	1.919E+00	-1.815E-02	-6.254E-02	1.927E+00	100.90	100.83	100.40
8.518	5.036E-01	-6.495E-01	4.568E+00	4.793E-01	-2.872E-01	3.930E+00	-2.428E-02	3.623E-01	-6.375E-01	-2.456E-02	3.652E-01	-6.403E-01	101.12	100.79	100.44
8.805	4.696E-01	-1.181E-01	3.111E+00	4.675E-01	5.651E-02	3.202E+00	-2.020E-03	1.746E-01	9.103E-02	-2.034E-03	1.765E-01	9.151E-02	100.68	101.06	100.53
9.284	5.314E-01	5.684E-01	-4.385E+00	5.551E-01	4.926E-01	1.398E-02	2.376E-02	-7.582E-02	4.399E+00	2.393E-02	-7.430E-02	4.417E+00	100.74	98.00	100.40
9.492	5.547E-01	4.912E-01	-1.064E-03	5.948E-01	5.927E-01	2.672E+00	4.008E-02	1.015E-01	2.673E+00	4.052E-02	1.017E-01	2.703E+00	101.10	100.23	101.10
9.806	6.343E-01	7.738E-01	1.302E+00	6.946E-01	6.116E-01	-2.960E+00	6.032E-02	-1.623E-01	-4.262E+00	6.076E-02	-1.658E-01	-4.310E+00	100.74	102.20	101.13
10.241	7.339E-01	4.123E-01	-2.126E+00	7.597E-01	2.761E-01	-1.390E+00	2.580E-02	-1.362E-01	7.363E-01	2.579E-02	-1.361E-01	7.356E-01	99.97	99.93	99.90
10.743	7.560E-01	-4.275E-01	-4.596E+00	7.340E-01	-6.699E-01	-7.462E+00	-2.194E-02	-2.425E-01	-2.866E+00	-2.191E-02	-2.431E-01	-2.864E+00	99.85	100.25	99.92
11.055	6.391E-01	-1.023E+00	8.143E+00	6.119E-01	-8.142E-01	5.818E+00	-2.728E-02	2.088E-01	-2.324E+00	-2.727E-02	2.111E-01	-2.327E+00	99.97	101.06	100.09
11.459	4.769E-01	-1.254E+00	3.662E+00	4.299E-01	-1.297E+00	-3.694E+00	-4.705E-02	-4.266E-02	-7.355E+00	-4.778E-02	-4.278E-02	-7.352E+00	101.55	100.30	99.95
11.775	3.585E-01	-1.459E+00	6.240E+00	2.816E-01	-5.575E-01	1.147E+01	-7.684E-02	9.014E-01	5.230E+00	-7.737E-02	9.051E-01	5.250E+00	100.69	100.41	100.37
12.127	2.643E-01	-2.578E-02	3.663E+00	2.631E-01	-1.451E-01	-5.498E+00	-1.197E-03	-1.193E-01	-9.161E+00	-1.206E-03	-1.198E-01	-9.203E+00	100.78	100.44	100.47
12.505	2.527E-01	1.007E-01	3.269E+00	2.622E-01	2.355E-01	2.920E+00	9.544E-03	1.348E-01	-3.491E-01	9.559E-03	1.355E-01	-3.503E-01	100.15	100.53	100.36
12.919	3.097E-01	6.297E-01	3.513E+00	3.513E-01	7.309E-01	-1.947E+00	4.164E-02	1.012E-01	-5.460E+00	4.177E-02	1.017E-01	-5.510E+00	100.32	100.45	100.91
13.220	3.895E-01	1.847E-01	-9.231E+00	3.893E-01	-1.924E-01	-9.460E+00	-1.940E-04	-3.771E-01	-2.285E-01	-1.958E-04	-3.804E-01	-2.299E-01	100.89	100.87	100.58
13.550	3.543E-01	-7.538E-01	-3.465E+00	3.118E-01	-6.990E-01	3.336E+00	-4.248E-02	5.473E-02	6.800E+00	-4.290E-02	5.517E-02	6.846E+00	100.99	100.82	100.68
13.731	2.868E-01	-5.582E-01	3.569E+00	2.685E-01	-4.323E-01	3.102E+00	-1.824E-02	1.259E-01	-4.661E-01	-1.855E-02	1.269E-01	-4.527E-01	101.70	100.77	97.12
14.099	2.412E-01	-2.033E-01	2.437E+00	2.339E-01	-6.811E-02	2.285E+00	-7.387E-03	1.352E-01	-1.521E-01	-7.448E-03	1.365E-01	-1.539E-01	100.82	100.95	101.17
14.320	2.326E-01	2.185E-02	2.320E+00	2.381E-01	1.581E-01	2.411E+00	5.545E-03	1.363E-01	9.142E-02	5.594E-03	1.370E-01	9.247E-02	100.88	100.54	101.15
14.651	2.654E-01	4.223E-01	3.179E+00	2.783E-01	5.136E-01	3.578E+00	1.290E-02	9.133E-02	3.988E-01	1.305E-02	9.154E-02	4.032E-01	101.10	100.23	101.10
15.066	3.846E-01	3.563E-01	-1.198E+01	3.891E-01	1.782E-01	-1.159E+01	4.453E-03	-1.782E-01	3.813E-01	4.452E-03	-1.780E-01	3.808E-01	99.97	99.94	99.88
15.420	3.659E-01	-7.411E-01	-1.022E+01	3.138E-01	-1.054E+00	-1.646E+00	-5.216E-02	-3.128E-01	8.573E+00	-5.203E-02	-3.129E-01	8.563E+00	99.74	100.03	99.88
15.790	2.330E-01	-3.089E-01	7.836E+00	2.242E-01	8.472E-02	7.637E+00	-8.753E-03	3.936E-01	-1.993E-01	-8.718E-03	3.948E-01	-1.997E-01	99.60	100.30	100.20
15.963	2.295E-01	1.615E-01	4.253E+00	2.405E-01	3.114E-01	5.179E+00	1.104E-02	1.499E-01	9.259E-01	1.096E-02	1.503E-01	9.278E-01	99.34	100.29	100.21
16.279	2.754E-01	7.737E-01	8.643E+00	3.508E-01	1.574E+00	1.467E+01	7.542E-02	8.008E-01	6.029E+00	7.611E-02	8.035E-01	6.039E+00	100.91	100.34	100.17

Figure 5.6f Sensitivity Verification for $u(t)$ due to Change of $\boldsymbol{B}^{x}_{8,8}$

5.5 Shape Design Optimization of B-Spline-Based Flume Sections

5.5.1 Flume Configuration for Optimization

The flume configuration for optimization is created from 14 basic B-Spline flume sections. The configuration was named William configuration by the author.

Table 5.1 Physical Sizes of William Configuration

Configuration	*S68D+CTL+LC45+LC90+LC90+LC90+LC90+CFL+S30 +CTR+RC45+RC90+RC90+RC90+CFR*
No. of Geometric Points	54×11
No. of Control Points	56×31
Knot Vector	$[u, w] \in [0, 10.6298] \times [0, 1]$
Size of Water Slide	W×L×H : 8.3 × 22.5 × 7.5 (ft)

Detailed shape representations in *Mathematica*® are shown in Figures 5.7a – 5.7c. Note that the representations in *Mathematica*® are much clearer and smoother than those in the *I-DEAS*® or *SolidWorks*® CAD Packages.

For this optimization, the Design Optimization Tool (*DOT*) [29] was used to carry out the optimization procedure. Interface programs were developed for retrieving information from the *Mathematica*® analysis software via specially coded FORTRAN programs. Once the initial control points were retrieved from *I-DEAS*®, the entire system was integrated and made functional. The environment was designed with the flexibility in mind to incorporate additional CAD packages, motion analyses, and/or optimization tools.

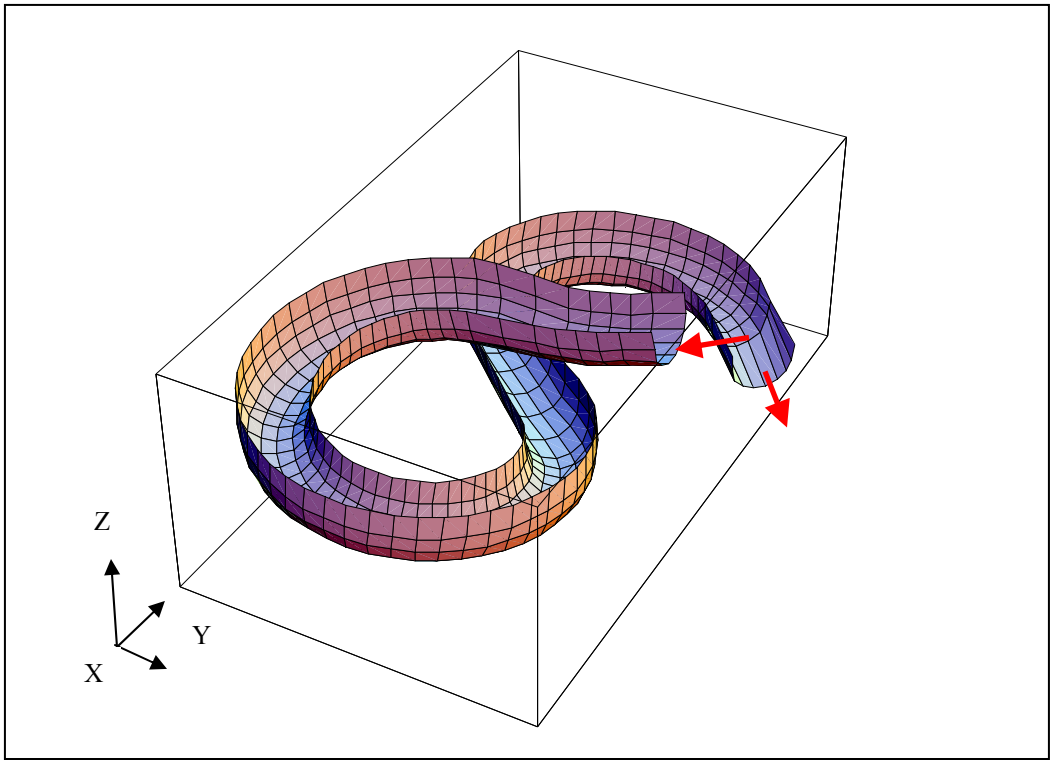


Figure 5.7a Isometric View of William Configuration

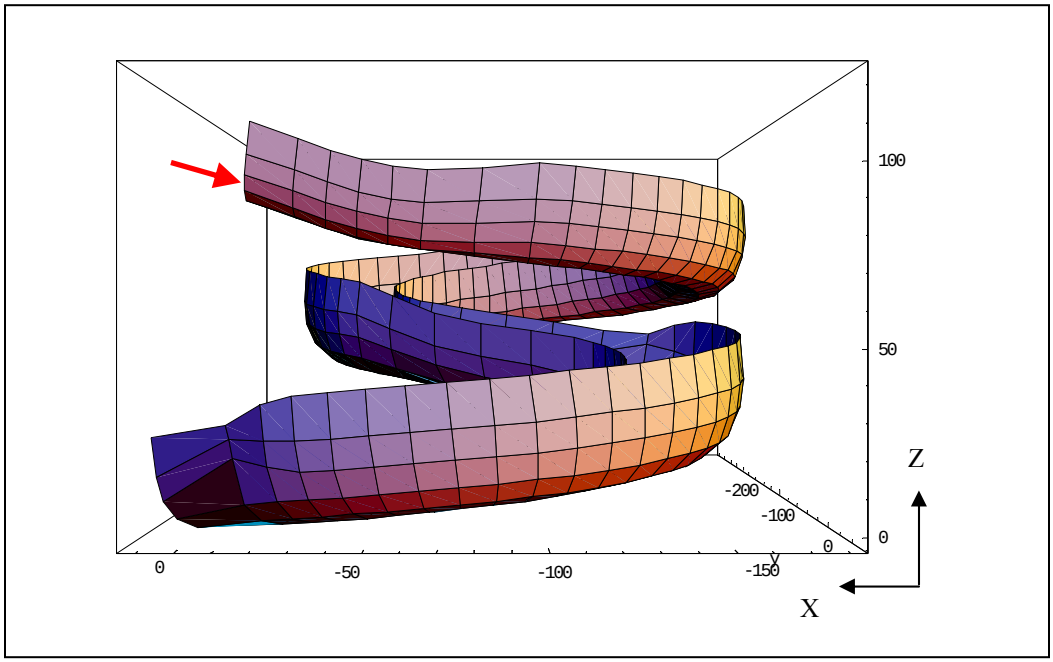


Figure 5.7b Front View of William Configuration

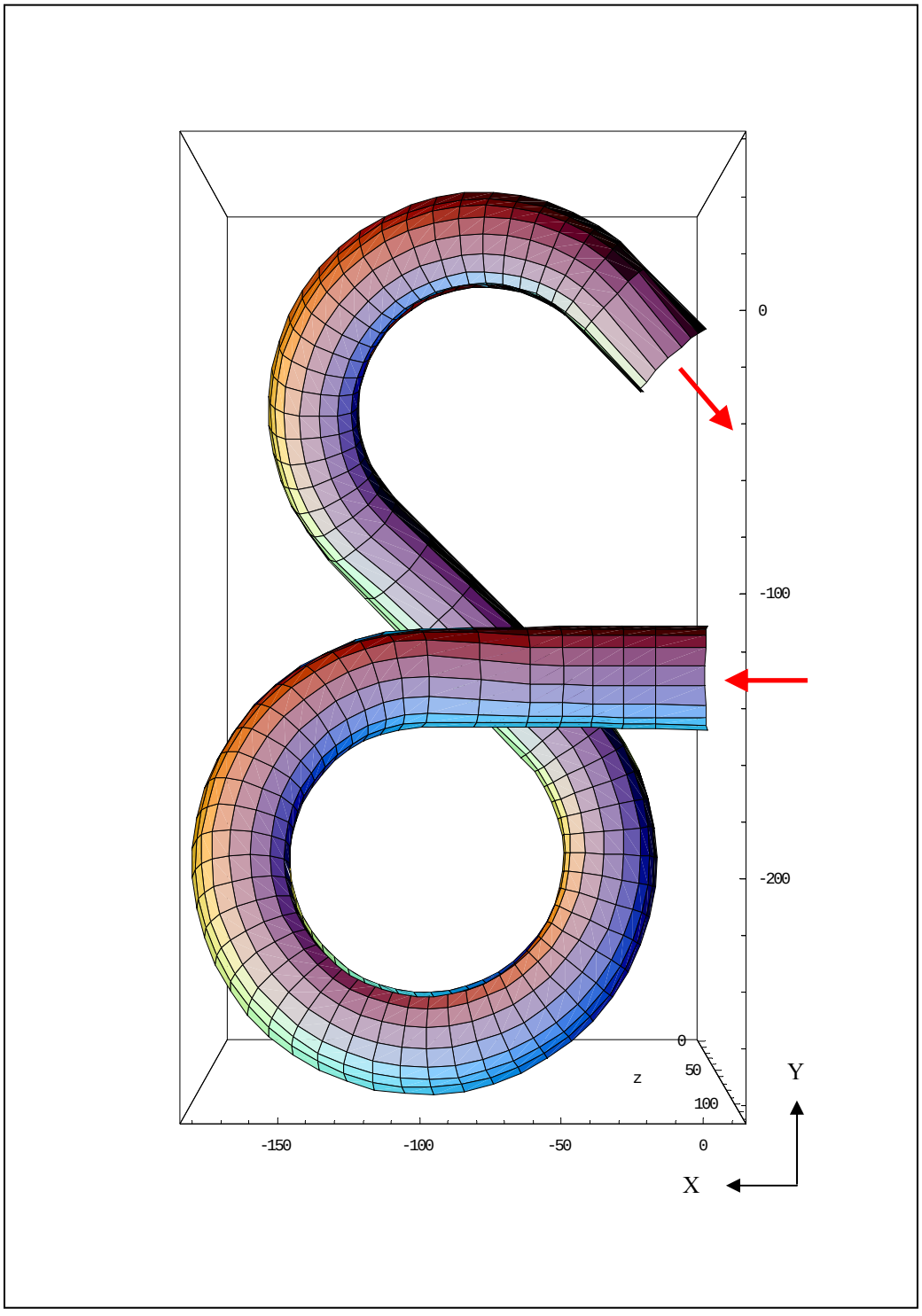


Figure 5.7c Top View of William Configuration

5.5.2 Design Optimization Problem

In the optimization of a water slide, the performance functions will be the rider's excitement level (= objective function) and safety (= constraints). Velocities and accelerations at specified locations can be designed for maximum recreational effect by altering the locations of the control points of the flume section. At the same time, safety consideration can be addressed by limiting the rider's lateral movement to stay within the flume section boundary.

The optimization problem of the B-Spline-based flume sections is presented as follows:

Minimize:

$$\text{OBJ} = (\alpha_1 \cdot \left|\ddot{u}(t)\right| - \alpha_2 \cdot \ddot{w}[t]) \text{ at each time step}$$

where

$$\alpha_1 = 0.7,\ \alpha_2 = 0.3, \text{ and } \alpha_1 + \alpha_2 = 1$$

Subject to:

$$0.2 \le u(t) \le 0.8$$

$$P_{xij_initial} - 20 \le P_{xij} \le P_{xij_initial} + 20 \qquad i = 1..31, \text{ except } 1,16,31 \quad j = 1..56$$

$$P_{yij_initial} - 20 \le P_{yij} \le P_{yij_initial} + 20 \qquad i = 1..31, \text{ except } 1,16,31 \quad j = 1..56$$

$$P_{zij_initial} - 5 \le P_{zij} \le P_{zij_initial} + 5 \qquad i = 1..31, \quad j = 1..56$$

$$P_{x1ij}, P_{x2ij}, P_{x3ij} \ge 0, \quad i = 1..13, \quad j = 1..68$$

$$w(t) \ge 0$$

where

$\ddot{u}(t)$: Lateral acceleration at each time step

$u(t)$: Lateral location at each time step

$\ddot{w}(t)$: Axial acceleration at each time step

$w(t)$: Axial location at each time step

$P_{xij}, P_{yij}, P_{zij}$: x, y, z Coordinate values of control points

$P_{xij_initial}, P_{yij_initial}, P_{zij_initial}$: Initial x, y, z coordinate values of control points

i : u Direction parameter

j : w Direction parameter

Note that the x, y locations of each edge point (i=1, 31) and the center point (i=16) in the u direction are fixed to prevent the shape of the flume configuration from becoming unreasonable. Otherwise, flume sections could turn sideways or even upside down.

5.5.3 Design Optimization Results

Figure 5.8a and Figure 5.8b show a rider's path in the William configuration before optimization. Initial conditions at the starting point are $u(0) = 0.5$ a the center of the flume section, $\dot{u}(0) = 0.0$, $w(0) = 0.0$, $\dot{w}(0) = 0.0$, the rider weighs 160 lbs and no friction is applied.

After optimization, path, velocity, and acceleration of the rider have changed significantly. The lateral accelerations are minimized and the axial acceleration is maximized. The rider's paths are compared in Figure 5.9. The rider travels closer to the center, which improves the safety of the traveling object. Also, due to the increase in acceleration, the total transit time has been reduced from 19.15 seconds to 16.32 seconds with a faster, smoother, and safer ride.

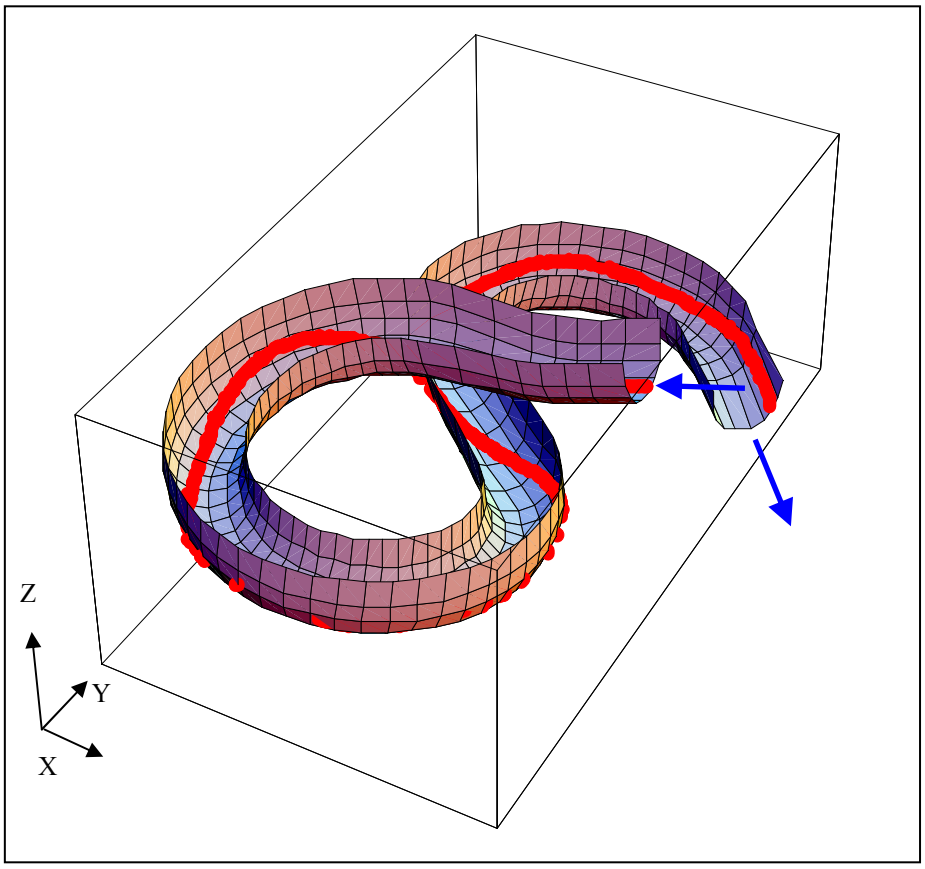


Figure 5.8a Isometric View of William Configuration with Particle Trace before Optimization

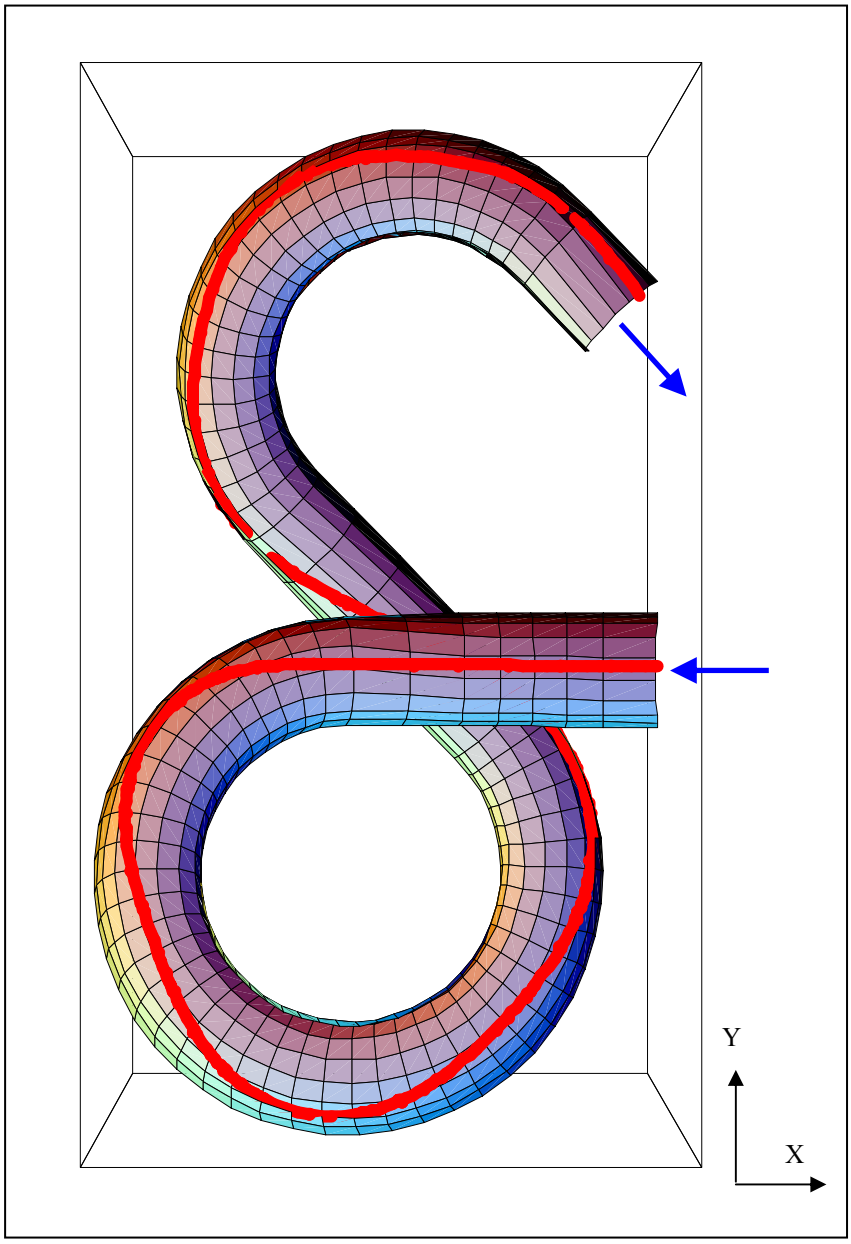


Figure 5.8b Top View of William Configuration with Particle Trace before Optimization

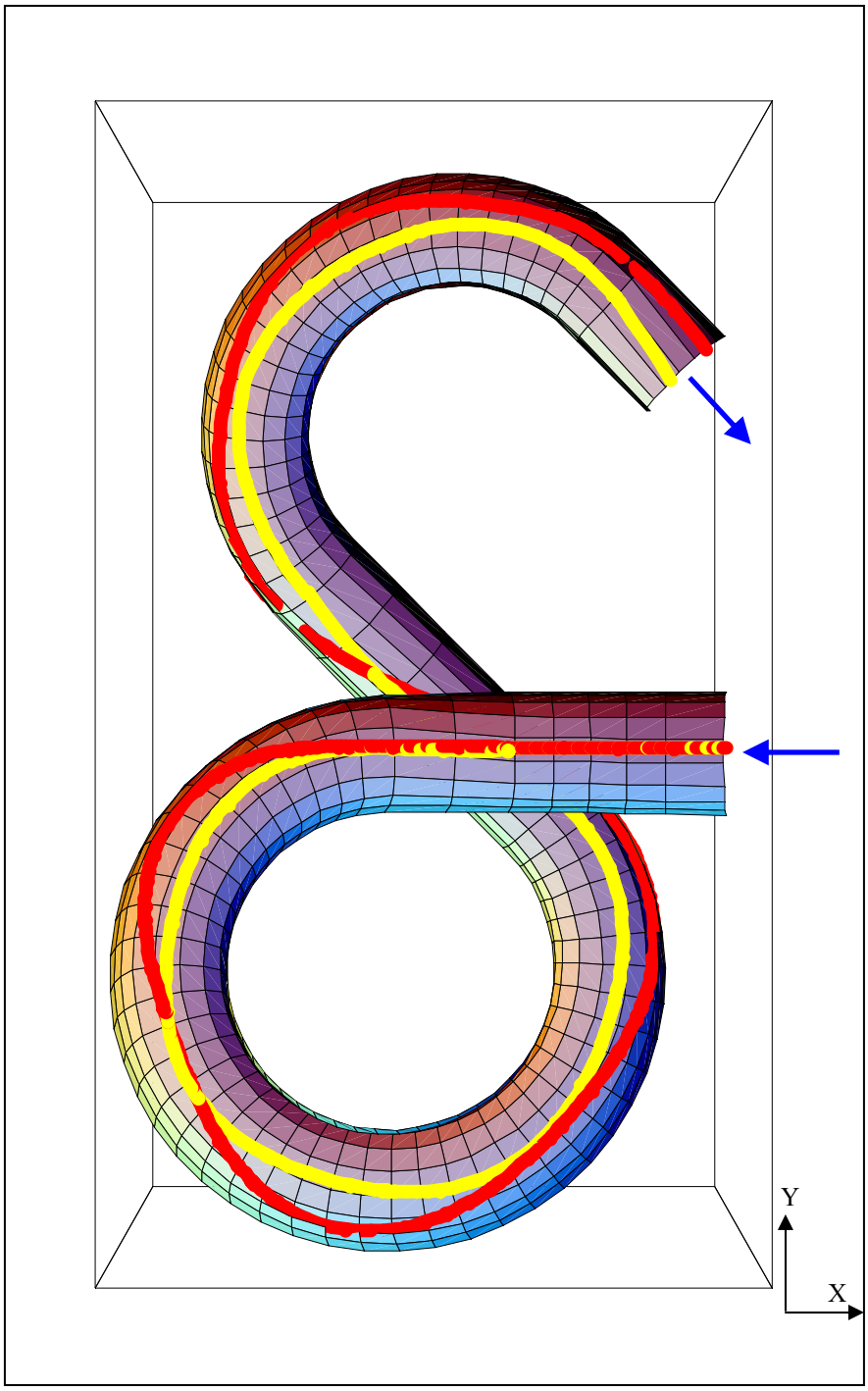


Figure 5.9 Comparisons of Particle Traces in William Configuration before and after Optimization

5.5.4 Off-Design Results

This optimized flume section is also analyzed with friction and different rider weights. Here, four different off-design friction/weight cases are tested on the optimized slide configuration (see Table 5.2). There are no noticeable differences between the paths as shown in Figure 2.10. The reason is that the cross sectional shape of the flume section has been optimized to keep the rider in the center as much as possible with no friction. With friction, the rider moves sideways less than with no friction. Thus, the rider just follows the path of the optimized shape of the flume section at a lower velocity and with a longer transit time. Figure 5.11 shows the combined paths of riders which show no noticeable differences.

Table 5.2 Physical Parameters for Off-Design Friction/Weight Cases

Color of Line	Weight (lbs)	Friction Coefficient
Blue – Design Case	160	0.0 (No Friction)
Green	40	0.05
Yellow	40	0.1
Light Blue	100	0.05
Magenta	100	0.1

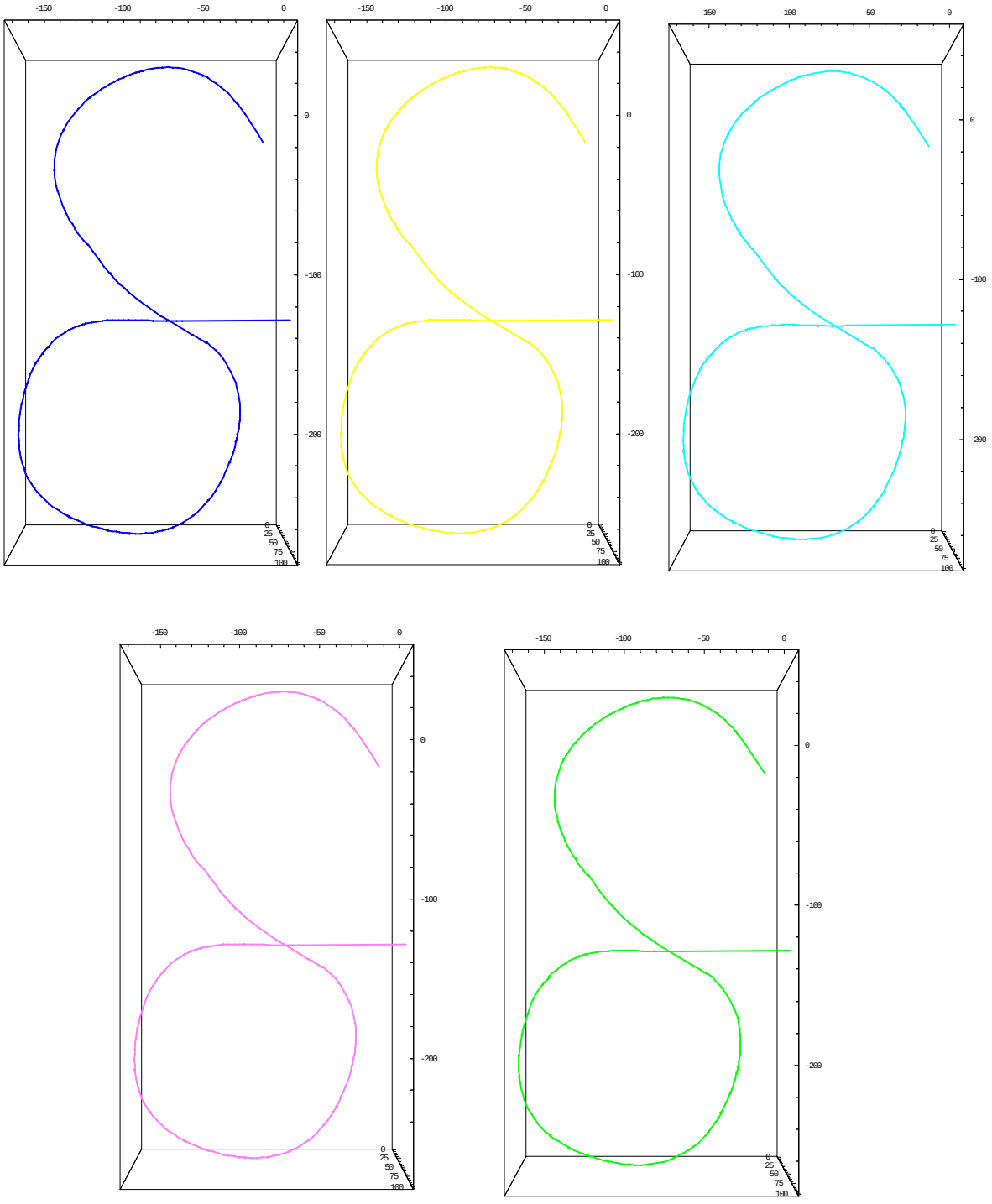


Figure 5.10 Paths of Friction Cases on B-Spline-Based Optimized Slide

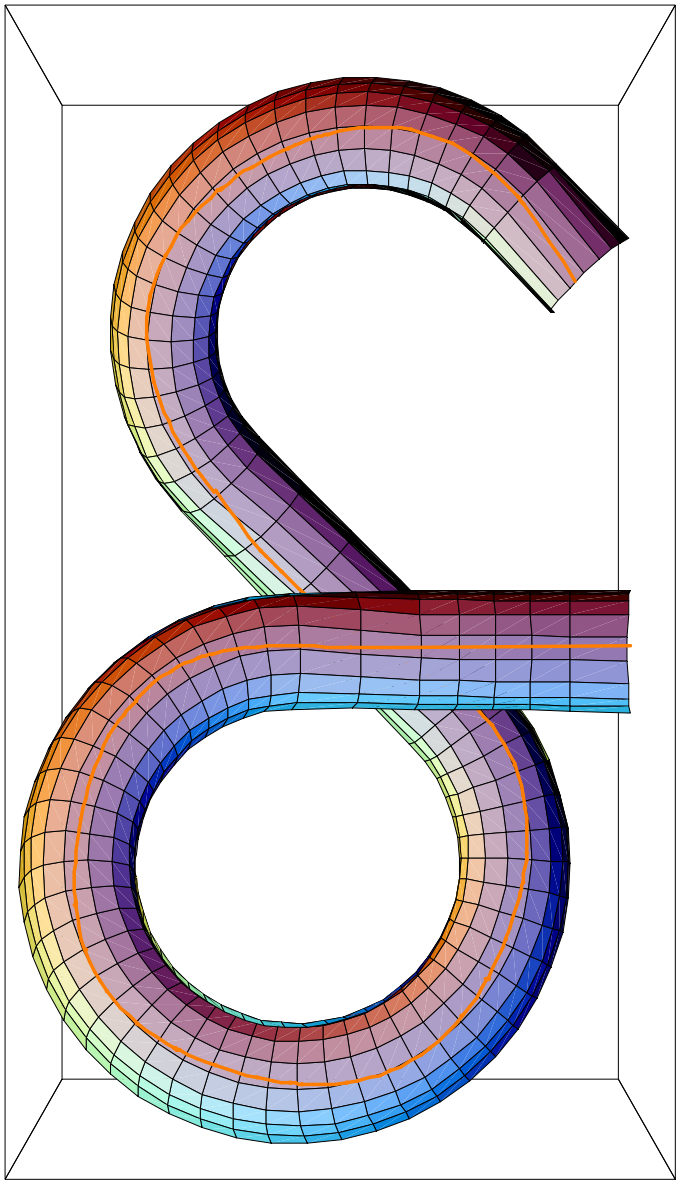


Figure 5.11 Combined Paths of Friction Cases in B-Spline-Based Optimized Slide

5.6 Shape Design Optimization of CAD Based Flume Sections

5.6.1 Flume Configuration for Optimization

The flume configuration for optimization is created from three straight flume sections and two cubic-curve flume sections with 33 and 36 piecewise cubic-curve segments. The dimensions (including the *x*, *y*, *z* locations) of the three straight flume sections, except for the radius of the cross section, are not included in the optimization to prevent the flume configuration from becoming just one straight flume section during optimization. Instead, these straight flume sections are used as anchors. This configuration is named David by the author.

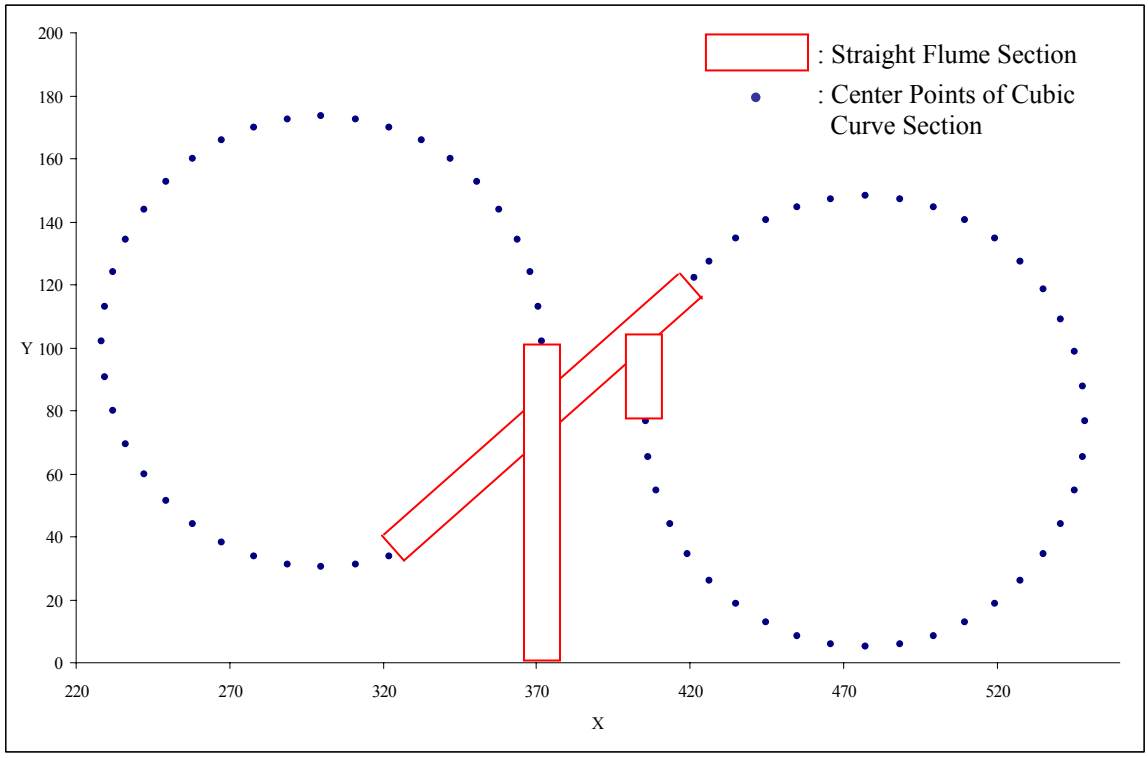


Figure 5.12 Top View of Center Points of Cubic-Curve Sections

Figure 5.12 shows the center points of the cubic-curve flume sections and three straight flume sections. Based on these center points and the straight flume sections, the flume configuration for optimization is constructed.

Detailed shape representations in *Mathematica*® are shown in Figures 5.13a – 5.13b.

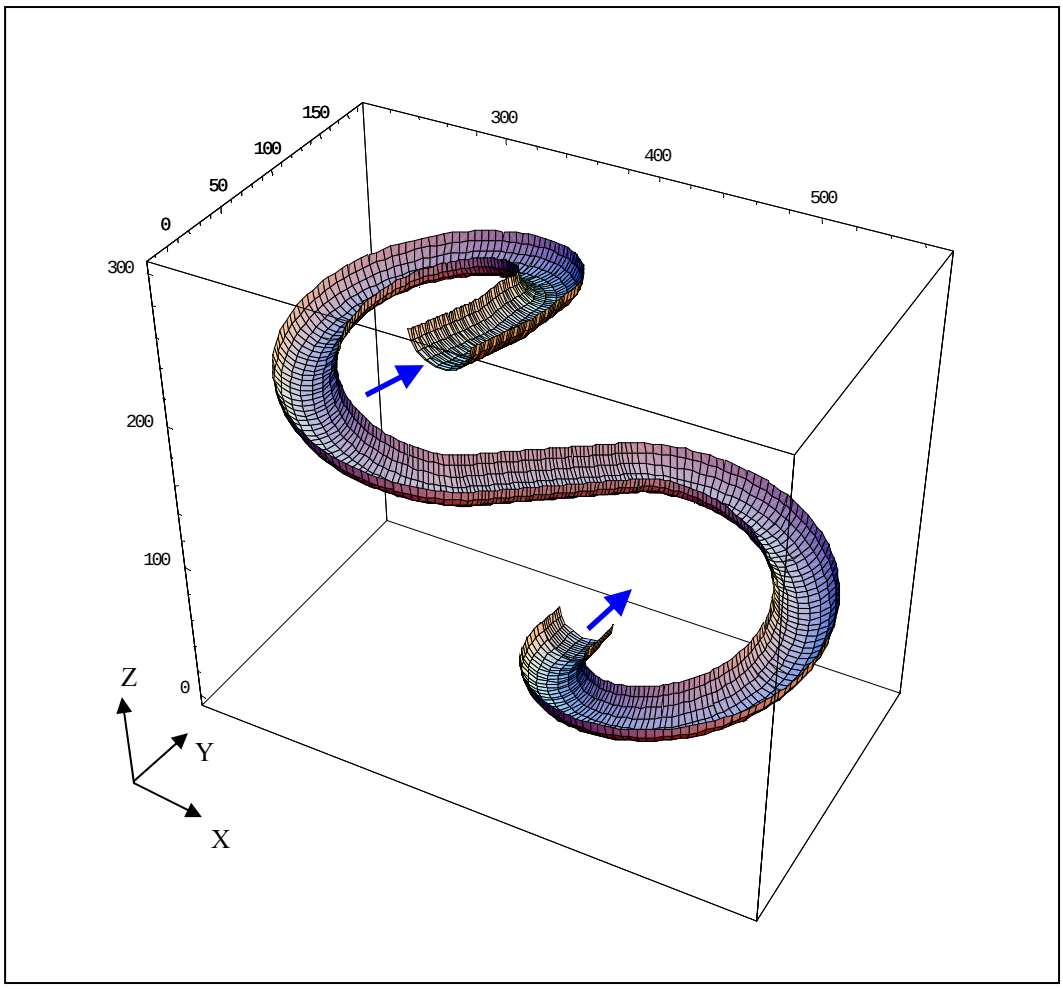


Figure 5.13a Isometric View of David Configuration

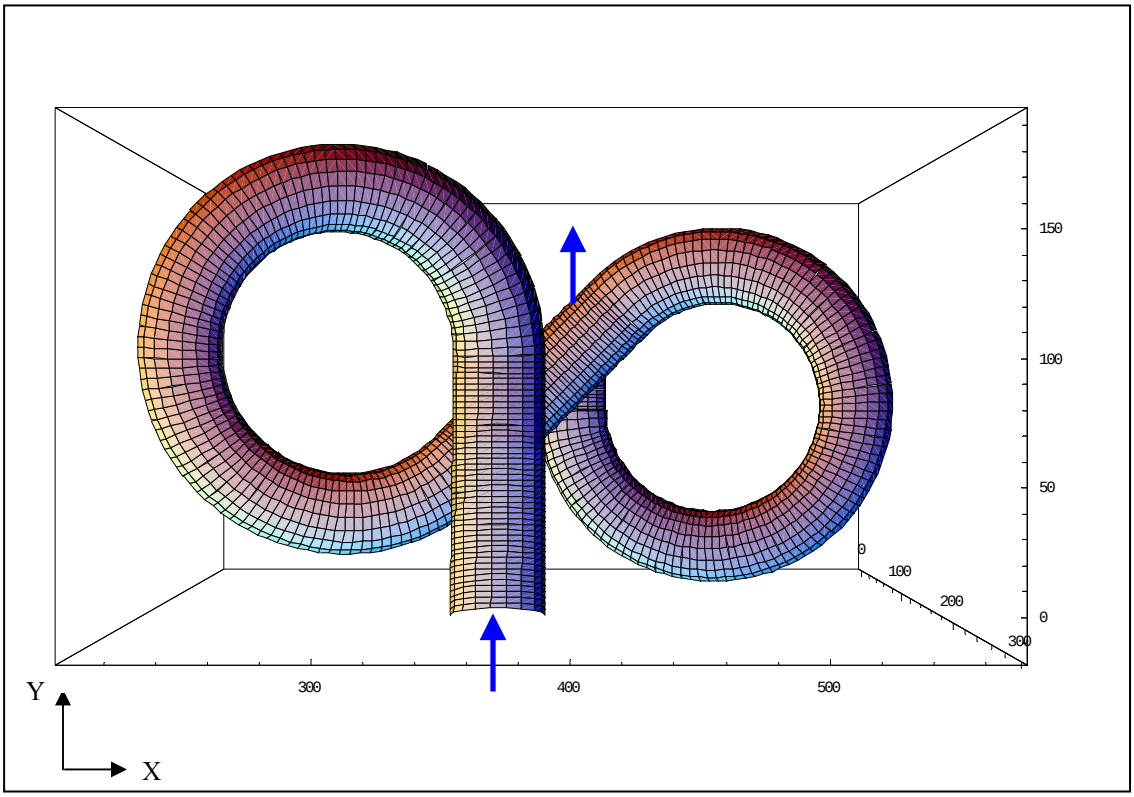


Figure 5.13b Top View of David Configuration

5.6.2 Design Optimization Problem

As in the previous optimization, the performance functions will be the rider's excitement level (= objective function) and safety (= constraints). Velocities and accelerations at specified locations can be designed for maximum safety and recreational effect by altering the locations of the center points of the cubic-curve flume sections and the radii of the flume section cross sections.

The optimization problem of the CAD-based flume sections is presented as follows:

Minimize:

$$\text{OBJ} = (\alpha_1 \cdot \left|\ddot{u}(t)\right| - \alpha_2 \cdot \ddot{w}[t]) \text{ at each time step}$$

where

$$\alpha_1 = 0.7,\ \alpha_2 = 0.3, \text{ and } \alpha_1 + \alpha_2 = 1$$

Subject to:

$$-\pi \le u(t) \le 0.0$$

$$14.505 \le r \le 19.624$$

$$P_{xk_initial} - 50 \le P_{xk} \le P_{xk_initial} + 50 \qquad k = 1..70$$

$$P_{yk_initial} - 50 \le P_{yk} \le P_{yk_initial} + 50 \qquad k = 1..70$$

$$P_{zk_initial} - 5 \le P_{zk} \le P_{zk_initial} + 5 \qquad k = 1..70$$

$$w(t) \ge 0$$

where

$\ddot{u}(t)$: Lateral acceleration at each time step

$u(t)$: Lateral location at each time step

$\ddot{w}(t)$: Axial acceleration at each time step

$w(t)$: Axial location at each time step

r : Radius of semi-circular cross section

P_{xk}, P_{yk}, P_{zk} : x, y, z Coordinate values of center point k of cubic curve

$P_{xk_initial}, P_{xk_initial}, P_{xk_initial}$: Initial x, y, z coordinate values of center point k of cubic curve

i : u Direction parameter

j : w Direction parameter

Note that the lower and upper limits of the u(t) constraint are –π and 0, respectively, instead of -0.8 π and -0.2 π, the equivalent to the optimization of the B-Spline-based flume sections. The reason is that a rider can more easily reach the edge of the CAD-based flume section because of the lower wall and the relatively small size of the cross section. This action will stop the motion analysis. Therefore, the safety constraint was loosened, allowing more movement from edge to edge in the CAD-based case, to let the optimization continue without stoppage due to strict safety constraints. In either case, the final path mostly follows the flume section centerline.

5.6.3 Design Optimization Results

Figure 5.14a and Figure 5.14b show the rider's path in the David configuration before optimization. Initial conditions at the starting point are $u(0)$ = -1.5707 (at the center of the flume section) , $\dot{u}(0) = 0.0$, $w(0) = 0.0$, $\dot{w}(0) = 0.0$, and no friction is applied. Note that there are several locations where the rider almost leaves the surface boundary.

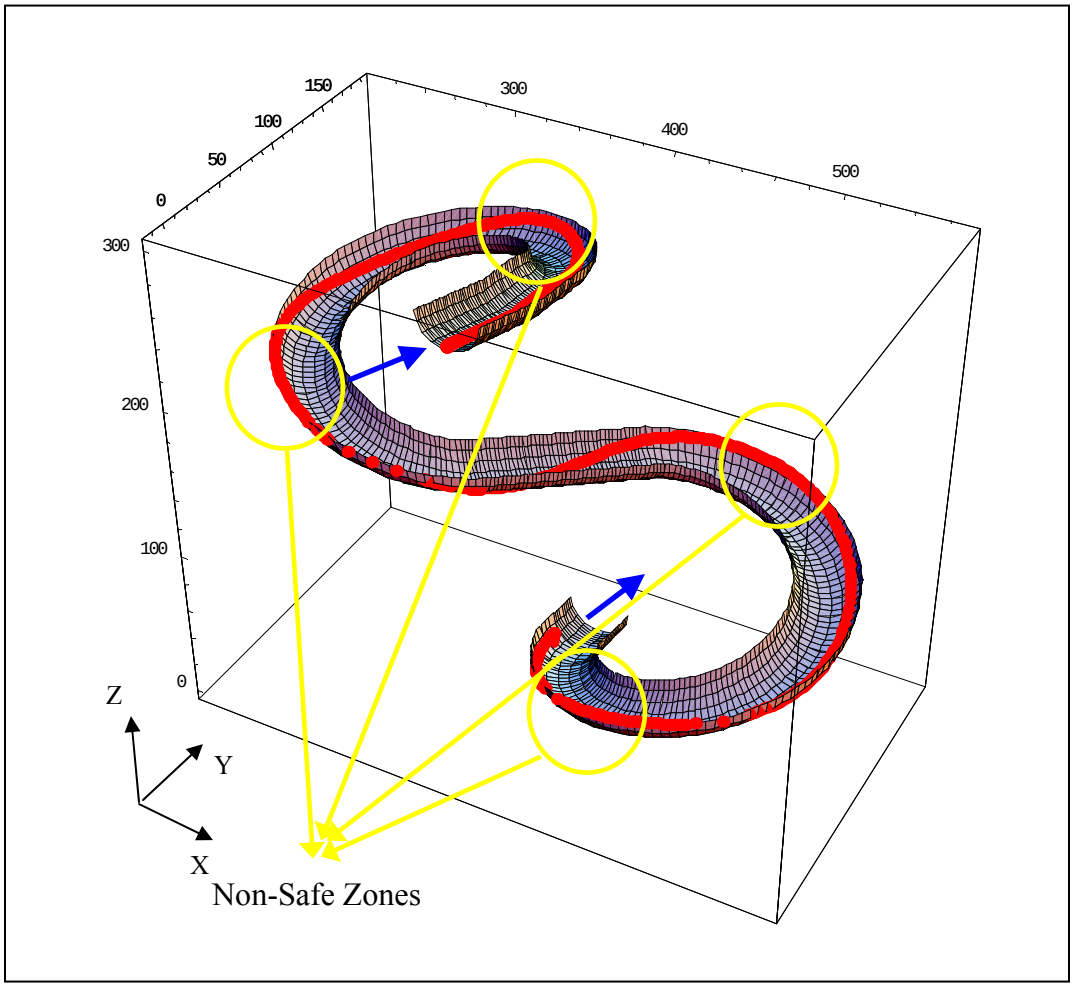


Figure 5.14a Isometric View of David Configuration with Particle Trace before Optimization

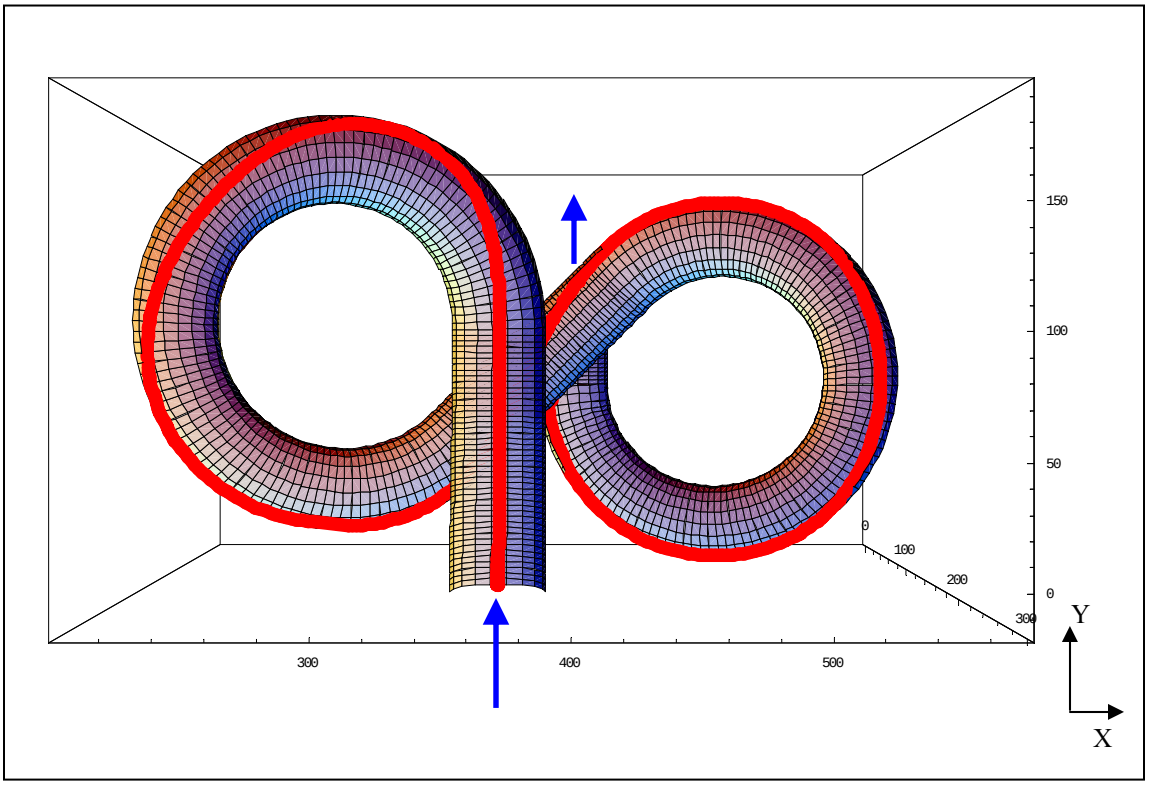


Figure 5.14b Top View of David Configuration with Particle Trace before Optimization

Figures 5.15 and 5.16 show the results for the CAD-based flume section optimization problem. As in the first optimization, the lateral accelerations are minimized and the axial acceleration is maximized. The total transit time has been reduced from 26.15 seconds to 25.32 seconds with a faster, smoother, and safer ride despite the fact that the optimization results in a longer overall configuration. Also, the radius of the flume cross section is increased from 17.061 inches to 19.624 inches. Changes of the center point locations of the cubic-curve flume sections are shown in Figure 5.15.

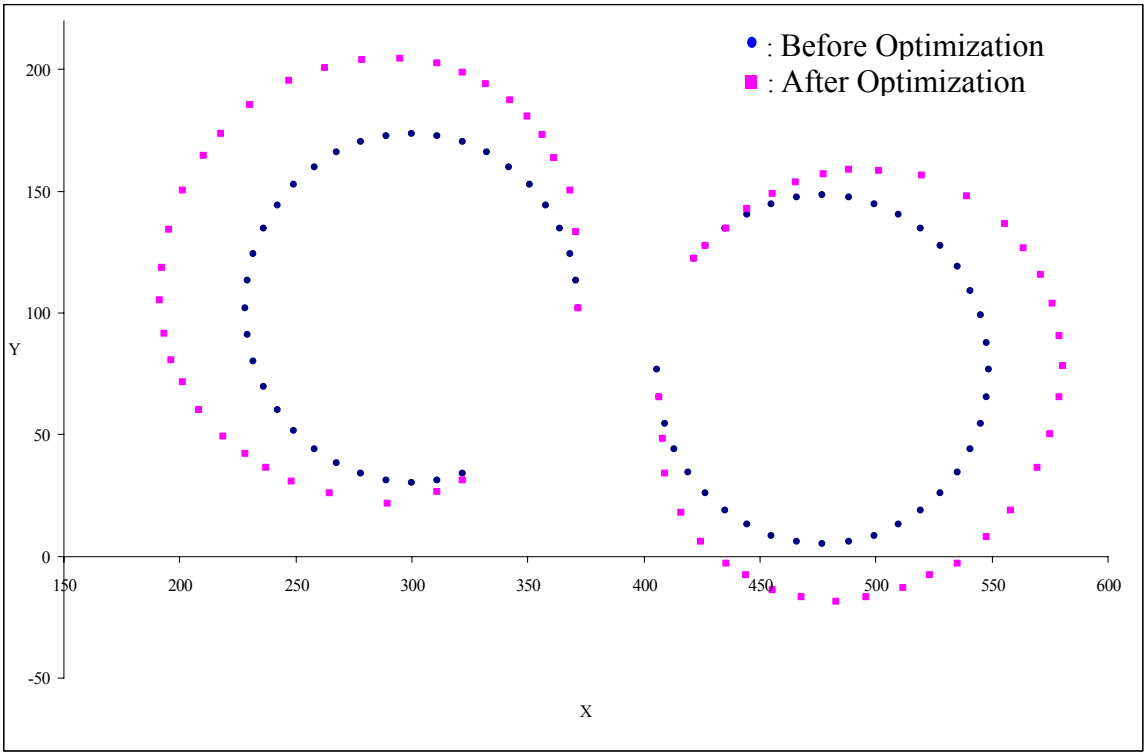


Figure 5.15 Comparisons of Center Points Before and After Optimization

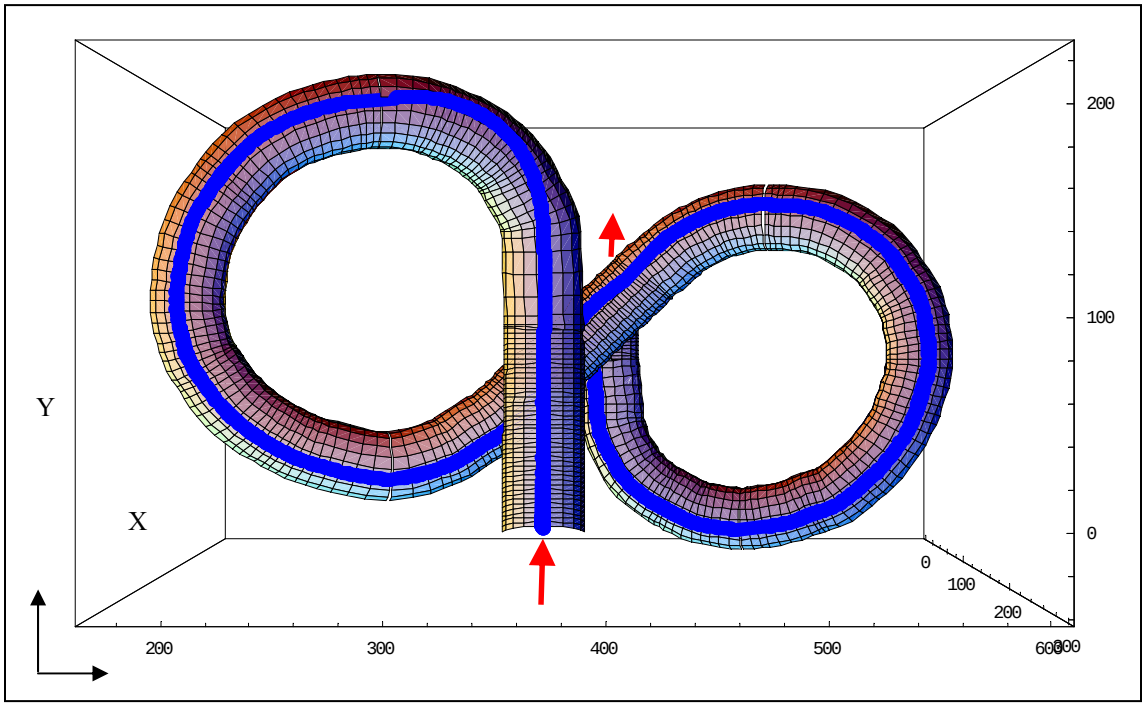


Figure 5.16a Top View of David Configuration with Particle Trace after Optimization

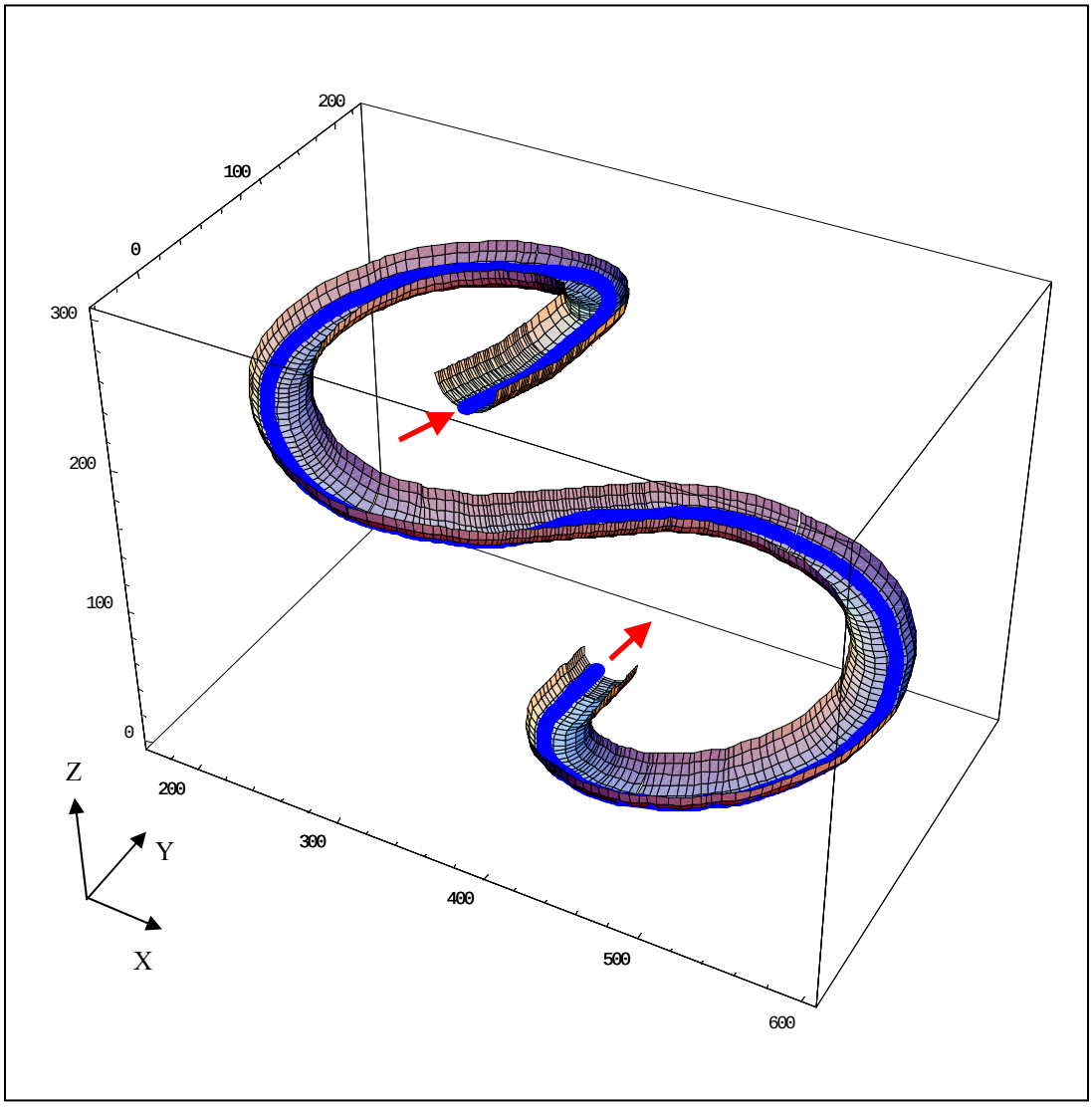


Figure 5.16b Isometric View of David Configuration with Particle Trace after Optimization

5.6.4 Off-Design Results

The same four off-design cases as shown in Table 5.2 are analyzed for the CAD-based optimized slide. Unlike in the B-Spline-based flume section case, there are noticeable differences between the paths. Since the CAD-based flume optimization hasn't changed the cross sectional shapes (except the width), the paths cannot be the same. However, since the friction coefficients are relatively small (0.05-0.1), the rider don't move out much from the original optimized path as shown in Figure 5.17 and 5.18. Some of paths are not even distinguishable. If the friction coefficients are increase more, a rider will move out of the original path more dramatically. However, a friction coefficient larger than 0.1 does not seem realistic.

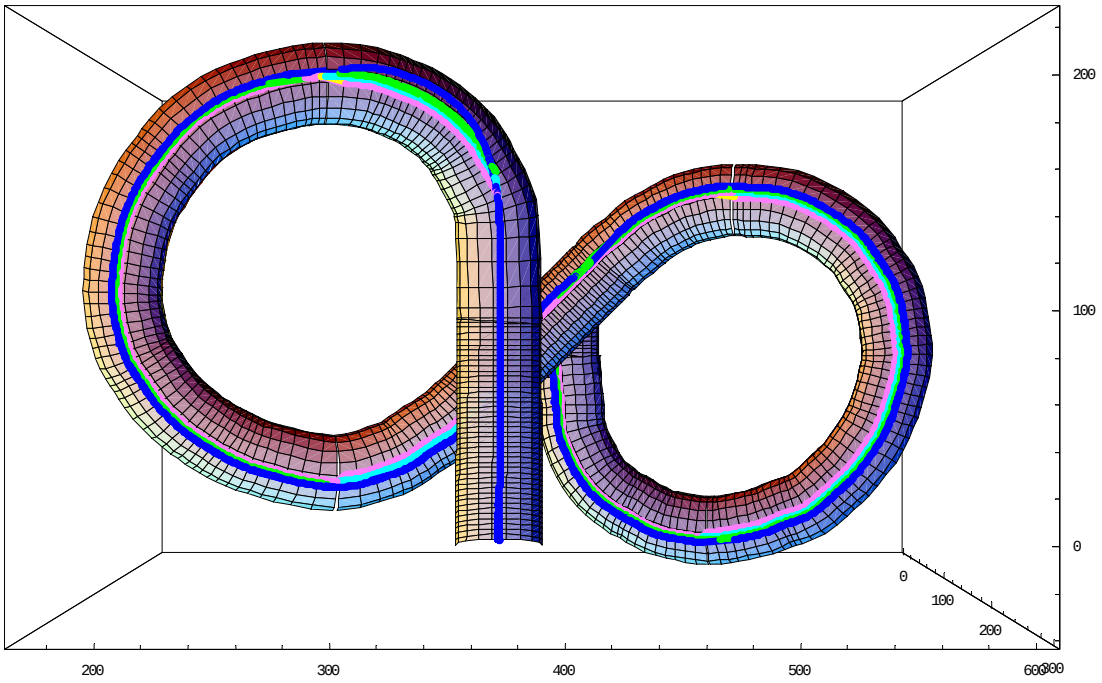


Figure 5.17 Combined Paths of Friction Cases on CAD-Based Optimized Slide

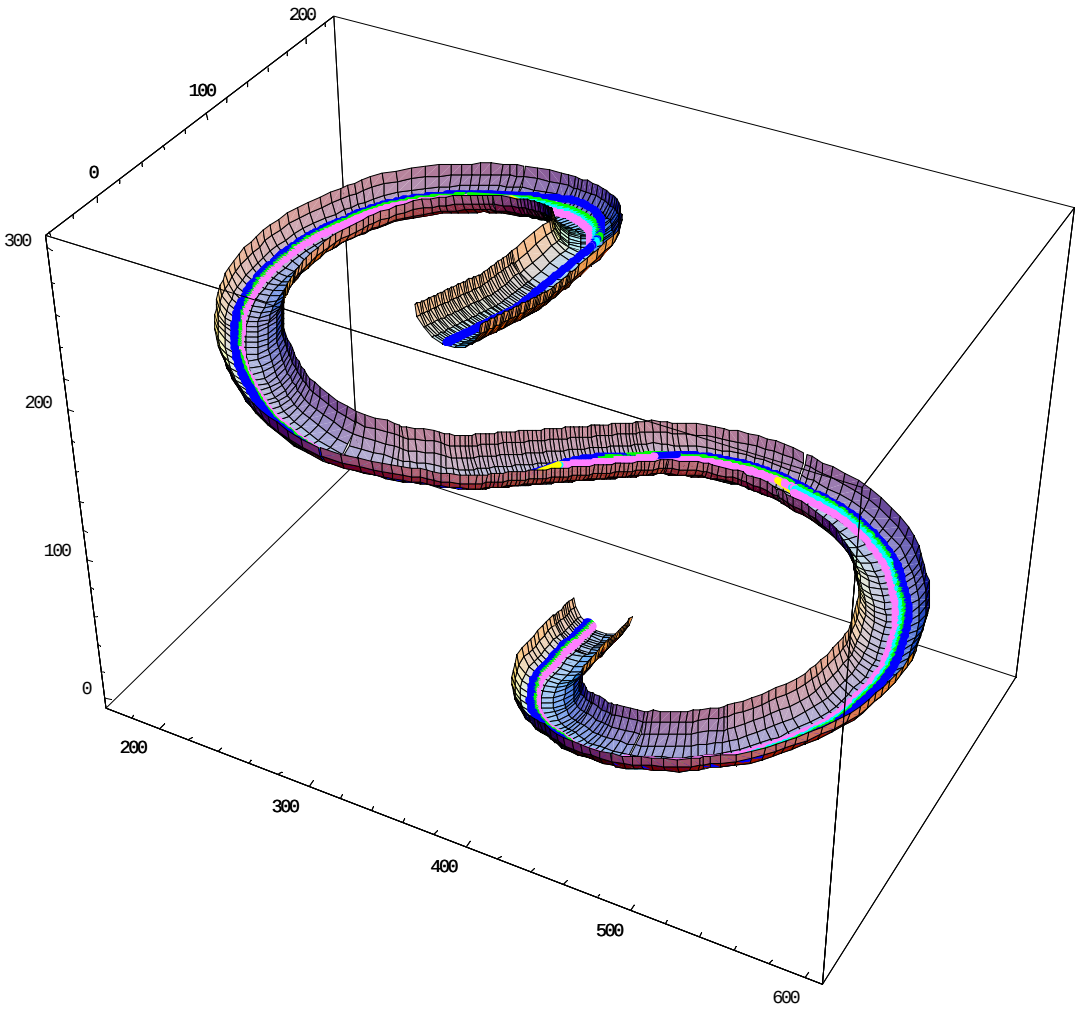


Figure 5.18 Combined Paths of Friction Cases on CAD-Based Optimized Slide

CHAPTER 6

DISCUSSION AND FUTURE WORK

In this dissertation, motion analysis, a shape DSA methodology, and shape design optimizations of flume section configurations have been presented. The traveling object is assumed to be a particle of concentrated mass with and without friction. An analytical shape DSA methodology has been developed and verified to be accurate. Design variables can be either the control points of a B-Spline-based flume section or the dimensions of a CAD-based flume section. Sensitivity verification based on sensitivity coefficients proves that conditions can be imposed on flume section configurations and their performance optimized, e.g., safety and excitement of a water slide can be ensured by modifying the geometry of the flume section configuration. Two optimization problems were defined and executed.

Some limitations of the present study are given here. The developed dynamic analysis methodology seems to have provided reasonable results, although they could not be verified on an actual water slide configuration. Friction coefficients are very hard to determine. However, these are needed to provide the most realistic slide environment. Educated guesses were made here. Another limitation is the assumption that the traveling object is a particle of concentrated mass. In a real water slide, the rider's path and velocity can be dramatically changed depending on a rider's body shape, orientation, and movement. Also, the current dynamic analysis code cannot generate an accurate path for

an object that jumps at the start point. The code always assumes that the object stays connected to the surface of the flow channel.

The CPU time for the optimization was long when the flume section was long, especially for the B-Spline-based flume section configuration. An optimized code and high-performance computing seem to be a must when a large number of design variables have to be deal with. Good CAD or mathematical packages, which support B-Spline curve fitting, and stronger graphics representation capabalities are also necessary. *I-DEAS*® has good curve fitting capabilities, but it's graphics representation capabilities seem to be poor, since it generated bad surface representations at times. *Mathematica*®'s external packages have very good graphics representations. However, its lack of good curve fitting and B-Spline control points generating capabilities significantly limits it as an independent design and graphics tool. *Solidworks*® and *Pro/E*® don't have curve fitting capabilities even though they have useful graphics capabilities

Several directions are worthy of future study. This dissertation provides theoretical and computational foundations for the design of flume sections. Following this research, it is desirable to develop a well-integrated user friendly tool to allow for the interactive design of flume sections. In addition, instead of using a particle, a dynamic system for a human body should be developed. Improving the calculations of the water-human and water-slide interaction by incorporating fluid mechanics will enhance the accuracy of the motion analysis. It is possible to expand this research and apply it to other areas, not just water slides. Since this program uses common programs like *Mathematica*® and

I-DEAS®, it should be easy to covert it to other platforms and to improve its compatibility by using a common programming language.

Finally, expanding the parametric surface representation to that of a moving surface can be another possible study. Instead of using fixed parametric flume sections, it is possible to use moving parametric surfaces such as free wave surfaces via a wave function. Such a module to calculate the movement of objects on waves is presently under development.

REFERENCES

[1] Kondragunta, N., Design of Water Slide, Class Project, The University of Oklahoma, Norman, OK, 1993.

[2] Kondragunta, N., "Rider Path Geometric Modeling and Simulation for Water Slide Configurations", *Master Thesis*, The University of Oklahoma, Norman, OK, 1995.

[3] White, F. M., *Fluid Mechanics*, McGraw-Hill, Inc., New York , NY, 1979.

[4] Schoenberg, N., "Contributions to the Problem of Approximation of Equidistant Data by Analytic Functions," *Quart. Appl. Math.,* Vol. 4, pp. 45–99 and 112–141, 1946.

[5] Bartels, R., Beatty, J., and Barsky, B, *An Introduction to Splines for Use in Computer Graphics and Geometric Modeling,* Morgan Kaufmann Publishers Inc., San Metao, CA, 1987.

[6] Birkhoff, G., and de Boor, C., "Piecewise Polynomial Interpolation and Approximation", in: H. L. Garabedian (ed.), *Proc. General Motors Symposium of 1964,* pp. 164–190. Elsevier, New York and Amsterdam, 1965.

[7] Ahlberg J. H., Nielson, E. N., and Walsh J.L., *The Theory of Splines and Their Applications*, Academic Press, New York, NY, 1967.

[8] Sarkar, B. and Menq, C.-H., "Parameter Optimization in Approximating Curves and Surfaces to Measurement Data," *Comput. Aided Geomet. Design,* Vol. 8, pp. 267—290, 1991.

[9] Speer, T., Kuppe, M., and Hoschek, J. "Global Reparameterization for Curve Approximation," *Comput. Aided Geomet. Design,* Vol. 15, pp 869-877, 1998.

[10] Laurent-Gengoux, P., and Mekhilef, M., " Optimization of a NURBS Representation," *Comput.-Aided Design*, Vol. 25, pp. 699-710, 2003.

[11] Joo, S-H., "Shape Design Optimization and What-If Study for Recreational Water Slides", *Master Thesis*, The University of Oklahoma, Norman, OK, 2000.

[12] Joo, S-H., and Chang K-H., "Design for Safety of Recreational Water Slides", *Mechanics of Structures and Machines*, Vol. 29, pp. 261-294, 2001.

[13] Joo, S.-H., Chang, K.-H., and Striz, A.G., "Shape Design Optimization of CAD-Based Flume Sections" , *11th AIAA/ISSMO Multidisciplinary Analysis and Optimization Conference*, Portsmouth, VA, 6-8 Sept, 2006 (accepted for presentation).

[14] Park, H., and Kim, K., "Smooth Surface Approximation to Serial Cross-Sections," *Journal of Computer Aided Design*, Vol. 28, No. 12, pp. 995–1005, 1996.

[15] Wolfram, S., *Mathematica Book*, Addison-Wesley, Reading, MA, 1998. ISBN 0-201- 51502-4.

[16] DeBoor, C., *A Practical Guide to Splines*, Springer-Verlag, New York, NY, 1978.

[17] Tang, P.S., "Integration of Topology and Shape Optimizations for Design of Structural Components," *M.S. Thesis*, The University of Oklahoma, Norman, OK, 1999.

[18] Petzold, L.R., "Automatic Selection of Methods for Solving Stiff and Non-Stiff Systems of Ordinary Differential Equations," *SIAM Journal of Scientific and Statistical Computing*, 4, pp. 136-148, 1983.

[19] Kincaid, D., and Cheney, W., *Numerical Analysis*, Brooks/Cole Publishing Co., Pacific Grove, CA, 1991. ISBN 0-534-13014-3.

[20] Rogers, D.F., and Adams, J.A., *Mathematical Elements for Computer Graphics*, McGraw-Hill, Inc., New York , NY, 1990. ISBN 0-07-100289-8.

[21] Piegl, L., and Tiller, W., *The NURBS Book*, Springer, New York, NY, 1997. ISBN 3-540-61545-8.

[22] Lawry, M.H., *I-DEAS Master Series Guide*, Structural Dynamics Research Corporation, Milford, OH, 1998. ISBN 0- 638178-3-3.

[23] Kane, T.R., and Levinson, D.A., *Dynamics: Theory and Applications*, McGraw-Hill, Inc., New York , NY, 1985. ISBN 0-07-037846-0.

[24] Chang, K.H., Choi, K.K., Tsai, C.S., Chen, C.J., Choi, B.S., and Yu, X. "Design Sensitivity Analysis and Optimization Tool (DSO) for Shape Design Applications," *Computing Systems in Engineering*, Vol. 6, No. 2, pp. 151-175, 1995.

[25] Parametric Technology Corporation, *Release 19.0 Pro/ENGINEER Fundamentals*, Parametric Technology Corporation, Waltham, MA, 1998.

[26] Stokes, H., "Solid Modeling and the Initial Graphics Exchange Specification (IGES)," Chapter 21 of *Handbook of Solid Modeling*, LaCourse, D.E. ed., McGraw-Hill, Inc., New York , NY, 1995.

[27] Mortenson, M. E., *Geometric Modeling*, Second Ed., John Wiley & Sons, Inc., New York, NY, 1997.

[28] Haug, E. J., Choi, K. K., and Komkov, V., *Design Sensitivity Analysis of Structural Systems*, Academic Press, New York, NY, 1986.

[29] DOT (Design Optimization Tools), Vanderplaats Research & Development, Inc., Colorado Springs, CO.

[30] Hagedorn, A.V., and Pritz, H.B., "Evaluation of the CRABI 12-Month-Old Infant Dummy and Its Comparison With the TNO P3/4," *NHTSA Docket* #99-5156, February 1999.

APPENDICES

APPENDIX A: THREE-DIMENSIONAL TRANSFORMATION

In this research (see also Reference 11), geometric transformations of basic flume sections are conducted in the so-called homogeneous coordinate system of three dimensions. The homogeneous coordinate system of two dimensions is easier to understand; therefore, it is discussed first.

Every single point $[x_1, x_2]$ in a 2-D x_1-x_2 plane has a corresponding set of homogeneous coordinates $[hx_1 , hx_2 , h]$ in the homogeneous coordinate system of two dimensions, as shown in Figure A.1. When $h = 1$, $[hx_1 , hx_2 , h]$ becomes $[x_1, x_2, 1]$ which projects the point $[hx_1 , hx_2 , h]$ onto the $h = 1$ plane in the homogeneous coordinate system. Therefore, the geometric representation in a two-dimensional Cartesian coordinate system is a special case of the more general homogeneous coordinate system of two dimensions.

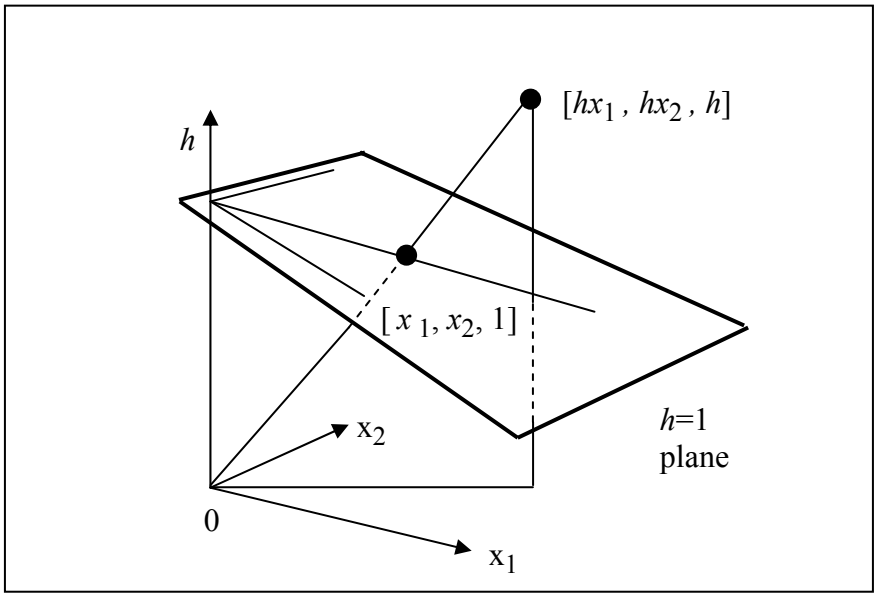


Figure A.1 Homogeneous Coordinate System of Two Dimensions

Similarly, a point in a three-dimensional Cartesian space $[x_1\ ,\ x_2\ ,\ x_3]$ has a corresponding set of homogeneous coordinates $[hx_1\ ,\ hx_2\ ,\ hx_3\ ,\ h]$ in the homogeneous coordinate system of three dimensions.

Three-dimensional transformations of geometric points can be handled more effectively in the homogeneous than the ordinary Cartesian coordinate system.

Let $\boldsymbol{P}_j$, j = 0, n, be n+1 geometric points in the homogeneous coordinate system of three-dimensions that define a flume section. Hence, for the j^{th} geometric point , $\boldsymbol{P}_j$ can be written as

$$P_j = [hx_{1\text{j}}\ ,\ hx_{2\text{j}}\ ,\ hx_{3\text{j}}\ ,\ h]_{1\times 4} \text{ or simply } [h\text{x}_1,\ h\text{x}_2,\ h\text{x}_3,\ h] \tag{A.1}$$

When h=1, one has $[x_1\ ,\ x_2\ ,\ x_3\ ,\ 1]$.

In the homogeneous coordinate system, the matrix for three-dimensional transformation can be represented as

$$\boldsymbol{T} = \left[\begin{array}{ccc:c} A & B & C & 0 \\ D & E & F & 0 \\ G & H & I & 0 \\ \hdashline J & K & L & S \end{array}\right] = \begin{bmatrix} \boldsymbol{T_r}_{3\times 3} & \boldsymbol{O}_{3\times 1} \\ \boldsymbol{T_t}_{1\times 3} & \boldsymbol{T_s}_{1\times 1} \end{bmatrix} \tag{A.2}$$

where $\boldsymbol{T_r}_{3\times 3}$, $\boldsymbol{T_t}_{1\times 3}$, and $\boldsymbol{T_s}_{1\times 1}$ take care of rotation, translation, and global scaling of the given geometric point $\boldsymbol{P}_j$ [17]. In this research, only rotational and translational transformations are needed.

Using Equation A.2, the transformed coordinates of the geometric point $\boldsymbol{P}_j$ can be obtained by

$$\boldsymbol{P}_{j1\times 4}{}' = \boldsymbol{P}_{j1\times 4} \times \boldsymbol{T}_{4\times 4} = \left[x_{1j}\ x_{2j}\ x_{3j} \right] \boldsymbol{T}_{4\times 4} \tag{A.3}$$

where $\boldsymbol{P}_j{}' = \left[x'_{1j}\ x'_{2j}\ x'_{3j}\ 1 \right]$.

For a set of n+1 geometric points, one has

$$\left[\boldsymbol{P}_j{}' \right]_{(n+1)\times 4} = \left[\boldsymbol{P}_j \right]_{(n+1)\times 4} \times \boldsymbol{T}_{4\times 4} = \begin{bmatrix} x_{10} & x_{20} & x_{30} & 1 \\ x_{11} & x_{21} & x_{31} & 1 \\ & \vdots & & \\ x_{13} & x_{23} & x_{33} & 1 \end{bmatrix} \times \boldsymbol{T}_{4\times 4} \tag{A.4}$$

APPENDIX B: CONTINUITY REQUIREMENTS OF CAD-BASED FLUME SECTIONS

1. Straight Flume Section *A* to Straight Flume Section *B* Connection

The general equation of a straight flume section can be expressed as

$$\boldsymbol{X}(u,w) = \boldsymbol{X}_0 + \boldsymbol{T}(\theta)\boldsymbol{x}(u,w) = \begin{bmatrix} X_{1_0} \\ X_{2_0} \\ X_{3_0} \end{bmatrix} + \begin{bmatrix} \cos\theta & \sin\theta & 0 \\ -\sin\theta & \cos\theta & 0 \\ 0 & 0 & 1 \end{bmatrix} \begin{bmatrix} x_1(u,w) \\ x_2(u,w) \\ x_3(u,w) \end{bmatrix} \tag{B.1}$$

where

$$\boldsymbol{x}(u,w) = \begin{bmatrix} r_c \cos u & \ell w & r_c(1+\sin u) - h \cdot w \end{bmatrix}^T \tag{B.2}$$

$\boldsymbol{T}(\theta)$ is the rotation matrix that orients the flume section by an orientation angle about the X_3 axis, X_{i_0} is the location of the local coordinate system of the flume section in the flow channel configuration, and $\boldsymbol{x}(u,w)$ is the surface function of the flume section referred to its local coordinate system. For a straight flume section, h and ℓ are the height and length of the section, respectively; r is the radius of the semicircular cross section of the flume section; u and w are the parametric coordinates along the circumferential and longitudinal directions of the flume section, respectively, and $u \in [0, -\pi], w \in [0, \ell]$ (see Figure B.1).

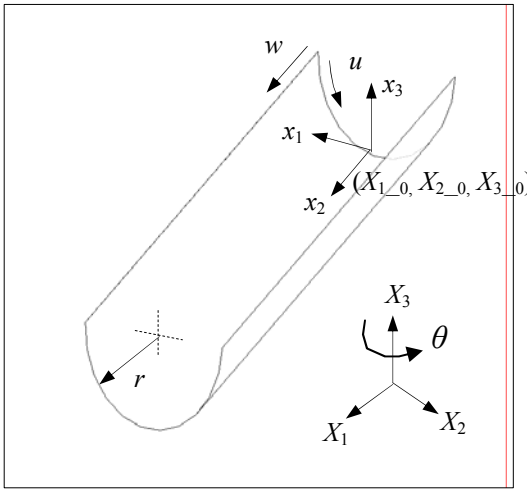


Figure B.1 Straight Flume Section

In this case, a straight flume section $\boldsymbol{X}^A$ (length ℓ_A, height h_A) and a straight flume section $\boldsymbol{X}^B$ (length ℓ_B, height h_B) are connected sequentially. In the present calculations, the cross-section directional parameter u is not considered and assumed the same in each flume section.

1) C^0 Continuity

The following relationship has to be satisfied for C^0 continuity:

$$\boldsymbol{X}^A(u,w)\Big|_{w=1} = \boldsymbol{X}^B(u,w)\Big|_{w=0} \tag{B.3}$$

$$\begin{bmatrix} X^A_{1_0} \\ X^A_{2_0} \\ X^A_{3_0} \end{bmatrix} + \begin{bmatrix} \cos\theta_A & \sin\theta_A & 0 \\ -\sin\theta_A & \cos\theta_A & 0 \\ 0 & 0 & 1 \end{bmatrix} \begin{bmatrix} r_c^A \cos u \\ \ell_A \\ r_c^A(1+\sin u) - h_A \end{bmatrix}$$

$$= \begin{bmatrix} X^B_{1_0} \\ X^B_{2_0} \\ X^B_{3_0} \end{bmatrix} + \begin{bmatrix} \cos\theta_B & \sin\theta_B & 0 \\ -\sin\theta_B & \cos\theta_B & 0 \\ 0 & 0 & 1 \end{bmatrix} \begin{bmatrix} r_c^B \cos u \\ 0 \\ r_c^B(1+\sin u) \end{bmatrix} \tag{B.4}$$

From Equation B.4, we have

$$\begin{aligned} &X^A_{1_0} + \cos\theta_A \cdot r_c^A \cdot \cos u + \ell_A \sin\theta_A = X^B_{1_0} + \cos\theta_B \cdot r_c^B \cdot \cos u \\ &X^A_{2_0} - \sin\theta_A \cdot r_c^A \cdot \cos u + \ell_A \cos\theta_A = X^B_{2_0} - \sin\theta_B \cdot r_c^B \cdot \cos u \\ &X^A_{3_0} + r_c^A(1+\sin u) - h_A = X^B_{3_0} + r_c^B(1+\sin u) \end{aligned} \tag{B.5}$$

Then, requirements for C^0 continuity are

$$\begin{aligned} &\theta_A = \theta_B, r_c^A = r_c^B \\ &X^A_{1_0} + \ell_A \sin\theta_A = X^B_{1_0} \\ &X^A_{2_0} + \ell_A \cos\theta_A = X^B_{2_0} \\ &X^A_{3_0} - h_A = X^B_{3_0} \end{aligned} \tag{B.6}$$

To satisfy the requirements, the radius (r) and rotational angle (θ) of each flume sections must be identical. Also, the X_1, X_2, X_3 coordinate values of each flume sections at the connection must be identical. When the above requirements are satisfied, C^1 continuity in the w-direction exists.

2) C^1 Continuity

Similarly, the following relationship has to be satisfied for C^1 continuity:

$$\left.\frac{\partial \boldsymbol{X}^A(u,w)}{\partial w}\right|_{w=\ell_A} = \left.\frac{\partial \boldsymbol{X}^B(u,w)}{\partial w}\right|_{w=0} \tag{B.7}$$

$$\begin{bmatrix} \cos\theta_A & \sin\theta_A & 0 \\ -\sin\theta_A & \cos\theta_A & 0 \\ 0 & 0 & 1 \end{bmatrix} \begin{bmatrix} 0 \\ 1 \\ -\frac{h_A}{\ell_A} \end{bmatrix} = \begin{bmatrix} \cos\theta_B & \sin\theta_B & 0 \\ -\sin\theta_B & \cos\theta_B & 0 \\ 0 & 0 & 1 \end{bmatrix} \begin{bmatrix} 0 \\ 1 \\ -\frac{h_B}{\ell_B} \end{bmatrix}$$

(B.8)

Then, requirements for C^1 continuity are $\frac{h_A}{\ell_A} = \frac{h_B}{\ell_B}, \theta_A = \theta_B$. To satisfy these requirements, the slope ($\frac{h}{\ell}$) and rotational angle (θ) of each of the two flume sections must be identical. When the above requirements are satisfied, C^1 continuity in the w-direction exists.

3) C^2 Continuity

Similarly, the following relationship has to be satisfied for C^2 continuity:

$$\left.\frac{\partial^2 \boldsymbol{X}^A(u,w)}{\partial w^2}\right|_{w=1} = \left.\frac{\partial^2 \boldsymbol{X}^B(u,w)}{\partial w^2}\right|_{w=0} \tag{B.9}$$

$$\begin{bmatrix} 0 \\ 0 \\ 0 \end{bmatrix} = \begin{bmatrix} 0 \\ 0 \\ 0 \end{bmatrix} \tag{B.10}$$

No requirements are needed here for C^2 continuity.

2. Arced Flume Section *C* to Arced Flume Section *D* Connection

The general equation of an arced flume section can be expressed as

$$\boldsymbol{X}(u,w) = \boldsymbol{X}_0 + \boldsymbol{T}(\theta)\boldsymbol{x}(u,w) = \begin{bmatrix} X_{1_0} \\ X_{2_0} \\ X_{3_0} \end{bmatrix} + \begin{bmatrix} \cos\theta & \sin\theta & 0 \\ -\sin\theta & \cos\theta & 0 \\ 0 & 0 & 1 \end{bmatrix} \begin{bmatrix} x_1(u,w) \\ x_2(u,w) \\ x_3(u,w) \end{bmatrix}$$

(B.11)

where

$$\boldsymbol{x}(u,w) = [\pm \cos w\phi\,(R + r\cos u) \mp R \qquad \sin w\phi\,(R + r\cos u) \qquad r(1 + \sin u) - h\,w]^T$$

(B.12)

$\boldsymbol{T}(\theta)$ is the rotation matrix that orients the flume section by an orientation angle about the X_3 axis, X_{i_0} is the location of the local coordinate system of the flume section in the flow channel configuration, and $\boldsymbol{x}(u,w)$ is the surface function of the flume section

referring to its local coordinate system. R is the radius of the arc of the flume section. The signs in the first entry of Equation B.12 are determined by the sign of the rotation angle ϕ of the flume section. h is the height of the arced flume section, r is the radius of the semicircular cross section of the flume section, and u and w are the parametric coordinates along the circumferential and longitudinal directions of the flume section, respectively, and $u \in [0, -\pi], w \in [0, \phi]$. An example of an arced flume section with ϕ = 90º is shown in Figure B.2.

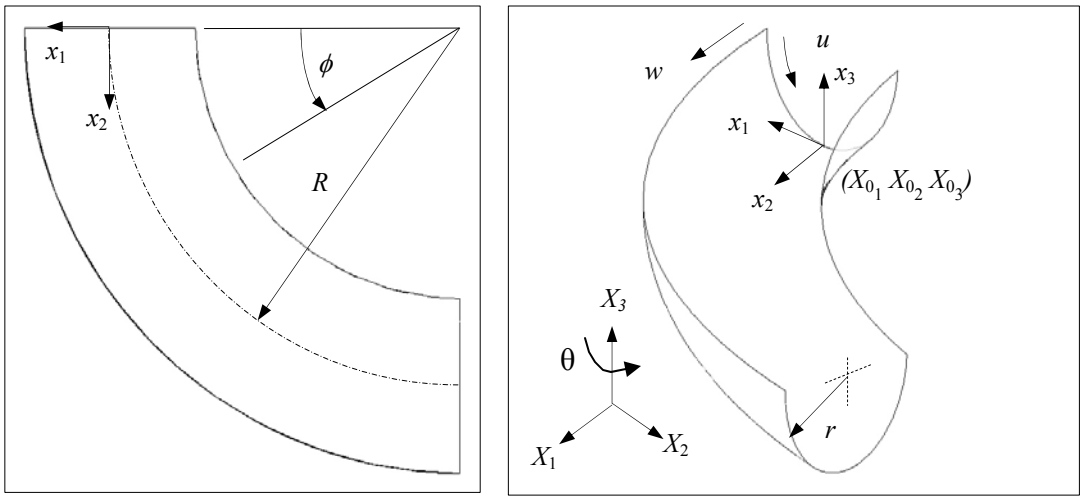


Figure B.2 90º Arced Flume Section

In this case, an arced flume section $\boldsymbol{X}^C$ (angle ϕ_C, rotation angle θ_C, height h_C) and an arced flume section $\boldsymbol{X}^D$ (angle ϕ_D, rotation angle θ_D, height h_D) are connected sequentially.

1) C^0 Continuity

The following relationship has to be satisfied for C^0 continuity:

$$\boldsymbol{X}^C(u,w)\Big|_{w=1} = \boldsymbol{X}^D(u,w)\Big|_{w=0} \tag{B.13}$$

$$\begin{bmatrix} X^C_{1_0} \\ X^C_{2_0} \\ X^C_{3_0} \end{bmatrix} + \begin{bmatrix} \cos\theta_C & \sin\theta_C & 0 \\ -\sin\theta_C & \cos\theta_C & 0 \\ 0 & 0 & 1 \end{bmatrix} \begin{bmatrix} \pm\cos w\phi_C(R_C + r_c^C\cos u) \mp R_C \\ \sin w\phi_C(R_C + r_c^C\cos u) \\ r_c^C(1+\sin u) - h_C \cdot w \end{bmatrix}\Bigg|_{w=1}$$

$$= \begin{bmatrix} X^D_{1_0} \\ X^D_{2_0} \\ X^D_{3_0} \end{bmatrix} + \begin{bmatrix} \cos\theta_D & \sin\theta_D & 0 \\ -\sin\theta_D & \cos\theta_D & 0 \\ 0 & 0 & 1 \end{bmatrix} \begin{bmatrix} \pm\cos w\phi_D(R_D + r_c^D\cos u) \mp R_D \\ \sin w\phi_D(R_D + r_c^D\cos u) \\ r_c^D(1+\sin u) - h_D \cdot w \end{bmatrix}\Bigg|_{w=0}$$

(B.14)

Substituting $w = 1$ and $w = 0$ into the respective sides of Equation B.14, one obtains

$$\begin{bmatrix} X^C_{1_0} \\ X^C_{2_0} \\ X^C_{3_0} \end{bmatrix} + \begin{bmatrix} \cos\theta_C & \sin\theta_C & 0 \\ -\sin\theta_C & \cos\theta_C & 0 \\ 0 & 0 & 1 \end{bmatrix} \begin{bmatrix} \pm\cos\phi_C(R_C + r_c^C\cos u) \mp R_C \\ \sin\phi_C(R_C + r_c^C\cos u) \\ r_c^C(1+\sin u) - h_C \end{bmatrix}$$

$$= \begin{bmatrix} X^D_{1_0} \\ X^D_{2_0} \\ X^D_{3_0} \end{bmatrix} + \begin{bmatrix} \cos\theta_D & \sin\theta_D & 0 \\ -\sin\theta_D & \cos\theta_D & 0 \\ 0 & 0 & 1 \end{bmatrix} \begin{bmatrix} \pm(R_D + r_c^D\cos u) \mp R_D \\ 0 \\ r_c^D(1+\sin u) \end{bmatrix}$$

(B.15)

From Equation B.15,

$$
\begin{aligned}
&X^C_{1_0} \pm \cos\theta_c \cdot \cos\phi_c (R_C + r_c^C \cdot \cos u) \mp \cos\theta_c \cdot R_C + \sin\theta_c \cdot \sin\phi_c (R_C + r_c^C \cdot \cos u) \\
&\qquad = X^D_{1_0} \pm \cos\theta_D \cdot (R_D + r_c^D \cdot \cos u) \mp \cos\theta_D \cdot R_D \\
&X^C_{2_0} \mp \sin\theta_c \cdot \cos\phi_c (R_C + r_c^C \cdot \cos u) \pm \sin\theta_c \cdot R_C + \cos\theta_c \cdot \sin\phi_c (R_C + r_c^C \cdot \cos u) \\
&\qquad = X^D_{2_0} \mp \sin\theta_D \cdot (R_D + r_c^D \cdot \cos u) \pm \sin\theta_D \cdot R_D \\
&X^C_{3_0} + r_c^C (1 + \sin u) - h_c = X^D_{3_0} + r_c^D (1 + \sin u)
\end{aligned}
\tag{B.16}
$$

Then, from Equation B.16, requirements for C^0 continuity are

$$
\begin{aligned}
&X^C_{1_0} \pm \cos(\theta_C \pm \phi_C) = X^D_{1_0} \pm \cos\theta_D \\
&X^C_{2_0} \pm \sin(\theta_C \mp \phi_C) = X^D_{2_0} \pm \sin\theta_D \\
&X^C_{3_0} - h_C = X^D_{3_0}, r_c^C = r_c^D, R_C = R_D
\end{aligned}
\tag{B.17}
$$

To satisfy these requirements, the radius of the cross section (r) and the radius of the arc (R) of the two flume sections must be identical. Also, the X_1, X_2, X_3 coordinate values of each flume section at the connection must be identical. When the above requirements are satisfied, C^0 continuity in the w-direction exists.

2) C^1 Continuity

The following relationship has to be satisfied for C^1 continuity:

$$
\left.\frac{\partial \boldsymbol{X}^C(u,w)}{\partial w}\right|_{w=1} = \left.\frac{\partial \boldsymbol{X}^D(u,w)}{\partial w}\right|_{w=0}
\tag{B.18}
$$

From Equation B.11,

$$\begin{bmatrix} \cos\theta_C & \sin\theta_C & 0 \\ -\sin\theta_C & \cos\theta_C & 0 \\ 0 & 0 & 1 \end{bmatrix} \begin{bmatrix} \mp\sin w_C\phi_C(R_C + r_c^C\cos u) \\ \cos w_C\phi_C(R_C + r_c^C\cos u) \\ -h_C \end{bmatrix} \tag{B.19}$$

$$= \begin{bmatrix} \cos\theta_D & \sin\theta_D & 0 \\ -\sin\theta_D & \cos\theta_D & 0 \\ 0 & 0 & 1 \end{bmatrix} \begin{bmatrix} 0 \\ (R_D + r_c^D\cos u) \\ -h_D \end{bmatrix}$$

Rearranging Equation B.19 with $w_C = 1$ results in

$$\begin{bmatrix} \mp\cos\theta_C \cdot \sin\phi_C(R_C + r_c^C\cos u) + \sin\theta_C \cdot \cos\phi_C(R_C + r_c^C\cos u) \\ -\sin\theta_C \cdot \sin\phi_C(R_C + r_c^C\cos u) + \cos\theta_C \cdot \cos\phi_C(R_C + r_c^C\cos u) \\ -h_C \end{bmatrix}$$

$$= \begin{bmatrix} \sin\theta_D \cdot (R_D + r_c^D\cos u) \\ \cos\theta_D \cdot (R_D + r_c^D\cos u) \\ -h_D \end{bmatrix}$$

(B.20)

Again, from Equation B.20, the requirements for C^1 continuity are

$$\begin{bmatrix} \sin(\theta_C \mp \phi_C)(R_C + r_c^C\cos u) \\ \cos(\theta_C \mp \phi_C)(R_C + r_c^C\cos u) \\ -h_C \end{bmatrix} = \begin{bmatrix} \sin\theta_D(R_D + r_c^D\cos u) \\ \cos\theta_D(R_D + r_c^D\cos u) \\ -h_D \end{bmatrix} \tag{B.21}$$

From the C^0 continuity requirements, $R_C = R_D, r_c^C = r_c^D$. To satisfy these requirements, height (h) of each flume sections must be identical. When the above requirements are satisfied, C^1 continuity in the w direction exists.

3) C^2 Continuity

The following relationship has to be satisfied for C^2 continuity:

$$\left.\frac{\partial^2 \boldsymbol{X}^C(u,w)}{\partial w^2}\right|_{w=\phi_C} = \left.\frac{\partial^2 \boldsymbol{X}^D(u,w)}{\partial w^2}\right|_{w=0} \tag{B.22}$$

From Equations B.11 and B.22, we have

$$\begin{bmatrix} \cos\theta_C & \sin\theta_C & 0 \\ -\sin\theta_C & \cos\theta_C & 0 \\ 0 & 0 & 1 \end{bmatrix} \begin{bmatrix} \mp\cos w_C(R_C + r_c^C \cos u) \\ -\sin w_C(R_C + r_c^C \cos u) \\ 0 \end{bmatrix} = \begin{bmatrix} \cos\theta_D & \sin\theta_D & 0 \\ -\sin\theta_D & \cos\theta_D & 0 \\ 0 & 0 & 1 \end{bmatrix} \begin{bmatrix} \mp\cos w_D(R_D + r_c^D \cos u) \\ -\sin w_D(R_D + r_c^D \cos u) \\ 0 \end{bmatrix} \tag{B.23}$$

Rearranging Equation B.23 with $w_C = 1$, $w_D = 0$, we have

$$\begin{bmatrix} \cos\theta_C & \sin\theta_C & 0 \\ -\sin\theta_C & \cos\theta_C & 0 \\ 0 & 0 & 1 \end{bmatrix} \begin{bmatrix} \mp\cos\phi_C(R_C + r_c^C \cos u) \\ -\sin\phi_C(R_C + r_c^C \cos u) \\ 0 \end{bmatrix}$$

$$= \begin{bmatrix} \cos\theta_D & \sin\theta_D & 0 \\ -\sin\theta_D & \cos\theta_D & 0 \\ 0 & 0 & 1 \end{bmatrix} \begin{bmatrix} \mp(R_D + r_c^D \cos u) \\ 0 \\ 0 \end{bmatrix}$$

(B.24)

From Equation B.24, requirements for C^2 continuity are

$$\begin{bmatrix} \mp\cos(\theta_C + \phi_C)(R_C + r_c^C \cos u) \\ -\sin(\theta_C + \phi_C)(R_C + r_c^C \cos u) \\ 0 \end{bmatrix} = \begin{bmatrix} \mp\cos\theta_D(R_D + r_c^D \cos u) \\ \pm\sin\theta_D(R_D + r_c^D \cos u) \\ 0 \end{bmatrix} \quad \text{(B.25)}$$

These requirements are already satisfied.

3. Straight Flume Section *A* to Cubic-Curve Flume Section *E* to Straight Flume Section *B* Connection

The general equation for a cubic-curve flume section can be expressed as [24]:

$$\boldsymbol{X}(u,w) = \boldsymbol{P}(w) + \boldsymbol{T}_0(\theta)\boldsymbol{x}(u,w) \quad \text{(B.26)}$$

where

$$\boldsymbol{x}(u,w) = \begin{bmatrix} r_c \cos u & 0 & r_c(1+\sin u) \end{bmatrix}$$

$$\boldsymbol{P}(w) = \boldsymbol{W}^T \boldsymbol{M}\boldsymbol{G} = \begin{bmatrix} w^3 & w^2 & w & 1 \end{bmatrix}^T \begin{bmatrix} 2 & -2 & 1 & 1 \\ -3 & 3 & -2 & -1 \\ 0 & 0 & 1 & 0 \\ 1 & 0 & 0 & 0 \end{bmatrix} \begin{bmatrix} \boldsymbol{P}_0 \\ \boldsymbol{P}_1 \\ \boldsymbol{P}_{0,w} \\ \boldsymbol{P}_{1,w} \end{bmatrix} \tag{B.27}$$

$$= \begin{bmatrix} w^3 & w^2 & w & 1 \end{bmatrix}^T \begin{bmatrix} 2 & -2 & 1 & 1 \\ -3 & 3 & -2 & -1 \\ 0 & 0 & 1 & 0 \\ 1 & 0 & 0 & 0 \end{bmatrix} \begin{bmatrix} P_{1_0} & P_{2_0} & P_{3_0} \\ P_{1_1} & P_{2_1} & P_{3_1} \\ P_{1_0,w} & P_{2_0,w} & P_{3_0,w} \\ P_{1_1,w} & P_{2_1,w} & P_{3_1,w} \end{bmatrix}$$

$\boldsymbol{M}$ is a constant 4×4 matrix, $\boldsymbol{P}_0$ and $\boldsymbol{P}_1$ are the start and end points of the curve, respectively, and $\boldsymbol{P}_{0,w}$ and $\boldsymbol{P}_{1,w}$ are the tangent vectors at the corresponding points.

In this case, a straight flume section $\boldsymbol{X}^A$ (length ℓ_A**,** height h_A**),** a cubic-curve flume section $\boldsymbol{X}^E$ (start point $\boldsymbol{P}_0$ and end point $\boldsymbol{P}_1$), and a straight flume section $\boldsymbol{X}^B$ (length ℓ_B**,** height h_B**)** are connected sequentially. The same straight flume sections *A* and *B* as in the previous cases are used.

Straight *A* to Cubic-Curve *E* Connection

1) C^0 Continuity

The following relationship has to be satisfied for C^0 continuity:

$$\boldsymbol{X}^{A}(u,w)\Big|_{w=1} = \boldsymbol{X}^{E}(u,w)\Big|_{w=0}$$

(B.28)

From Equations B.1, B.26, B.27, and B.28, we have

$$\begin{bmatrix} X^{A}_{1_0} \\ X^{A}_{2_0} \\ X^{A}_{3_0} \end{bmatrix} + \begin{bmatrix} \cos\theta_A & \sin\theta_A & 0 \\ -\sin\theta_A & \cos\theta_A & 0 \\ 0 & 0 & 1 \end{bmatrix} \begin{bmatrix} r_c^A \cos u \\ \ell_A \cdot w_A \\ r_c^A(1+\sin u_A) - h_A \cdot w_A \end{bmatrix}$$

$$= \begin{bmatrix} w_E^3 & w_E^2 & w_E & 1 \end{bmatrix}^T \begin{bmatrix} 2 & -2 & 1 & 1 \\ -3 & 3 & -2 & -1 \\ 0 & 0 & 1 & 0 \\ 1 & 0 & 0 & 0 \end{bmatrix} \begin{bmatrix} \boldsymbol{P}_0 \\ \boldsymbol{P}_1 \\ \boldsymbol{P}_{0,w} \\ \boldsymbol{P}_{1,w} \end{bmatrix} + \begin{bmatrix} \cos\theta_E & \sin\theta_E & 0 \\ -\sin\theta_E & \cos\theta_E & 0 \\ 0 & 0 & 1 \end{bmatrix} \begin{bmatrix} r_c^E \cos u \\ w_E \\ r_c^E(1+\sin u) \end{bmatrix}$$

$$= \begin{bmatrix} w_E^3 & w_E^2 & w_E & 1 \end{bmatrix}^T \begin{bmatrix} 2 & -2 & 1 & 1 \\ -3 & 3 & -2 & -1 \\ 0 & 0 & 1 & 0 \\ 1 & 0 & 0 & 0 \end{bmatrix} \begin{bmatrix} P_{1_0} & P_{2_0} & P_{3_0} \\ P_{1_1} & P_{2_1} & P_{3_1} \\ P_{1_0,w} & P_{2_0,w} & P_{3_0,w} \\ P_{1_1,w} & P_{2_1,w} & P_{3_1,w} \end{bmatrix}$$

$$+ \begin{bmatrix} \cos\theta_E & \sin\theta_E & 0 \\ -\sin\theta_E & \cos\theta_E & 0 \\ 0 & 0 & 1 \end{bmatrix} \begin{bmatrix} r_c^E \cos u \\ w_E \\ r_c^E(1+\sin u) \end{bmatrix}$$

(B.29)

Rearranging Equation B.29 with $w_A = 1$ and $w_E = 0$ results in

$$\begin{bmatrix} X^A_{1_0} \\ X^A_{2_0} \\ X^A_{3_0} \end{bmatrix} + \begin{bmatrix} \cos\theta_A & \sin\theta_A & 0 \\ -\sin\theta_A & \cos\theta_A & 0 \\ 0 & 0 & 1 \end{bmatrix} \begin{bmatrix} r_c^A \cos u \\ \ell_A \\ r_c^A(1+\sin u_A) - h_A \end{bmatrix} \tag{B.30}$$

$$= \begin{bmatrix} \cos\theta_E & \sin\theta_E & 0 \\ -\sin\theta_E & \cos\theta_E & 0 \\ 0 & 0 & 1 \end{bmatrix} \begin{bmatrix} r_c^E \cos u \\ 0 \\ r_c^E(1+\sin u) \end{bmatrix} + \begin{bmatrix} P_{1_0} \\ P_{2_0} \\ P_{3_0} \end{bmatrix}$$

From Equation B.30,

$$\begin{bmatrix} X^A_{1_0} + \cos\theta_A \cdot r_c^A \cos u + \sin\theta_A \cdot \ell_A \\ X^A_{2_0} - \sin\theta_A \cdot r_c^A \cos u + \cos\theta_A \cdot \ell_A \\ X^A_{3_0} + r_c^A(1+\sin u_A) - h_A \end{bmatrix} = \begin{bmatrix} P_{1_0} + \cos\theta_E \cdot r_c^E \cos u \\ P_{2_0} - \sin\theta_E \cdot r_c^E \cos u \\ P_{3_0} + r_c^E(1+\sin u) \end{bmatrix} \tag{B.31}$$

Then, from Equation B.31, the requirements for C^0 continuity are

$$\begin{aligned} &P_{1_0} = X^A_{1_0} + \sin\theta_A \ell_A \\ &P_{2_0} = X^A_{2_0} + \cos\theta_A \ell_A, \theta_A = \theta_E, r_c^A = r_c^E \\ &P_{3_0} = X^A_{3_0} - h_A \end{aligned} \tag{B.32}$$

To satisfy these requirements, the radius (r) and rotational angle (θ) of the two flume sections must be identical. Also, the X_1, X_2, X_3 coordinate values of each flume section at the connection must be identical. When the above requirements are satisfied, C^0 continuity in the w-direction exists.

2) C^1 Continuity

The following relationship has to be satisfied for C^1 continuity:

$$\left.\frac{\partial \boldsymbol{X}^{A}(u,w)}{\partial w}\right|_{w=\ell_A} = \left.\frac{\partial \boldsymbol{X}^{E}(u,w)}{\partial w}\right|_{w=0} \tag{B.33}$$

From Equations B.1, B.26, B.27, and B.33, we have

$$\begin{bmatrix} \cos\theta_A & \sin\theta_A & 0 \\ \sin\theta_A & \cos\theta_A & 0 \\ 0 & 0 & 1 \end{bmatrix} \begin{bmatrix} 0 \\ \ell_A \\ -h_A \end{bmatrix}$$

$$= \begin{bmatrix} 3w_E^{\,2} & 2w_E & 1 & 0 \end{bmatrix}^T \begin{bmatrix} 2 & -2 & 1 & 1 \\ -3 & 3 & -2 & -1 \\ 0 & 0 & 1 & 0 \\ 1 & 0 & 0 & 0 \end{bmatrix} \begin{bmatrix} P_{1_0} & P_{2_0} & P_{3_0} \\ P_{1_1} & P_{2_1} & P_{3_1} \\ P_{1_0,w} & P_{2_0,w} & P_{3_0,w} \\ P_{1_1,w} & P_{2_1,w} & P_{3_1,w} \end{bmatrix}$$

(B.34)

Rearranging Equation B.34 results in

$$\begin{bmatrix} \cos\theta_A & \sin\theta_A & 0 \\ \sin\theta_A & \cos\theta_A & 0 \\ 0 & 0 & 1 \end{bmatrix} \begin{bmatrix} 0 \\ \ell_A \\ h_A \end{bmatrix} = \begin{bmatrix} P_{1_0,w} & P_{2_0,w} & P_{3_0,w} \end{bmatrix} \tag{B.35}$$

Then, requirements for C^1 continuity are

$$\begin{bmatrix} \sin\theta_A \cdot \ell_A \\ \cos\theta_A \cdot \ell_A \\ h_A \end{bmatrix} = \boldsymbol{P}_{0,w} = \begin{bmatrix} P_{1_0,w} & P_{2_0,w} & P_{3_0,w} \end{bmatrix}$$

(B.36)

$$\begin{aligned} P_{1_0,w} &= \sin\theta_A \cdot \ell_A \\ P_{2_0,w} &= \cos\theta_A \cdot \ell_A \\ P_{3_0,w} &= -h_A \end{aligned} \tag{B.37}$$

To satisfy these requirements, the tangent vector at the start point $\begin{bmatrix} P_{1_0,w} & P_{2_0,w} & P_{3_0,w} \end{bmatrix}$ of the cubic-curve flume section must be identical to the values $\begin{bmatrix} \sin\theta_A \cdot \ell_A & \cos\theta_A \cdot \ell_A & h_A \end{bmatrix}$ of the straight flume section, respectively. When the above requirements are satisfied, C^1 continuity in the *w*-direction exists.

3) C^2 Continuity

The following relationship has to be satisfied for C^2 continuity:

$$\left.\frac{\partial^2 \boldsymbol{X}^A(u,w)}{\partial w^2}\right|_{w=1} = \left.\frac{\partial^2 \boldsymbol{X}^E(u,w)}{\partial w^2}\right|_{w=0} \tag{B.38}$$

From Equations B.1, B.26, B.27, and B.38 with $w_A = 1$, we have

$$\begin{bmatrix}0\\0\\0\end{bmatrix} = \begin{bmatrix}6w_E & 2 & 0 & 0\end{bmatrix}^T \begin{bmatrix}2 & -2 & 1 & 1\\ -3 & 3 & -2 & -1\\ 0 & 0 & 1 & 0\\ 1 & 0 & 0 & 0\end{bmatrix} \begin{bmatrix}\boldsymbol{P}_0\\ \boldsymbol{P}_1\\ \boldsymbol{P}_{0,w}\\ \boldsymbol{P}_{1,w}\end{bmatrix}$$

$$= \begin{bmatrix}6w_E & 2 & 0 & 0\end{bmatrix}^T \begin{bmatrix}2 & -2 & 1 & 1\\ -3 & 3 & -2 & -1\\ 0 & 0 & 1 & 0\\ 1 & 0 & 0 & 0\end{bmatrix} \begin{bmatrix}P_{1_0} & P_{2_0} & P_{3_0}\\ P_{1_1} & P_{2_1} & P_{3_1}\\ P_{1_0,w} & P_{2_0,w} & P_{3_0,w}\\ P_{1_1,w} & P_{2_1,w} & P_{3_1,w}\end{bmatrix} \quad \text{(B.39)}$$

Rearranging Eqaution B.39 with $w_E = 0$, we get

$$\begin{bmatrix}0\\0\\0\end{bmatrix} = \begin{bmatrix}-6 & 6 & -4 & -2\end{bmatrix} \begin{bmatrix}P_{1_0} & P_{2_0} & P_{3_0}\\ P_{1_1} & P_{2_1} & P_{3_1}\\ P_{1_0,w} & P_{2_0,w} & P_{3_0,w}\\ P_{1_1,w} & P_{2_1,w} & P_{3_1,w}\end{bmatrix}$$

(B.40)

Then, requirements for C^2 continuity are

$$\begin{aligned}0 &= 6P_{1_1} - 4P_{1_0,w} - 2P_{1_1,w} - 6P_{1_0}\\ 0 &= 6P_{2_1} - 4P_{2_0,w} - 2P_{2_1,w} - 6P_{2_0}\\ 0 &= 6P_{3_1} - 4P_{3_0,w} - 2P_{3_1,w} - 6P_{3_0}\end{aligned}$$

(B.41)

Existence of C^2 continuity will be discussed with Equation B.54.

Cubic-Curve *E* to Straight *B* Connection

1) C^0 Continuity

The following relationship has to be satisfied for C^0 continuity:

$$\boldsymbol{X}^{E}(u,w)\Big|_{w=1} = \boldsymbol{X}^{B}(u,w)\Big|_{w=0}$$

(B.42)

From Equations, B.1, B.26, B.27, and B.42, we have

$$\begin{bmatrix} w_E^3 & w_E^2 & w_E & 1 \end{bmatrix}^T \begin{bmatrix} 2 & -2 & 1 & 1 \\ -3 & 3 & -2 & -1 \\ 0 & 0 & 1 & 0 \\ 1 & 0 & 0 & 0 \end{bmatrix} \begin{bmatrix} P_{1_0} & P_{2_0} & P_{3_0} \\ P_{1_1} & P_{2_1} & P_{3_1} \\ P_{1_0,w} & P_{2_0,w} & P_{3_0,w} \\ P_{1_1,w} & P_{2_1,w} & P_{3_1,w} \end{bmatrix}$$

$$+ \begin{bmatrix} \cos\theta_E & \sin\theta_E & 0 \\ -\sin\theta_E & \cos\theta_E & 0 \\ 0 & 0 & 1 \end{bmatrix} \begin{bmatrix} r_c^E \cos u \\ 0 \\ r_c^E(1+\sin u) \end{bmatrix} = \begin{bmatrix} X_{1_0}^B \\ X_{2_0}^B \\ X_{3_0}^B \end{bmatrix} + \begin{bmatrix} \cos\theta_B & \sin\theta_B & 0 \\ -\sin\theta_B & \cos\theta_B & 0 \\ 0 & 0 & 1 \end{bmatrix} \begin{bmatrix} r_c^B \cos u \\ \ell_B \cdot w_B \\ r_c^B(1+\sin u) - h_B \cdot w_B \end{bmatrix}$$

(B.43)

Rearranging Equation B.43 with $w_E = 1$ and $w_B = 0$ results in

$$\begin{bmatrix} P_{1_1} \\ P_{2_1} \\ P_{3_1} \end{bmatrix} + \begin{bmatrix} \cos\theta_E & \sin\theta_E & 0 \\ -\sin\theta_E & \cos\theta_E & 0 \\ 0 & 0 & 1 \end{bmatrix} \begin{bmatrix} r_c^E \cos u \\ 0 \\ r_c^E(1+\sin u) \end{bmatrix} = \begin{bmatrix} X_{1_0}^B \\ X_{2_0}^B \\ X_{3_0}^B \end{bmatrix} + \begin{bmatrix} \cos\theta_B & \sin\theta_B & 0 \\ -\sin\theta_B & \cos\theta_B & 0 \\ 0 & 0 & 1 \end{bmatrix} \begin{bmatrix} r_c^B \cos u \\ 0 \\ r_c^B(1+\sin u) \end{bmatrix}$$

(B.44)

Again, rearranging Equation B.44, we get

$$\begin{bmatrix} P_{1_1} + \cos\theta_E \cdot r_c^E \cos u \\ P_{2_1} - \sin\theta_E \cdot r_c^E \cos u \\ P_{3_1} + r_c^E (1 + \sin u) \end{bmatrix} = \begin{bmatrix} X_{1_0}^B + \cos\theta_B \cdot r_c^B \cos u \\ X_{2_0}^B - \sin\theta_B \cdot r_c^B \cos u \\ X_{3_0}^B + r_c^B (1 + \sin u) \end{bmatrix} \quad \text{(B.45)}$$

Then, requirements for C^0 continuity are:

$$\begin{aligned} &\theta_E = \theta_B, r_c^E = r_c^B \\ &P_{1_1} = X_{1_0}^B \\ &P_{2_1} = X_{2_0}^B \\ &P_{3_1} = X_{3_0}^B \end{aligned} \quad \text{(B.46)}$$

To satisfy these requirements, the radius (r) and rotational angle (θ) of the two flume sections must be identical. Also, the X_1, X_2, X_3 coordinate values of each flume section at the connection must be identical. When the above requirements are satisfied, C^0 continuity in the w-direction exists.

2) C^1 Continuity

The following relationship has to be satisfied for C^1 continuity:

$$\left.\frac{\partial \boldsymbol{X}^{E}(u,w)}{\partial w}\right|_{w=1} = \left.\frac{\partial \boldsymbol{X}^{B}(u,w)}{\partial w}\right|_{w=0} \tag{B.47}$$

From Equations B.1, B.26, B.27, and B.47, we have

$$\begin{aligned}\begin{bmatrix} 3\cdot w_E^2 & 2\cdot w_E & 1 & 0 \end{bmatrix}^T \begin{bmatrix} 2 & -2 & 1 & 1 \\ -3 & 3 & -2 & -1 \\ 0 & 0 & 1 & 0 \\ 1 & 0 & 0 & 0 \end{bmatrix} \begin{bmatrix} P_{1_0} & P_{2_0} & P_{3_0} \\ P_{1_1} & P_{2_1} & P_{3_1} \\ P_{1_0,w} & P_{2_0,w} & P_{3_0,w} \\ P_{1_1,w} & P_{2_1,w} & P_{3_1,w} \end{bmatrix} \\ = \begin{bmatrix} \cos\theta_B & \sin\theta_B & 0 \\ -\sin\theta_B & \cos\theta_B & 0 \\ 0 & 0 & 1 \end{bmatrix} \begin{bmatrix} 0 \\ \ell_B \\ h_B \end{bmatrix}\end{aligned} \tag{B.48}$$

Rearranging Equation B.48 with $w_E = 1$, $w_B = 0$ results in

$$\begin{aligned}\begin{bmatrix} 3 & 2 & 1 & 0 \end{bmatrix}^T \begin{bmatrix} 2 & -2 & 1 & 1 \\ -3 & 3 & -2 & -1 \\ 0 & 0 & 1 & 0 \\ 1 & 0 & 0 & 0 \end{bmatrix} \begin{bmatrix} P_{1_0} & P_{2_0} & P_{3_0} \\ P_{1_1} & P_{2_1} & P_{3_1} \\ P_{1_0,w} & P_{2_0,w} & P_{3_0,w} \\ P_{1_1,w} & P_{2_1,w} & P_{3_1,w} \end{bmatrix} \\ = \begin{bmatrix} P_{1_1,w} & P_{2_1,w} & P_{3_1,w} \end{bmatrix} = \begin{bmatrix} \sin\theta_B \cdot \ell_B \\ \cos\theta_B \cdot \ell_B \\ h_B \end{bmatrix}\end{aligned} \tag{B.49}$$

From Equation B.49, we can get the requirements for C^1 continuity.

They are

$$
\begin{aligned}
P_{1_1,w} &= \sin\theta_B \cdot \ell_B \\
P_{2_1,w} &= \cos\theta_B \cdot \ell_B \\
P_{3_1,w} &= -h_B
\end{aligned}
\tag{B.50}
$$

To satisfy these requirements, the tangent vector at the end point $\begin{bmatrix} P_{1_1,w} & P_{2_1,w} & P_{3_1,w} \end{bmatrix}$ of the cubic-curve flume section must be identical to the values $\begin{bmatrix} \sin\theta_B \cdot \ell_B & \cos\theta_B \cdot \ell_B & h_B \end{bmatrix}$ of the straight flume section, respectively. When the above requirements are satisfied, C^1 continuity in the *w*-direction exists.

3) C^2 Continuity

The following relationship has to be satisfied for C^2 continuity:

$$
\left.\frac{\partial^2 \boldsymbol{X}^E(u,w)}{\partial w^2}\right|_{w=1} = \left.\frac{\partial^2 \boldsymbol{X}^B(u,w)}{\partial w^2}\right|_{w=0} \tag{B.51}
$$

From Equations B.1, B.26, B.27, and B.51, we have

$$\begin{bmatrix} 6 & 2 & 0 & 0 \end{bmatrix}^T \begin{bmatrix} 2 & -2 & 1 & 1 \\ -3 & 3 & -2 & -1 \\ 0 & 0 & 1 & 0 \\ 1 & 0 & 0 & 0 \end{bmatrix} \begin{bmatrix} P_{1_0} & P_{2_0} & P_{3_0} \\ P_{1_1} & P_{2_1} & P_{3_1} \\ P_{1_0,w} & P_{2_0,w} & P_{3_0,w} \\ P_{1_1,w} & P_{2_1,w} & P_{3_1,w} \end{bmatrix}$$

$$= \begin{bmatrix} \cos\theta_B & \sin\theta_B & 0 \\ -\sin\theta_B & \cos\theta_B & 0 \\ 0 & 0 & 1 \end{bmatrix} \begin{bmatrix} 0 \\ 0 \\ 0 \end{bmatrix} \tag{B.52}$$

$$\begin{bmatrix} 6 & -6 & 2 & 4 \end{bmatrix} \begin{bmatrix} P_{1_0} & P_{2_0} & P_{3_0} \\ P_{1_1} & P_{2_1} & P_{3_1} \\ P_{1_0,w} & P_{2_0,w} & P_{3_0,w} \\ P_{1_1,w} & P_{2_1,w} & P_{3_1,w} \end{bmatrix} = \begin{bmatrix} 6P_{1_0} - 6P_{1_1} + 2P_{1_0,w} + 4P_{1_1,w} \\ 6P_{2_0} - 6P_{2_1} + 2P_{2_0,w} + 4P_{2_1,w} \\ 6P_{3_0} - 6P_{3_1} + 2P_{3_0,w} + 4P_{4_1,w} \end{bmatrix} = \begin{bmatrix} 0 \\ 0 \\ 0 \end{bmatrix}$$

(B.53)

Then, requirements for C^2 continuity are

$$\begin{aligned} 0 &= -6P_{1_1} + 2P_{1_0,w} + 4P_{1_1,w} + 6P_{1_0} \\ 0 &= -6P_{2_1} + 2P_{2_0,w} + 4P_{2_1,w} + 6P_{2_0} \\ 0 &= -6P_{3_1} + 2P_{3_0,w} + 4P_{3_1,w} + 6P_{3_0} \end{aligned} \tag{B.54}$$

From Equation B.37, B.41, B.50, and B.54, we have

$$\begin{aligned} P_{1_0,w} &= P_{1_1,w} \\ P_{2_0,w} &= P_{2_1,w} \\ P_{3_0,w} &= P_{3_1,w} \end{aligned} \quad \text{, and} \quad \begin{aligned} \sin\theta_A \cdot \ell_A &= \sin\theta_B \cdot \ell_B \\ \cos\theta_A \cdot \ell_A &= \cos\theta_B \cdot \ell_B \\ -h_A &= -h_B \end{aligned}$$

To satisfy these requirements, the tangent vector at the start point $\begin{bmatrix} P_{1_0,w} & P_{2_0,w} & P_{3_0,w} \end{bmatrix}$ and at the end point $\begin{bmatrix} P_{1_1,w} & P_{2_1,w} & P_{3_1,w} \end{bmatrix}$ of the cubic-curve flume section must be identical, and the lengths (ℓ) and rotational angles (θ) of the two straight flume sections must be identical. When the above requirements are satisfied, C^2 continuity in the *w*-direction exists.

4. Arced Flume Section *C* to Straight Flume Section *B* Connection

In this case, an arced flume section $\boldsymbol{X}^C$ (angle ϕ_C, rotation angle θ_C, height h_C) and a straight flume section $\boldsymbol{X}^B$ (length ℓ_B, height h_B) are connected sequentially.

1) C^0 Continuity

The following relationship has to be satisfied for C^0 continuity:

$$\boldsymbol{X}^C(u,w)\Big|_{w=1} = \boldsymbol{X}^B(u,w)\Big|_{w=0} \tag{B.55}$$

From Equations B.1, B.11, and B.55, we have

$$\begin{bmatrix} X^C_{1_0} \\ X^C_{2_0} \\ X^C_{3_0} \end{bmatrix} + \begin{bmatrix} \cos\theta_C & \sin\theta_C & 0 \\ -\sin\theta_C & \cos\theta_C & 0 \\ 0 & 0 & 1 \end{bmatrix} \begin{bmatrix} \pm\cos w_C\phi_C(R_C + r_c^C\cos u) \mp R_C \\ \sin w_C\phi_C(R_C + r_c^C\cos u) \\ r_c^C(1+\sin u) - h_C \cdot w_C \end{bmatrix}$$

$$= \begin{bmatrix} X^B_{1_0} \\ X^B_{2_0} \\ X^B_{3_0} \end{bmatrix} + \begin{bmatrix} \cos\theta_B & \sin\theta_B & 0 \\ -\sin\theta_B & \cos\theta_B & 0 \\ 0 & 0 & 1 \end{bmatrix} \begin{bmatrix} r_c^B\cos u \\ \ell_B \cdot w_B \\ r_c^B(1+\sin u) - h_B \cdot w_B \end{bmatrix} \qquad \text{(B.56)}$$

Rearranging Equation B.56 with $w_C = 1$ and $w_B = 0$, we have the requirements for C^0 continuity.

They are

$$\begin{aligned} &X^C_{1_0} \pm \cos(\theta_C \pm \phi_C) \mp \cos\theta_C R_C = X^B_{1_0} + \cos\theta_B r_c^B \cos u \\ &X^C_{2_0} \pm \sin(\theta_C \pm \phi_C) \pm \sin\theta_C R_C = X^B_{2_0} - \sin\theta_B r_c^B \cos u \\ &X^C_{3_0} + r_c^C(1+\sin u) - h_C \cdot \phi_C = X^B_{3_0} + r_c^B(1+\sin u) \end{aligned} \qquad \text{(B.57)}$$

To satisfy these requirements, the X_1, X_2, X_3 coordinate values of the two flume sections at the connection must be identical. When the above requirements are satisfied, C^0 continuity in the *w*-direction exists.

2) C^1 Continuity

Similarly, the following relationship has to be satisfied for C^1 continuity:

$$\left.\frac{\partial \boldsymbol{X}^{C}(u,w)}{\partial w}\right|_{w=1} = \left.\frac{\partial \boldsymbol{X}^{B}(u,w)}{\partial w}\right|_{w=0} \tag{B.58}$$

From Equations B.1, B.11, and B.58 with $w_C = 1$ and $w_B = 0$, we have

$$\begin{bmatrix} \cos\theta_C & \sin\theta_C & 0 \\ -\sin\theta_C & \cos\theta_C & 0 \\ 0 & 0 & 1 \end{bmatrix} \begin{bmatrix} \mp \sin w_C (R_C + r_c^C \cos u) \\ \cos w_C (R_C + r_c^C \cos u) \\ -h_C \end{bmatrix} = \begin{bmatrix} \cos\theta_B & \sin\theta_B & 0 \\ \sin\theta_B & \cos\theta_B & 0 \\ 0 & 0 & 1 \end{bmatrix} \begin{bmatrix} 0 \\ 1 \\ -\dfrac{h_B}{\ell_B} \end{bmatrix} \tag{B.59}$$

Then, requirements for C^1 continuity are

$$\begin{aligned} &\sin(\theta_C \pm \phi_C)(R_C + r_c^C \cos u) = \sin\theta_B \\ &\cos(\theta_C \pm \phi_C)(R_C + r_c^C \cos u) = \cos\theta_B \\ &-h_C = -h_B \end{aligned} \tag{B.60}$$

Existence of C^1 continuity in w-direction will be discussed with C^2 continuity.

3) C^2 Continuity

The following relationship has to be satisfied for C^2 continuity:

$$\left.\frac{\partial^2 \boldsymbol{X}^{C}(u,w)}{\partial w^2}\right|_{w=1} = \left.\frac{\partial^2 \boldsymbol{X}^{B}(u,w)}{\partial w^2}\right|_{w=0} \tag{B.61}$$

From Equations B.1, B.11, and B.61, we have

$$\begin{bmatrix} \cos\theta_C & \sin\theta_C & 0 \\ -\sin\theta_C & \cos\theta_C & 0 \\ 0 & 0 & 1 \end{bmatrix} \begin{bmatrix} \mp\cos w_C(R_C + r_c^C \cos u) \\ -\sin w_C(R_C + r_c^C \cos u) \\ 0 \end{bmatrix} = 0$$

(B.62)

Rearranging Equation B.62 with w_C =1, and w_B = 0, we have the requirements for C^2 continuity.

They are

$$\begin{aligned} &\pm\cos(\theta_C \mp \phi_C)(R_C + r_c^C \cos u) = 0 \\ &\pm\sin(\theta_C \mp \phi_C)(R_C + r_c^C \cos u) = 0 \\ &0 = 0 \end{aligned} \qquad \text{(B.63)}$$

However, if we compare Equations B.60 and B.63, both requirements cannot be satisfied at the same time. Either C^1 or C^2 continuity cannot be satisfied. Therefore, arced flume sections cannot be connected to straight flume sections with C^2 continuity.

APPENDIX C: FRICTIONAL FORCES

C.1. Frictional Forces due to Centrifugal Forces

The tangent vectors of the particle trace along the *u* and *w*-directions, as shown in Figure C.1, can be written as

$$\boldsymbol{P}_{,u} = \frac{\partial \boldsymbol{P}}{\partial u} = \left[\frac{\partial x}{\partial u} \quad \frac{\partial y}{\partial u} \quad \frac{\partial z}{\partial u}\right] = \left[x_{1,u} \quad x_{2,u} \quad x_{3,u}\right] \tag{C.1}$$

and

$$\boldsymbol{P}_{,w} = \frac{\partial \boldsymbol{P}}{\partial w} = \left[\frac{\partial x}{\partial w} \quad \frac{\partial y}{\partial w} \quad \frac{\partial z}{\partial w}\right] = \left[x_{1,w} \quad x_{2,w} \quad x_{3,w}\right] \tag{C.2}$$

The unit vectors along the *u*- and *w*-tangent directions can be defined as

$$\hat{\boldsymbol{e}}_u \equiv \frac{\boldsymbol{P}_{,u}}{\left\|\boldsymbol{P}_{,u}\right\|}$$

(C.3)

and

$$\hat{\boldsymbol{e}}_w = \frac{\boldsymbol{P}_{,w}}{\left\|\boldsymbol{P}_{,w}\right\|} \tag{C.4}$$

where $\left\|\bullet\right\|$ is the Euclidean norm of the vector.

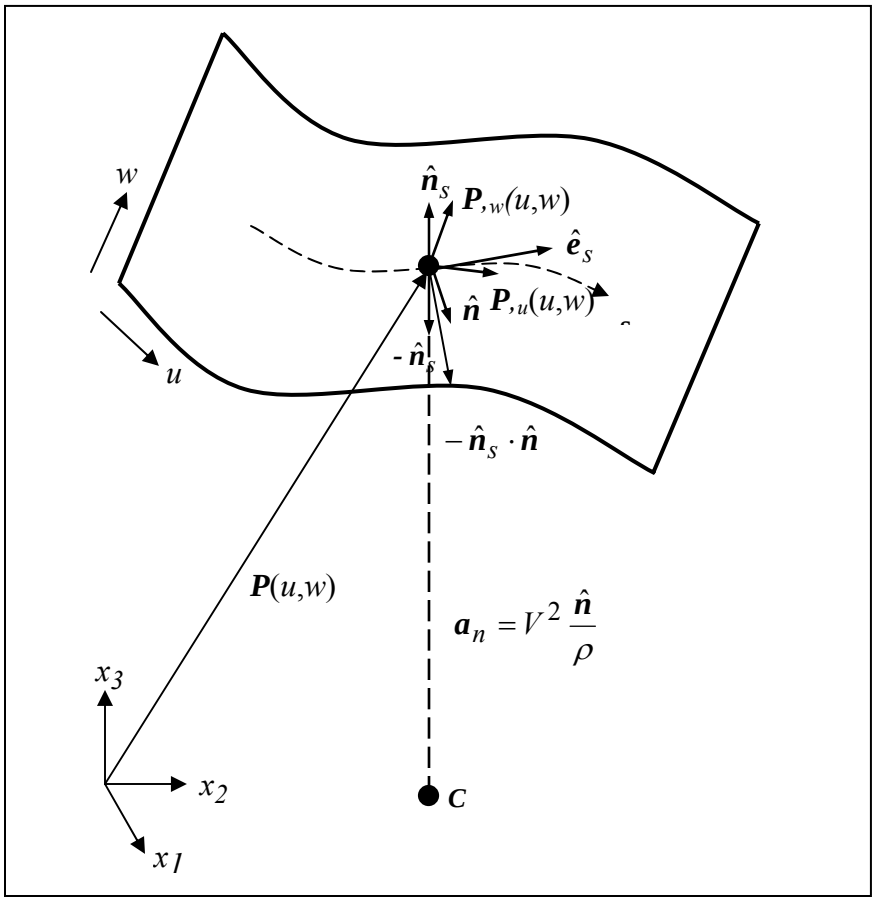


Figure C.1 Vectors of Particle on Surface

The velocity of the particle is given by the expression

$$\boldsymbol{V} = \frac{d\boldsymbol{P}}{dt} = \dot{\boldsymbol{P}} = \left[x_{1,u}\dot{u} + x_{1,w}\dot{w} \qquad x_{2,u}\dot{u} + x_{2,w}\dot{w} \qquad x_{3,u}\dot{u} + x_{3,w}\dot{w} \right] \tag{C.5}$$

$$= \|\boldsymbol{V}\| \hat{\boldsymbol{e}}_s = V\hat{\boldsymbol{e}}_s$$

where $\hat{\boldsymbol{e}}_s$ is the unit vector in the $\boldsymbol{V}$ direction and V is the magnitude of the vector $\boldsymbol{V}$.

The acceleration of the particle is defined as

$$\boldsymbol{a} = \frac{d\mathbf{V}}{dt} = \frac{d}{dt}\left(V\hat{\boldsymbol{e}}_s\right) = \frac{dV}{dt}\hat{\boldsymbol{e}}_s + V\frac{d\hat{\boldsymbol{e}}_s}{dt} = \dot{V}\hat{\boldsymbol{e}}_s + V\dot{\hat{\boldsymbol{e}}}_s \tag{C.6}$$

with

$$\frac{d\hat{\boldsymbol{e}}_s}{dt} = \dot{\hat{\boldsymbol{e}}}_s = \frac{d\hat{\boldsymbol{e}}_s}{ds}\cdot\frac{ds}{dt} = V\frac{d\hat{\boldsymbol{e}}_s}{ds} \tag{C.7}$$

where s is the arclength along the curve.

Then, the acceleration can be written as

$$\boldsymbol{a} = \frac{d\mathbf{V}}{dt} = \dot{V}\hat{\boldsymbol{e}}_s + V^2\frac{d\hat{\boldsymbol{e}}_s}{ds} \tag{C.8}$$

Note that

$$\frac{d\hat{\boldsymbol{e}}_s}{ds} = \frac{1}{\rho}\hat{\boldsymbol{n}} \tag{C.9}$$

where $\hat{\boldsymbol{n}}$ is the unit vector perpendicular to $\hat{\boldsymbol{e}}_s$ and ρ is the radius of curvature of the path of the particle shown in Figure C.1. Hence,

$$\boldsymbol{a} = \boldsymbol{a}_S + \boldsymbol{a}_n = \dot{V}\hat{\boldsymbol{e}}_{\mathrm{S}} + \frac{V^2}{\rho}\hat{\boldsymbol{n}} \tag{C.10}$$

In the above expression, $\dot{V}\hat{\boldsymbol{e}}_{\mathrm{s}}$ and $\frac{V^2}{\rho}\hat{\boldsymbol{n}}$ represent the accelerations along the tangential and normal directions along the particle trace, respectively. The later part is the centripetal acceleration.

Since the centrifugal force acting on the particle is known, the friction force that is acting on the particle can be calculated. This friction force will be perpendicular to the centrifugal force vector and will be opposite to the direction of the velocity vector. Only the component of $\frac{\hat{\boldsymbol{n}}}{\rho}$ that is normal to the surface is of interest for calculating the friction force. The unit vector that is normal to the surface, as shown in Figure C.1., can be defined as $\hat{\boldsymbol{n}}_S = \frac{\boldsymbol{P}_{,u} \times \boldsymbol{P}_{,w}}{\left|\boldsymbol{P}_{,u} \times \boldsymbol{P}_{,w}\right|}$.

Thus, the magnitude of the centrifugal force normal to the surface is $\frac{mV^2}{\rho}\left(\hat{\boldsymbol{n}} \cdot \hat{\boldsymbol{n}}_s\right)$.

Since $\hat{\boldsymbol{n}} \cdot \hat{\boldsymbol{n}}_s = \cos\phi$ (Figure C.1), the magnitude of the friction force is $\frac{\mu m V^2}{\rho}\cos\phi$, where μ is the coefficient of dynamic friction and *m* is the mass of the particle.

The direction of the friction force, which is opposite to the direction of the velocity of the particle, is given by $-\hat{\boldsymbol{e}}_s$. Now, the component of the friction force that is acting in the *u*-direction is given by $-\hat{\boldsymbol{e}}_S \cdot \boldsymbol{P}_{,u}$ and, for the *w*-direction, by $-\hat{\boldsymbol{e}}_S \cdot \boldsymbol{P}_{,w}$.

C.2 Friction Forces due to Particle Mass

Let $\boldsymbol{R}$ be the normal reaction force acting on the particle from the surface due to the weight of the particle, i.e.,

$$\boldsymbol{R} = \begin{bmatrix} R_{x_1} & R_{x_2} & R_{x_3} \end{bmatrix}^T \tag{C.11}$$

Then,

$$\boldsymbol{R} = \|\boldsymbol{R}\|\hat{\boldsymbol{n}}_S = R\hat{\boldsymbol{n}}_S \tag{C.12}$$

where R is the magnitude of the reaction force $\boldsymbol{R}$, $\hat{\boldsymbol{n}}_s$ is the unit vector normal to the surface as shown in Figure C.2, and

$$\hat{\boldsymbol{n}}_s = \begin{bmatrix} \cos\alpha_{x_1} & \cos\alpha_{x_2} & \cos\alpha_{x_3} \end{bmatrix}^T \tag{C.13}$$

From geometry, $$R = W \cdot \hat{\boldsymbol{n}}_s = mg\cos\alpha_z \tag{C.14}$$

and

$$R_{x_1} = R\cos(\alpha_{x_1})$$

$$R_{x_2} = R\cos(\alpha_{x_2}) \qquad \text{(C.15)}$$

$$R_{x_3} = R\cos(\alpha_{x_3})$$

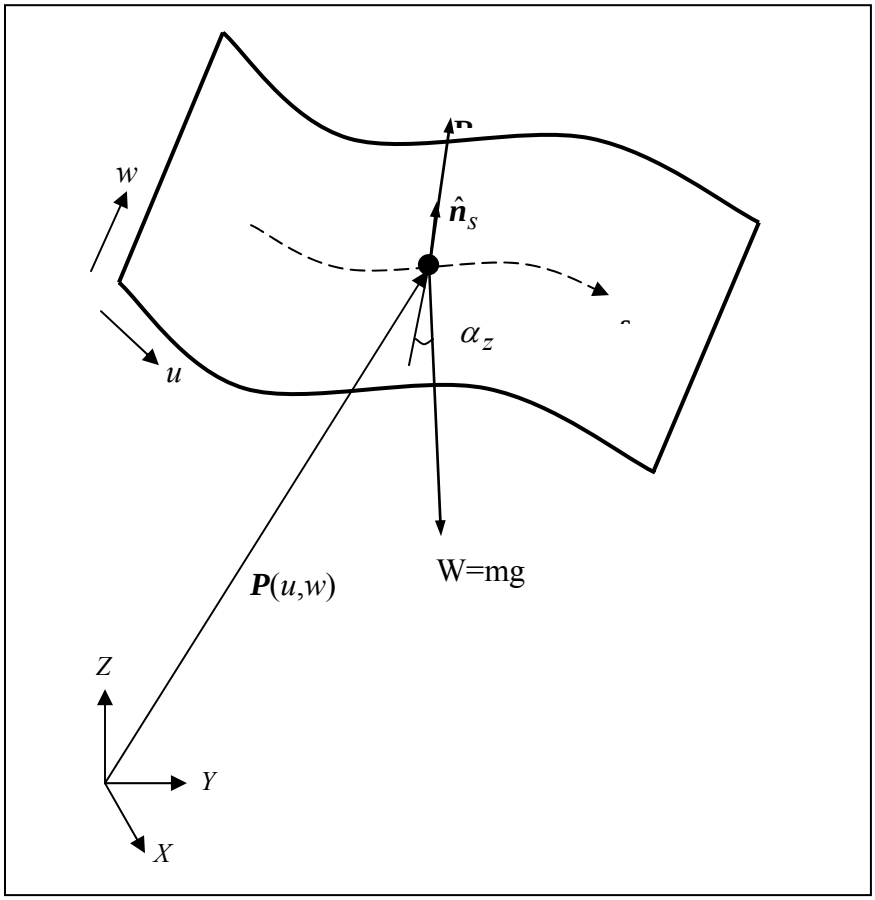


Figure C.2 Normal Reaction Force and Unit Normal Vector

Let $\boldsymbol{F}$ be the friction force due to the weight of the particle and μ be the friction coefficient. Then, one has

$$\boldsymbol{F} = \left[F_{x_1}, \quad F_{x_2}, \quad F_{x_3} \right]^T \tag{C.16}$$

and

$$\begin{aligned} F_{x_1} &= \mu R_{x1} \\ F_{x_2} &= \mu R_{x_2} \\ F_{x_3} &= \mu R_{x_3} \end{aligned} \tag{C.17}$$

C.3 Total Friction Force

The total friction force will be given by the summation of the friction force due to the normal reaction forces and the centrifugal forces. The total friction forces acting in the *u*- and *w*-directions are

$$\boldsymbol{F}_u = \left(\mu R + \frac{\mu m V^2}{\rho} \cos\phi \right) \left(-\hat{\boldsymbol{e}}_{\mathrm{s}} \cdot \boldsymbol{P}_{,u} \right) \tag{C.18}$$

and

$$\boldsymbol{F}_w = \left(\mu R + \frac{\mu m V^2}{\rho} \cos\phi \right) \left(-\hat{\boldsymbol{e}}_{\mathrm{S}} \cdot \boldsymbol{P}_{,w} \right) \tag{C.19}$$

APPENDIX D: DERIVATIONS OF SENSITIVITY EQUATIONS

In this appendix, detailed derivations of the sensitivity equations are presented.

From Equations 5.1 and 5.2., we get

$$k_0\ddot{u} = k_1\dot{u}^2 + k_2\dot{w}^2 + k_3\dot{u}\dot{w} + k_4 \tag{D.1}$$

$$k_0\ddot{w} = k_5\dot{u}^2 + k_6\dot{w}^2 + k_7\dot{u}\dot{w} + k_8 \tag{D.2}$$

where

$$\begin{aligned}
k_0 &= ac - b^2 \\
k_1 &= -0.5\cdot c\cdot a_{,u} - 0.5\cdot b\cdot a_{,w} + b\cdot b_{,u} \\
k_2 &= 0.5\cdot c\cdot c_{,u} + 0.5\cdot b\cdot c_{,w} - c\cdot b_{,w} \\
k_3 &= b\cdot c_{,u} - c\cdot a_{,w} \\
k_4 &= g\cdot(b\cdot x_{3,w} - c\cdot x_{3,u}) \\
k_5 &= 0.5\cdot a\cdot a_{,w} + 0.5\cdot b\cdot a_{,u} - a\cdot b_{,u} \\
k_6 &= -0.5\cdot a\cdot c_{,w} - 0.5\cdot b\cdot c_{,u} + b\cdot b_{,w} \\
k_7 &= b\cdot a_{,w} - a\cdot c_{,u} \\
k_8 &= g\cdot(b\cdot x_{3,u} - a\cdot x_{3,w})
\end{aligned} \tag{D.3}$$

Taking derivatives of Equations D.1 and D.2 with respect to D (a design variable, can be either a control point or a dimension), one has

$$\begin{aligned}
\frac{dk_0}{dD}\ddot{u} + k_0\frac{d\ddot{u}}{dD} = \frac{dk_1}{dD}\dot{u}^2 + k_1\cdot 2\cdot\dot{u}\frac{d\dot{u}}{dD} + \frac{dk_2}{dD}\dot{w}^2 \\
+ k_2\cdot 2\cdot\dot{w}\frac{d\dot{w}}{dD} + \frac{dk_3}{dD}\dot{u}\dot{w} + k_3\frac{d\dot{u}}{dD}\dot{w} + k_4\frac{d\dot{w}}{dD}\dot{u} + \frac{dk_4}{dD}
\end{aligned} \tag{D.4}$$

$$\frac{dk_0}{dD}\ddot{w}+k_0\frac{d\ddot{w}}{dD}=\frac{dk_5}{dD}\dot{u}^2+k_5\cdot 2\cdot\dot{u}\frac{d\dot{u}}{dD}+\frac{dk_6}{dD}\dot{w}^2 \\ +k_6\cdot 2\cdot\dot{w}\frac{d\dot{w}}{dD}+\frac{dk_7}{dD}\dot{u}\dot{w}+k_7\frac{d\dot{u}}{dD}\dot{w}+k_8\frac{d\dot{w}}{dD}\dot{u}+\frac{dk_8}{dD} \tag{D.5}$$

where the coefficient terms $\frac{dk_i}{dD}$ (i=1…8) are shown in

Equations D.6a – D.6i:

$$\frac{dk_0}{dD}=\frac{da}{dD}\cdot c+a\cdot\frac{dc}{dD}-2\cdot b\cdot\frac{db}{dD} \tag{D.6a}$$

$$\frac{dk_1}{dD}=-0.5(\frac{dc}{dD}\cdot a_{,u}+c\cdot\frac{da_{,u}}{dD})-0.5(\frac{db}{dD}\cdot a_{,w}+b\cdot\frac{da_{,w}}{dD})+(\frac{db}{dD}\cdot b_{,u}+b\cdot\frac{db_{,u}}{dD}) \tag{D.6b}$$

$$\frac{dk_2}{dD}=0.5(\frac{dc}{dD}\cdot c_{,u}+c\cdot\frac{dc_{,u}}{dD})+0.5(\frac{db}{dD}\cdot c_{,w}+b\cdot\frac{dc_{,w}}{dD})-(\frac{dc}{dD}\cdot b_{,w}+c\cdot\frac{db_{,w}}{dD}) \tag{D.6c}$$

$$\frac{dk_3}{dD}=-(\frac{dc}{dD}\cdot a_{,w}+c\cdot\frac{da_{,w}}{dD})+(\frac{db}{dD}\cdot c_{,u}+b\cdot\frac{dc_{,u}}{dD}) \tag{D.6d}$$

$$\frac{dk_4}{dD}=-g\left\{(\frac{dc}{dD}\cdot x_{3,u}+c\cdot\frac{dx_{3,u}}{dD})-(\frac{db}{dD}\cdot x_{3,w}+b\cdot\frac{dx_{3,w}}{dD})\right\} \tag{D.6e}$$

$$\frac{dk_5}{dD}=0.5(\frac{db}{dD}\cdot a_{,u}+b\cdot\frac{da_{,u}}{dD})+0.5(\frac{da}{dD}\cdot a_{,w}+a\cdot\frac{da_{,w}}{dD})-(\frac{da}{dD}\cdot b_{,u}+a\cdot\frac{db_{,u}}{dD}) \tag{D.6f}$$

$$\frac{dk_6}{dD} = -0.5\left(\frac{db}{dD}\cdot c_{,u} + b\cdot\frac{dc_{,u}}{dD}\right) - 0.5\left(\frac{da}{dD}\cdot c_{,w} + a\cdot\frac{dc_{,w}}{dD}\right) + \left(\frac{db}{dD}\cdot b_{,w} + b\cdot\frac{db_{,w}}{dD}\right) \tag{D.6g}$$

$$\frac{dk_7}{dD} = \left(\frac{db}{dD}\cdot a_{,w} + b\cdot\frac{da_{,w}}{dD}\right) - \left(\frac{da}{dD}\cdot c_{,u} + a\cdot\frac{dc_{,u}}{dD}\right) \tag{D.6h}$$

$$\frac{dk_8}{dD} = g\left\{\left(\frac{db}{dD}\cdot x_{3,u} + b\cdot\frac{dx_{3,u}}{dD}\right) - \left(\frac{da}{dD}\cdot x_{3,w} + a\cdot\frac{dx_{3,w}}{dD}\right)\right\} \tag{D.6i}$$

The terms from Equations D.3 and D.6a – D.6i, a, b, c, $a_{,u}$, $b_{,u}$, $c_{,u}$, $a_{,w}$, $b_{,w}$, and $c_{,w}$ are given below:

$$a = \sum_{i=1}^{3} x_{i,u} \;,\; b = \sum_{i=1}^{3}\left(x_{i,u}\cdot x_{i,w}\right) \;,\; c = \sum_{i=1}^{3} x_{i,w} \tag{D.7a}$$

$$a_{,u} = 2\cdot\sum_{i=1}^{3} x_{i,u}\cdot x_{i,uu} \tag{D.7b}$$

$$b_{,u} = \sum_{i=1}^{3}\left(x_{i,uu}\cdot x_{i,w} + x_{i,u}\cdot x_{i,wu}\right) \tag{D.7c}$$

$$c_{,u} = 2\cdot\sum_{i=1}^{3} x_{i,w}\cdot x_{i,wu} \tag{D.7d}$$

$$a_{,w} = 2\cdot\sum_{i=1}^{3} x_{i,u}\cdot x_{i,uw} \tag{D.7e}$$

$$b_{,w} = \sum_{i=1}^{3}\left(x_{i,uw}\cdot x_{i,w} + x_{i,u}\cdot x_{i,ww}\right) \tag{D.7f}$$

$$c_{,w} = 2 \cdot \sum_{i=1}^{3} x_{i,w} \cdot x_{i,ww} \tag{D.7g}$$

Taking derivatives of Equations D.7a - D.7g with respect to D, one has

$$\frac{da}{dD} = 2 \cdot \sum_{i=1}^{3} x_{i,u} \cdot \frac{dx_{i,u}}{dD} \tag{D.8a}$$

$$\frac{db}{dD} = \sum_{i=1}^{3} \left(\frac{dx_{i,u}}{dD} \cdot x_{i,w} + x_{i,u} \cdot \frac{dx_{i,w}}{dD} \right) \tag{D.8b}$$

$$\frac{dc}{dD} = 2 \cdot \sum_{i=1}^{3} x_{i,w} \cdot \frac{dx_{i,w}}{dD} \tag{D.8c}$$

$$\frac{da_{,u}}{dD} = 2 \cdot \sum_{i=1}^{3} \left(\frac{dx_{i,u}}{dD} \cdot x_{i,uu} + x_{i,u} \cdot \frac{dx_{i,uu}}{dD} \right) \tag{D.8d}$$

$$\frac{da_{,w}}{dD} = 2 \cdot \sum_{i=1}^{3} \left(\frac{\partial x_{i,u}}{\partial D} \cdot x_{i,uw} + x_{i,u} \cdot \frac{\partial x_{i,uw}}{\partial D} \right) \tag{D.8e}$$

$$\frac{db_{,u}}{dD} = \sum_{i=1}^{3} \left(\frac{dx_{i,uu}}{dD} \cdot x_{i,w} + x_{i,uu} \cdot \frac{dx_{i,w}}{dD} + \frac{dx_{i,u}}{dD} \cdot x_{i,wu} + x_{i,u} \cdot \frac{dx_{i,wu}}{dD} \right) \tag{D.8f}$$

$$\frac{\partial b_{,w}}{\partial D} = \sum_{i=1}^{3} \left(\frac{\partial x_{i,uw}}{\partial D} \cdot x_{i,w} + x_{i,uw} \cdot \frac{\partial x_{i,w}}{\partial D} + \frac{\partial x_{i,u}}{\partial D} \cdot x_{i,ww} + x_{i,u} \cdot \frac{\partial x_{i,ww}}{\partial D} \right) \tag{D.8g}$$

$$\frac{\partial c_{,u}}{\partial D} = 2 \cdot \sum_{i=1}^{3} \left(\frac{\partial x_{i,w}}{\partial D} \cdot x_{i,wu} + x_{i,w} \cdot \frac{\partial x_{i,wu}}{\partial D} \right) \tag{D.8h}$$

$$\frac{\partial c_{,w}}{\partial D} = 2 \cdot \sum_{i=1}^{3} \left(\frac{\partial x_{i,w}}{\partial D} \cdot x_{i,ww} + x_{i,w} \cdot \frac{\partial x_{i,ww}}{\partial D} \right) \tag{D.8i}$$

Derivatives of D with respect to $\boldsymbol{x}_{i,u}$, $\boldsymbol{x}_{i,uu}$, $\boldsymbol{x}_{i,w}$, $\boldsymbol{x}_{i,ww}$, $\boldsymbol{x}_{i,uw}$, $\boldsymbol{x}_{i,wu}$ can be described as follows:

The last terms on the right-hand sides of following Equations D.9a and D.9f represent the explicit dependence of $\boldsymbol{x}_{i,u}$, $\boldsymbol{x}_{i,w}$, $\boldsymbol{x}_{i,w}$, $\boldsymbol{x}_{i,ww}$, $\boldsymbol{x}_{i,uw}$, $\boldsymbol{x}_{i,wu}$ on the design variable *D*.

The remaining terms describe the implicit dependence of $\boldsymbol{x}_{i,u}$, $\boldsymbol{x}_{i,w}$, $\boldsymbol{x}_{i,w}$, $\boldsymbol{x}_{i,ww}$, $\boldsymbol{x}_{i,uw}$, $\boldsymbol{x}_{i,wu}$ on the design variable *D* through $u(t)$ and $w(t)$.

$$\frac{d\boldsymbol{x}_{i,u}}{dD} = \frac{\partial \boldsymbol{x}_{i,u}}{\partial u} \cdot \frac{\partial u}{\partial D} + \frac{\partial \boldsymbol{x}_{i,u}}{\partial w} \cdot \frac{\partial w}{\partial D} + \frac{\partial \boldsymbol{x}_{i,u}}{\partial t} \cdot \frac{\partial t}{\partial D} + \frac{\partial \boldsymbol{x}_{i,u}}{\partial D} \qquad i=1,3 \tag{D.9a}$$

$$\frac{d\boldsymbol{x}_{i,w}}{dD} = \frac{\partial \boldsymbol{x}_{i,w}}{\partial u} \cdot \frac{\partial u}{\partial D} + \frac{\partial \boldsymbol{x}_{i,w}}{\partial w} \cdot \frac{\partial w}{\partial D} + \frac{\partial \boldsymbol{x}_{i,w}}{\partial t} \cdot \frac{\partial t}{\partial D} + \frac{\partial \boldsymbol{x}_{i,w}}{\partial D} \qquad i=1,3 \tag{D.9b}$$

$$\frac{d\boldsymbol{x}_{i,uu}}{dD} = \frac{\partial \boldsymbol{x}_{i,uu}}{\partial u} \cdot \frac{\partial u}{\partial D} + \frac{\partial \boldsymbol{x}_{i,uu}}{\partial w} \cdot \frac{\partial w}{\partial D} + \frac{\partial \boldsymbol{x}_{i,uu}}{\partial t} \cdot \frac{\partial t}{\partial D} + \frac{\partial \boldsymbol{x}_{i,uu}}{\partial D} \qquad i=1,3 \tag{D.9c}$$

$$\frac{d\boldsymbol{x}_{i,ww}}{dD} = \frac{\partial \boldsymbol{x}_{i,ww}}{\partial u} \cdot \frac{\partial u}{\partial D} + \frac{\partial \boldsymbol{x}_{i,ww}}{\partial w} \cdot \frac{\partial w}{\partial D} + \frac{\partial \boldsymbol{x}_{i,ww}}{\partial t} \cdot \frac{\partial t}{\partial D} + \frac{\partial \boldsymbol{x}_{i,ww}}{\partial D} \qquad i=1,3 \tag{D.9d}$$

$$\frac{d\boldsymbol{x}_{i,uw}}{dD} = \frac{\partial \boldsymbol{x}_{i,uw}}{\partial u} \cdot \frac{\partial u}{\partial D} + \frac{\partial \boldsymbol{x}_{i,uw}}{\partial w} \cdot \frac{\partial w}{\partial D} + \frac{\partial \boldsymbol{x}_{i,uw}}{\partial t} \cdot \frac{\partial t}{\partial D} + \frac{\partial \boldsymbol{x}_{i,uw}}{\partial D} \qquad i=1,3 \qquad \text{(D.9e)}$$

$$\frac{d\boldsymbol{x}_{i,wu}}{dD} = \frac{\partial \boldsymbol{x}_{i,wu}}{\partial u} \cdot \frac{\partial u}{\partial D} + \frac{\partial \boldsymbol{x}_{i,wu}}{\partial w} \cdot \frac{\partial w}{\partial D} + \frac{\partial \boldsymbol{x}_{i,wu}}{\partial t} \cdot \frac{\partial t}{\partial D} + \frac{\partial \boldsymbol{x}_{i,wu}}{\partial D} \qquad i=1,3 \qquad \text{(D.9f)}$$